An overview of coupled GCM biases in the tropics

Ingo Richter[1,2], Ping Chang[3,4], Takeshi Doi[1,2], Takahito Kataoka[5], Motoki Nagura[2], Pascal Oettli[2,5], Simon de Szoeke[6], Tomoki Tozuka[5], Zhao Xu[3,4]

1 Research Institute for Global Change, JAMSTEC, Yokohama, Japan

2 Application Laboratory, JAMSTEC, Yokohama, Japan

3 Texas A&M University, College Station, Texas, USA

4 Ocean University of China, Qingdao, Shandong, China

5 Department of Earth and Planetary Science, Graduate School of Science, University of Tokyo, Tokyo, Japan

6 College of Oceanic and Atmospheric Sciences, Oregon State University, Corvallis, Oregon, USA

Corresponding author:

Ingo Richter

Research Institute for Global Change, JAMSTEC

3173-25 Showa-machi, Kanazawa-ku, Yokohama

Tel.: +81-45-778-5523

Fax: +81-45-778-5707

E-mail: richter@jamstec.go.jp

ABSTRACT

This chapter examines the performance of complex numerical climate models with respect to several aspects of mean tropical climate and its variability. While substantial progress has been made since the early days of climate modeling, many challenges remain. A problem common to most coupled ocean-atmosphere general circulation models (GCMs) is the cold sea-surface temperature (SST) bias in the tropics. Despite this cold SST bias GCMs tend to produce too much precipitation over the tropical oceans, particularly south of the equator. Due to the close link between convection and surface winds, the precipitation biases in GCMs are also accompanied by surface wind biases. Particularly on the equator this strongly affects the simulated ocean currents and vertical temperature stratification. Precipitation biases over land surfaces likely contribute to biases over the equatorial oceans through their influence on the Walker circulation. This influence is particularly strong for the Atlantic basin where GCMs typically underpredict precipitation over tropical South America and overpredict it over tropical Africa. Despite cold SST biases over much of the tropical oceans, warm SST biases dominate in the southeastern tropical Pacific and Atlantic. These warm biases appear to be due to a combination of surface wind biases (both on the equator and locally), excessive shortwave solar radiation due to insufficient low-level cloud, and weak oceanic stratification reducing the cooling effect of upwelling. The failure to capture the equatorial thermocline (the sharp temperature gradient separating the deep ocean from the warm surface layer) is also an important error source in coupled GCMs.

Moving ahead will require further improvements in the representation of deep convection and its relation to surface winds in atmospheric GCMs. On the oceanic side, one major challenge is to better understand and simulate the processes responsi-

ble for the equatorial thermocline. While increased model resolution can solve some of the problems of current GCMs it certainly cannot solve all of them. Additionally, long-term climate simulations will likely have to rely on convective and other parameterizations for a long time to come. Further improving these parameterizations must therefore remain one of the main targets for model development. Such efforts should increase model performance but, on the other hand, many issues will probably remain. Effort should therefore be spent on understanding how model biases affect seasonal forecasts and climate change projections, in order to maximize their utility as predictive tools.

1 Introduction

The history of numerical modeling of geophysical fluids may have started with the pioneering work of Vilhelm Bjerknes (1900, 1904), who outlined the steps necessary for numerical weather prediction based on the Navier-Stokes and thermodynamical equations. These ideas were further developed by Richardson (1922), who wrote the exact form of the required equations and described ways of solving them numerically. Both researchers were, however, far ahead of their time in the sense that neither weather observations nor computational power where anywhere near the levels required to make useful predictions feasible. Efforts were reinvigorated in the late 1940s with the advent of electronic computers. On the advice of mathematician John von Neumann, the U.S. funded research into numerical weather prediction (Edwards 2000), and this eventually led to the first successful geophysical simulations with a 2D barotropic model in 1950 (Charney et al. 1950). The first general circulation model (GCM) is usually attributed to Phillips (1956), who developed a global quasi-geostrophic model with two vertical levels. Further efforts at the Geophysical Fluid Dynamics Laboratory in Princeton led to models based on the less simplified primitive equations (Smagorinsky 1958). Benefitting from the experience gained in atmospheric GCMs, numerical simulation of the ocean started in the 1960s (Sarkisyan 1962; Bryan 1963; Bryan and Cox 1967, 1968; see also review by McWilliams 1996). The first coupled ocean-atmosphere models appeared in the late 1960s (Manabe and Bryan 1969) but still employed idealized land-ocean distributions. Global coupled ocean-atmosphere GCMs (CGCMs) were developed in the 1970s and 1980s (Manabe et al. 1975; Bryan et al. 1975; Washington et al. 1980; Gates et al. 1985). Starting from the late 1980s they were increasingly used to investigate issues such as global warming (e.g. Washington and Meehl 1989; Manabe et al. 1990) and interannual cli-

mate variability associated with the El Niño/Southern Oscillation (ENSO) phenomenon (e.g. Latif et al. 1988). The coupling of oceanic and atmospheric GCMs brought with it new challenges in reproducing the observed circulation. When integrated with prescribed forcing at the air-sea boundary, the individual atmospheric and oceanic components showed some success in reproducing features of the observed climate. Upon coupling, however, the model climate tended to drift into an unrealistic state due to positive air-sea feedbacks that amplify the systematic errors in either component. This climate drift proved to be a serious problem for simulating and predicting climate variability and projecting climate change, and led many modeling groups to employ so-called "flux correction" (also flux adjustment) schemes. These overrode the model generated air-sea fluxes to ensure a realistic mean state while still allowing the coupled system to develop internal variability and to respond to external forcing. Naturally, such an approach puts heavy constraints on CGCM behavior and has therefore been criticized (Neelin and Dijkstra 1995) and regarded as a temporary rather than a permanent solution. Efforts were made to eliminate flux-correction schemes from CGCMs and from the 1990s onward the majority of models do not use them though the latest coupled model intercomparison project phase 5 (CMIP5; Taylor et al. 2012) still contains a few flux-corrected GCMs.

The fact that most current CGCMs do not use any flux correction schemes is indicative of the progress models have made since the early days. Nevertheless, CGCMs continue to face serious challenges in reproducing observed and past climate. In the following three paragraphs we introduce three of the issues that feature prominently in the present overview.

One of the most challenging aspects in GCMs is the representation of tropical convection because it involves spatial scales that are much smaller than those of the

general circulation but nevertheless have a profound influence on it (see e.g. Arakawa 2004 for a review of the representation of convection in GCMs). Moreover tropical convection not only involves subgrid-scale dynamics but also several other processes that need to be parameterized, such as cloud microphysics, radiation, and turbulence. Since the precipitation that results from tropical convection is relatively well observed, it provides an integrative measure of model performance and has been the focus of many diagnostic studies. While in recent years there have been efforts to explicitly resolve tropical convection (see subsection 6.1), which requires grid resolutions of 4 km or finer, current computer speeds do not permit to integrate global models of this kind beyond a few months. Even assuming that the rapid increase in computational power over the last few decades will continue into the future, it seems likely that long-term climate simulations will depend on some kind of convective parameterizations in the near term and possibly beyond.

Another challenge for GCMs in the tropics is resolving the sharp vertical gradients that characterize the atmospheric planetary boundary layer (PBL) and oceanic thermocline (OT). In the atmosphere this is particularly problematic in the marine boundary layer over the eastern subtropical oceans where sharp gradients of temperature and moisture occur over a vertical distance as short as a few 10s of meters (e.g. Roach et al. 1982). In the ocean, the equatorial thermocline, which separates the warm and thin upper layer from the cool deep ocean, presents similar sharp gradients. Both PBL and OT are difficult to simulate in GCMs (Suarez et al. 1983; Moeng and Stevens 2000; Xu et al. 2013a), whose typical vertical grid spacing is too coarse to fully resolve such sharp gradients.

The representation of land-surface processes poses another challenge to current GCMs. Fluxes of sensible and latent heat are crucial in determining PBL structure and

hence terrestrial precipitation. These fluxes, however, depend on the complex interaction among atmospheric radiation, soil moisture and various vegetation types. Current observations of the relevant properties are not sufficient to validate GCMs on a global scale, which hampers efforts toward improving existing models. While satellite observations can help to infer properties such as soil moisture over some areas, they are of limited use over the rainforests that cover large portions of the tropics. Due to these reasons there are large uncertainties associated with the representation of land-surface processes in GCMs.

The aim of this chapter is to give an overview of the challenges facing current coupled GCMs. It should be stressed that the choice of issues covered is highly selective and guided by the authors' individual areas of expertise. While these are fairly diverse the authors lay no claim to a comprehensive review. Nevertheless we hope that the material covers a wide enough range to be helpful to model users and developers alike. To the former, as an overview of the limitations of current GCMs; to the latter as a guide to target areas for model improvement. We also hope that the synthesis provided in section 7 will give the community some food for thought regarding the common aspects of GCM biases in different tropical regions. The focus will mostly be on mean state errors, but the influence of these errors on interannual variability will also be discussed. Variability on intraseasonal timescales, such as the Madden-Julian oscillation (MJO; Zhang 2005), will not be covered here due to our limited expertise in this area and due to length considerations. We note, however, that correct representation of the MJO remains one of the major challenges of current GCMs and refer the reader to a model evaluation by Kim et al. (2009).

Since this overview will rely heavily on the comparison of GCMs and observations we briefly summarize here the relevant datasets. In addition to the CMIP5 inter-

comparison described above, many studies have used models from the previous inter-comparison, CMIP3 (Meehl et al. 2007; see Table 1 for a list of models). While CMIP3 models formed the basis of the Intergovernmental Panel on Climate Change's (IPCC) fourth Assessment Report (AR4), the CMIP5 models form the basis of the AR5. Since there are about 6 years between the two, most CMIP5 models feature further development relative to CMIP3.

On the observational side, the following datasets feature in this overview. For the sea-surface temperatures (SST) the OISST (Reynolds et al. 2002) and GISST (Rayner et al. 1996) data are featured. The former is a blend of satellite and in-situ observations while the latter consists of in-situ observations only, with gaps filled in through statistical techniques. Precipitation data is from the Global Precipitation Climatology Project (GPCP; Adler et al. 2003), the Climate Prediction Center Merged Analysis of Precipitation (CMAP; Xie and Arkin (1996), and the Tropical Rainfall Measurement Mission (TRMM; Adler et al. 2000). The first two present a blend of satellite and rain-gauge data, while the third one is based on satellite data only. Surface winds are from the International Comprehensive Ocean-Atmosphere Data Set (ICOADS; Woodruff et al. 2011), while surface wind stress is from TropFlux (http://www.locean-ipsl.upmc.fr/tropflux/). Subsurface ocean temperatures are from the World Ocean Atlas 2009 observations (Locarnini et al. 2006).

Reanalysis is a technique that essentially blends observations and GCM simulations to derive a gapless record of relevant atmospheric and oceanic variables. Several reanalysis products feature in this overview. These are the European Center for Medium Range Forecast (ECMWF) Reanalysis (ERA40; Uppala et al. 2005), the satellite era ECMWF Interim reanalysis (ERA-Interim; Dee et al. 2011), the National Center for Environment Prediction (NCEP) and National Center for Atmospheric Research

(NCAR) reanalysis (NCEP; Kalnay et al. 1996), and the NCEP Climate Forecast System reanalysis (CFSR; Saha et al. 2010).

Sections 2, 3 and 4 look at GCM performance in the Pacific, Atlantic and Indian Ocean basins, in that order. Challenges regarding the representation of land-surface process are treated in section 5, with some illustrative examples from agro-hydrological models. The potential benefits of increasing model resolution are evaluated in section 6. In section 7, we summarize sections 2-6 and discuss the challenges that lie ahead for GCMs and how these might be addressed.

2 GCM biases in the tropical Pacific Ocean

2.1 The mean state of the tropical Pacific and its representation in GCMs

Latent heat of condensation over precipitating regions of the Pacific Ocean drives a significant part of the upward branches of the Hadley and Walker circulations. These features of the mean general circulation export heat, moisture, and angular momentum to the subtropics and midlatitudes. The Pacific Ocean specifically is host to ENSO, the mode of air-sea interaction that dominates global interannual climate variability. Atmospheric teleconnections originating from atmospheric heating anomalies in the central Pacific propagate poleward and eastward as stationary Rossby waves, steering the jet stream and affecting midlatitude weather in the winter hemisphere (Hoskins and Karoly 1981; Wallace and Gutzler 1981). A schematic diagram of tropical Pacific mean climate and El Niño conditions is given in Fig. 1. More detailed explanations follow below.

The observed climatology of precipitation (Fig. 2a) over the tropical Pacific features a narrow zonal band of precipitation known as the intertropical convergence zone (ITCZ). This band merges into a broader region of precipitation over the warm-

est waters in the western Pacific Ocean (Fig. 3a). A third arm of precipitation, the South Pacific convergence zone (SPCZ), stretches southeast from the equatorial West Pacific. The Walker cell (Walker 1923, 1924, 1928; Bjerknes 1969) dominates the mean zonal circulation, with easterly trade winds at the surface (Fig. 4) and ascent in the precipitating regions of the West Pacific warm pool (Fig. 2). The Hadley cell (Halley 1686) dominates the mean meridional circulation, with surface convergence, precipitation, and mean upward motion in the deep tropics, notably in the zonally symmetric ITCZ, and adiabatic descent of dry air outside convective regions and throughout the subtropical latitudes.

Atmospheric heating and surface convergence in the western Pacific component of the Walker circulation, and zonal angular momentum conservation in the Hadley circulation, give rise to the easterly trade winds along the equatorial Pacific (Fig. 4). The easterly wind stress pushes the mean sea level up and the thermocline depth down in the western equatorial Pacific, increasing its warm water volume. It also lowers sea level and shoals thermocline depth in the eastern equatorial Pacific Ocean, enabling cold sub-thermocline water entrainment into the mixed layer there. The deep warm mixed layer in the western Pacific is known as the western Pacific warm pool, while the region of shallow mixed layer and cold sea-surface temperature (SST) in the eastern Pacific is known as equatorial cold tongue.

The distribution of annual mean SST and precipitation in the eastern and central Pacific is markedly asymmetric about the equator, with SST and precipitation higher to the north than to the south (Figs. 2a and 3a). This meridional asymmetry is surprising in view of the fact that annual mean insolation is approximately symmetric about the equator. Only in March and April are SST and precipitation nearly symmetric and precipitation maxima found both north and south of the equator (observations in Fig.

5). From May through October the meridional asymmetry strengthens and matures, with SST and precipitation decreasing south of the equator. This results in a single ITCZ north of the equator that reaches its northernmost latitude in October. The annual cycle of meridional asymmetry is closely tied to an annual cycle of meridional wind stress magnitude on the equator, where cross-equatorial winds are weakest in boreal spring and strongest in boreal fall. The associated upwelling and mixing on the equator maintain a pronounced annual cycle of equatorial SST (despite the semiannual cycle of solar radiation) with October being the coldest month of the equatorial Pacific cold tongue (Mitchell and Wallace 1992).

Philander et al. (1996) suggested that the ultimate reason for the eastern Pacific meridional asymmetry lies in the orientation of the eastern boundary (American west coast), which is parallel to the southeast trades in the Southern Hemisphere, but perpendicular to the northeast trades in the Northern Hemisphere. Thus alongshore winds in the Southern Hemisphere drive coastal upwelling, while offshore winds in the Northern Hemisphere do not. The resulting initial meridional SST asymmetry is amplified by the wind-evaporation-SST (WES; Xie and Philander 1994) feedback. Warm SST anomalies in the Northern Hemisphere, for example, are associated with southerly wind anomalies that strengthen the southeast trades and weaken the northeast trades, and the resulting latent heat flux anomalies amplify the initial asymmetry. The positive WES feedback reduces the damping of SST anomalies by evaporation and thus facilitates the westward propagation of long atmospheric Rossby waves that propagate initial asymmetries from the eastern boundary toward the basin interior (Xie 1996). For a detailed review of the mechanisms governing the meridional asymmetry of the Hadley circulation the reader is referred to Xie et al. (2005).

Most coupled GCMs face similar problems in reproducing the meridional asymmetry of the eastern Pacific. Mechoso et al. (1995) noted that instead of an ITCZ that mostly stayed in the Northern Hemisphere, many models had a so-called *double ITCZ bias*: two zonal bands of surface convergence and precipitation between 5-10° latitude, one in each hemisphere. Though there has been improvement over the intervening years of model development, many of the same biases persist in today's GCMs (Fig. 2b). De Szoeke and Xie (2008) found that while the CMIP3 models often simulated some meridional asymmetry, many underestimated it (Figs. 2b and Figs. 3b), and as a result simulated an ITCZ alternating between the hemispheres with the seasons (Fig. 5).

Dai et al. (2006) found that the double ITCZ bias in coupled GCMs is amplified by the excessive westward extension of the equatorial cold tongue, which tends to split the ITCZ into two branches straddling the equator. Lin (2007) analyzed tropical biases in 22 coupled GCMs from CMIP3 and 12 of their atmospheric GCM counterparts. They found that the double ITCZ and the cold equatorial bias in these models mostly stem from an overly strong Walker circulation related to excessive warm pool precipitation, and from excessive sensitivity of precipitation to SST. Excessive precipitation is also present in the atmospheric components of the models forced with observed SST (Schneider 2002), which is likely due to deficiencies in their convective schemes. Regarding the equatorial easterly and cold SST biases, Luo et al. (2005) have shown that considering the surface ocean current speed in the momentum transfer calculations reduces the easterly stress and thus alleviates some of the SST bias in their coupled model.

The excessive sensitivity of precipitation to SST in models is often compounded by inadequate radiative effects of clouds associated with precipitation (Lin 2007).

Many GCMs produce too little cirrus and cumulus cloud in response to deep convection, and thus underrepresent the net reduction of surface shortwave radiation associated with these cloud types (Ramanathan and Collins 1991). Thus surface shortwave radiation and SST decrease less than they should, which facilitates continued deep convection.

Another potential source of GCM deficiencies concerns the response of latent heat flux (LHF) to SST anomalies (Lin 2007). Due to the excessive surface winds, most models overpredict *mean* LHF over the tropical oceans, contributing to the cold SST biases that prevail over much of the tropical oceans. On the other hand, the simulated LHF *anomalies* tend to erroneously enhance SST anomalies. This can be seen by expanding the LHF anomaly as a product of a friction velocity u^* and a moisture component q^*,

$$\mathrm{LHF}' = u^*q^* - \langle u^*q^* \rangle = u^{*\prime}\langle q^* \rangle + \langle u^* \rangle q^{*\prime} + u^{*\prime}q^{*\prime} - \langle u^{*\prime}q^{*\prime} \rangle,$$

where angular brackets and primes denote mean fields and deviations from the mean over the tropics, respectively.

LHF anomalies are dominated by the first two terms on the right hand side. Negative $u^{*\prime}$ anomalies tend to occur in the weak converging winds over warm SST anomalies. $q^{*\prime}$ anomalies, on the other hand, are only weakly correlated to SST because the sea-air specific humidity difference stays small. As a result simulated LHF anomalies are too weak over warm SST, amplifying SST anomalies associated with the Walker circulation.

The double ITCZ problem is exacerbated by a coupled feedback involving the equatorial trades. In observations the equatorial trades (both zonal and meridional components) are weakest in boreal spring, when the ITCZ is closest to the equator. In GCMs, however, the boreal spring ITCZ often migrates farther into the Southern

Hemisphere, which leads to a spurious second maximum in the strength of the equatorial trades. Upwelling and mixing associated with the meridional wind cools the SST, thus further discouraging deep convection close to the equator. This causes the annual average SST, and even the minimum SST, on the equator to be colder in simulations with an alternating ITCZ (de Szoeke and Xie 2008; Fig. 3b).

Stratocumulus clouds reduce surface insolation preferentially in the Southern Hemisphere (Hartmann et al. 1992; Klein and Hartmann 1993). Errors in the representation of these low clouds in GCMs contribute to the underestimation of meridional asymmetry of the East Pacific climate (Ma et al. 1996; Philander et al. 1996; Gordon et al. 2000; de Szoeke et al. 2006). Low-cloud radiative forcing is quite varied in present state-of-the-art climate models, partly because of its sensitivity to the underlying surface temperature (Lauer et al. 2010; de Szoeke et al. 2012). This has a large impact on the simulated surface radiation budget and remains the largest source of uncertainty to climate change projections (Bony and Dufresne 2005; Lauer et al. 2010).

Low-level cloud cover is closely linked to the underlying SST (Klein and Hartmann 1993), which could potentially amplify meridional asymmetries in the eastern Pacific. Using an ensemble of CMIP3 CGCMs de Szoeke and Xie (2008) show that the intermodel SST spread in the southeastern Pacific is correlated to the overlying stratocumulus incidence yet surface solar flux does not seem to determine the meridional ITCZ asymmetry in the eastern Pacific. Several CMIP3 models have weak asymmetry despite having strong cloud forcing and cold SST in the Southern Hemisphere. Among these models the meridional asymmetry in February-April is correlated much better to winter wind speed in the northern tropical Pacific near Central America. The stronger-than-observed winds in that region are consistent with the absence of the northern ITCZ and convergence into the Southern Hemisphere. These

winds keep SST cool and thus prevent the ITCZ from migrating into the Northern Hemisphere in the following spring (de Szoeke and Xie 2008).

2.2 The simulation of tropical Pacific interannual variability

In addition to the Walker cell, Bjerknes (1969) also noted a positive feedback between equatorial easterly trade wind anomalies and cold SST in the eastern equatorial Pacific Ocean. The easterly anomalies associated with an enhanced Walker circulation act to enhance the gradient of SST by advecting warm surface water toward the western Pacific and raising the thermocline in the eastern equatorial Pacific. Due to the Earth's rotation, easterly wind stress drives poleward divergence off the equator that further raises the thermocline and cools the SST. The cycle of enhancement of the Walker circulation: easterly wind stress, thermocline tilt, and zonal SST gradient along the equator are known as the *Bjerknes feedback*. Anomalously warm SST during November-December-January and the collapse of the fishery dependent on nutrient-rich upwelling off the coast of Ecuador and Peru are known as El Niño; a seesaw of Indo-Australian sea level pressure anomalies anti-correlated to the Pacific basin are called the Southern Oscillation (Walker 1923, 1924, 1928). Combined, the El Niño-Southern Oscillation (ENSO) phenomenon is one of the most famous examples of interannual climate variability (see Fig. 1b for a schematic diagram). Reproducing its statistical behavior and predicting its temporal evolution remain a challenge for GCMs.

While the too-strong Walker circulation and meridionally alternating double ITCZ biases (see subsection 2.1) are common to many GCMs, errors in the simulation of ENSO are less consistent though some commonalities exist. Whereas observed SST anomalies are positively skewed, with stronger interannual warm SST events than cool events, model distributions tend to be more symmetric (though the inter-

model variability is large). A multi-model study by An et al. (2005) suggests that the lack of skewness is due to insufficient nonlinear oceanic advection (both in the horizontal and vertical direction).

ENSO events recur quasi-regularly every 3-8 years and typically peak in December. While early models tended toward regular biennial ENSO cycles, most models in the CMIP3 and CMIP5 ensembles have improved substantially in this regard, with realistic power in the 3-8 year band and reduced power in the 1-3 year band (Bellenger et al. 2013). The seasonality of ENSO anomalies, however, remains too symmetric in GCMs, with models simulating relatively too little SST variability in November-January compared to March-May (AchutaRao and Sperber 2006, Bellenger et al. 2013).

The recharge oscillator model (Jin 1997) simulates many of the salient features of ENSO by modeling its essential feedbacks with linear parameters. Bellenger et al. (2013) find that the atmospheric wind stress feedback (wind stress anomaly per SST anomaly) is too weak in all but 3 of the CMIP3 and CMIP5 models. On the other hand damping of SST anomalies due to surface fluxes, comprised chiefly of solar cloud forcing (Lloyd et al. 2012) and latent heat flux, in the CMIP3 and CMIP5 models is too strong, indicating compensating errors may be partly responsible for the reasonable ENSO amplitudes simulated by these models. Regarding errors in amplitude, an interesting relation to the mean state exists in that models with too weak an annual cycle in the eastern tropical Pacific suffer from excessively strong ENSO amplitude (Guilyardi 2006).

Due to its dominant influence on global climate anomalies, prediction of ENSO remains one of the major targets of modeling centers. Through the turn of the millennium dynamical models demonstrated no additional predictive skill relative to statisti-

cal models, but recent generations of dynamical models do provide useful predictability over their statistical counterparts (Luo et al. 2008). Models were long troubled by a "predictability barrier" in the seasonal cycle such that forecasts initialized before March-April had no useful prediction skill after March-April. Recent dynamical ocean-atmosphere models (e.g. the NCEP Coupled Forecast System CFS version 2) have improved and offer predictability beyond statistical models, even when making seasonal forecasts through March-April (Luo et al. 2008; Barnston et al. 2012).

3 GCM biases in the tropical Atlantic

In the early days of CGCMs, research interest was focused mainly on studying ENSO and simulating the climatic response to greenhouse gas forcing. While CGCMs of the 1980s typically suffered from severe biases in the tropical Pacific (see section 2; also Neelin et al. 1992) substantial progress has been made over the last two decades, though several issues remain (see section 2 and de Szoeke and Xie 2008). In the tropical Atlantic, on the other hand, improvements have been more limited. During the 1980s and 1990s, modelers mainly paid attention to the simulation of the tropical Pacific. The study by Davey et al. (2002) was perhaps the first CGCM intercomparison that included the Atlantic basin. They found that the annual mean SST gradient along the equator had the wrong sign, relative to observations, in all GCMs except one (note, however, that that GCM was only fully coupled in the tropical Atlantic and Pacific). Thus the GCMs produced cold SST in the western warm pool and warm SST in the eastern cold tongue (see Fig. 6a). In the equatorial Pacific, on the other hand, the zonal SST gradient had the right sign in all the models. The severity of the equatorial Atlantic biases prompted several studies into their origins, the results of which will be discussed in subsection 3.1.

Another persistent problem exists in the southeastern tropical Atlantic close to the African coast, where simulated SSTs are often 5 K warmer than observed (Fig. 6a; Wahl et al. 2011; Huang et al. 2007). This bias is very similar to the one in the southeast Pacific (see section 2) and often attributed to under-representation of stratocumulus decks in GCMs. A significant difference between the southeast Pacific and Atlantic is that the latter features surface current convergence at around 16ºS, where the poleward Angola current and the equatorward Benguela current meet. The strong temperature gradient associated with this Angola-Benguela frontal zone (ABFZ) presents an additional challenge for GCMs (Xu et al. 2013a), as will be further discussed in subsection 3.2.

The biases in CGCMs are often attributed to coupled processes amplifying small initial errors in the individual components. While error amplification certainly does exist in the tropical Atlantic, e.g. through the Bjerknes feedback (Richter and Xie 2008; see subsection 2.1 for an explanation of the Bjerknes feedback), it has also become clear that substantial biases already exist in the atmospheric and oceanic components with prescribed forcing (Chang et al. 2007; Richter and Xie 2008; Patricola et al. 2012). In terms of improving CGCMs it is helpful to identify the errors in their uncoupled components since this more readily points to specific issues that need to be addressed. Following this philosophy, we describe the biases in the atmospheric and oceanic components in subsections 3.1 and 3.2, respectively. Subsection 3.3 discusses to what extent Atlantic biases affect seasonal predictions and climate change projections.

3.1 Biases originating in the atmospheric component

Davey et al. (2002) noted that the equatorial easterlies in the CGCMs are weaker than observed, particularly in boreal spring, when some models even feature wester-

lies on the equator. Subsequent studies confirmed this feature and showed that it was already present in uncoupled AGCMs (Okumura and Xie 2004; DeWitt 2005; Chang et al. 2007; Richter and Xie 2008). Okumura and Xie (2004) speculated that the weak equatorial easterlies in spring were responsible for the failure of CGCMs to capture the annual evolution of the Atlantic cold tongue. This was confirmed by DeWitt (2005) who performed sensitivity tests with one particular CGCM. His results showed that unrealistically weak equatorial easterlies reduce thermocline slope and upwelling velocity, both of which contribute to the equatorial SST biases. Later sensitivity studies by Wahl et al. (2009) and Richter et al. (2012a) gave further support to this idea.

Richter and Xie (2008) demonstrated that the westerly bias and thermocline deepening are ubiquitous among CGCMs participating in CMIP3. They also confirmed the robustness of the westerly surface wind bias in the standalone atmospheric components of the CGCMs. Various factors have been found to contribute to the weak easterlies in uncoupled GCMs. 1) Deficient precipitation over the Amazon basin (Chang et al. 2008; Richter and Xie 2008; Patricola et al. 2012) and excessive precipitation over the Congo basin (Richter and Xie 2008; Patricola et al. 2012) weaken the Atlantic Walker cell and thus the equatorial surface winds. The continental influence on surface winds is supported by experiments with a quasi-geostrophic atmospheric model with prescribed heating over equatorial South America (Chang et al. 2008), by GCM experiments with modified convection strength over equatorial South America and Africa (Tozuka et al. 2011; Wahl et al. 2011; Richter et al. 2012a), and by regional high-resolution atmospheric model experiments with different convection and radiation schemes (Patricola et al. 2012). 2) Migration of the marine ITCZ into the Southern Hemisphere (Richter and Xie 2008; Grodsky et al. 2012; Doi et al. 2012; Richter et al. 2012b) leads to weak surface easterlies on the equator. Weakening of equatorial

trades in relation to southward ITCZ migration is also found in observed interannual variability. Theoretical explanations for this phenomenon are the meridional advection of zonal momentum (Okumura and Xie 2004) and the shallow westerly jet that accompanies the Atlantic ITCZ in the central basin (Grodsky et al. 2003). Both 1) and 2) appear to contribute to the westerly surface wind biases in the equatorial Atlantic but further studies are needed to determine their relative importance. An additional explanation has been put forward by Zermeno and Zhang (2013) who argue that insufficient moment entrainment across the PBL top is one of the root causes. A more recent evaluation by Richter et al. (manuscript submitted), however, suggests that this is only a minor factor. Other factors may be at play but have not been discussed in the literature so far. Relating these biases to particular shortcomings in the AGCM parameterizations remains a major challenge.

Apart from playing a central role in the AGCMs' westerly surface wind bias, tropical convection itself is also of major interest due to its vital importance to water resources. Since convection cannot be explicitly resolved in GCMs but has to be parameterized it is a potential source for GCM errors. We therefore discuss in some more detail here the role of convective parameterizations in tropical Atlantic GCMs biases (see Arakawa (2004) and Stensrud (2007) for reviews of different schemes). We note, however that other parameterizations, such as microphysics, turbulence, and land surface schemes may also have a large impact on the simulated equatorial surface winds (see e.g. Wahl et al. 2009) and climate in general.

Braconnot et al. (2007) compared results from a CGCM using the convection scheme of Tiedtke (1989) and Emanuel (1991). They found that the seasonal march of the ITCZ, which plays an important role in the SST simulation over the equatorial Atlantic, is better reproduced when the Emanuel scheme is used. In addition, the Eman-

uel scheme also achieves a better representation of the South American and West African monsoon systems, which are known to play an important role in the development of the equatorial Atlantic cold tongue. The cloud cover simulated by the Emanuel scheme also enhances the monsoon flow by strengthening the meridional surface temperature gradient between deep convective regions at the equator and subsidence regions to the south.

More recently, Tozuka et al. (2011) analyzed three versions of the same CGCM differing only in their cumulus convection scheme. The three schemes tested were developed by Kuo (1974), Tiedtke (1989), and Emanuel (1991). Only the version using the Kuo scheme was successful in simulating the mean zonal SST gradient of the equatorial Atlantic with warm SST in the west and cool SST in the east (Fig. 7). Tozuka et al. (2011) attributed the success of the Kuo scheme version to three major reasons. 1) It correctly places the ITCZ to the north of the equator, while the two other versions erroneously place the ITCZ in the Southern Hemisphere. 2) It reproduces the intense precipitation over the northern part of South America, which provides favorable conditions for equatorial easterly winds. Further sensitivity experiments by Tozuka et al. (2011) using the atmospheric component of the CGCM indicated that remote forcing from the tropical Pacific plays an important role in suppressing convection over the region in the other two versions. 3) The Kuo scheme version simulates southerly winds along the southwestern coast of Africa that are comparable to observations, while the southerlies in the other two versions are much weaker than observed. This is consistent with the notion that the seasonal cold tongue development is associated with the onset of the West African monsoon through its influence on cross-equatorial winds (Mitchell and Wallace 1992; Okumura and Xie 2004).

While the results of Tozuka et al. (2011) highlight the performance of the Kuo scheme it should be noted that this scheme has long been criticized because it assumes that convection is controlled by the large-scale atmospheric moisture supply, which is often not the case in observations (Stensrud 2007). Moreover, the contrasting results of Braconnot et al. (2007) and Tozuka (2011) suggest that the performance of a given scheme is model dependent. Thus, rather than assessing the performance of convection schemes, the results should be seen as highlighting the fundamental influence that these schemes exert on the simulated climate. Changes in other parameterization schemes (e.g. microphysics, turbulence, or land surface) may also have large impacts (see Wahl et al. 2009) on tropical climate. Since these schemes also interact with the model's convective parameterization, pinpointing the causes of atmospheric biases remains a difficult task.

Warm SST biases along the southwest African coast are a problem in all CMIP5 GCMs. Equatorial surface wind biases may also play a role here (Patricola et al. 2012; Richter et al. 2012a; Grodsky et al. 2012; see subsection 3.2) via oceanic Kelvin waves that travel along the equatorial and coastal waveguides and adjust the thermal stratification (Florenchie et al. 2003; Rouault et al. 2007; Luebbecke et al. 2010). There is, however, also evidence that underestimation of along-shore winds contribute to the biases (Richter et al. 2012a) and that local feedbacks in the eastern tropical Atlantic affect the biases (Patricola et al. 2012). Such an influence of local along-shore winds on Ekman pumping has been documented in observations of interannual-to-intraseasonal variability in the region (Polo et al. 2008; Richter et al. 2010; DeWitt et al. 2011). To what extent the oceanic model components contribute to the warm SST bias in the southeast Atlantic is discussed in subsection 3.2.

While the contribution of surface wind stress to the southeast Atlantic SST biases has gained attention in recent years, there is a longer history of examining the contribution of subtropical stratocumulus decks. This cloud type covers large portions of both the southeast Atlantic and Pacific oceans and, due to its high reflectivity, has a net cooling effect on the ocean surface (Stephens and Greenwald 1991; Hartmann et al. 1992; Klein and Hartmann 1993). AGCMs have notorious difficulties in representing low-level cloud (e.g. Mechoso et al. 1995; see also section 2) and this has been shown to contribute to the warm SST biases in the stratocumulus regions of the southeast Pacific (Ma et al. 1996; Yu and Mechoso 1999) and Atlantic (Huang et al. 2007; Hu et al. 2011). The dependence of stratocumulus on lower tropospheric stability (LTS; Klein and Hartmann 1993) suggests a coupled feedback (Randall 1980): warm SSTs reduce LTS (commonly defined as the potential temperature difference between 700 hPa and the surface) and thereby create an environment that is less favorable to stratocumulus. This leads to reduced cloud cover and increased net shortwave heating at the surface, which further warms SST and completes the feedback loop. Due to this positive feedback mechanism, initial errors in simulated cloud cover and coastal upwelling are quickly amplified and can lead to nearly cloud-free conditions over the eastern subtropical oceans. To what extent stratocumulus deficiencies can explain the southeastern SST biases, however, needs further study. SST errors are most pronounced just off the coast while stratocumulus decks typically extend more than 1000 km offshore. The coastal signature of the SST errors indicates that the underrepresentation of coastal upwelling plays a large role as well. Errors in coastal upwelling might be partly related to errors in surface wind forcing, as discussed in the previous paragraph. A large portion, however, is likely related to problems in the oceanic component, as will be discussed in subsection 3.2.

Regarding the relative importance of surface wind stress and shortwave radiation in the southeastern SST biases there is still some degree of uncertainty. Based on sensitivity studies with the NCAR Community Climate System Model (CCSM) version 2, Large and Danabasoglu (2006) estimate that both contribute in roughly equal parts. However, the combined contribution of these two effects to the total SST bias was only 40%, which indicates that other significant error sources have yet to be identified. It is interesting to note that regional coupled models that do not include the equatorial region typically produce southeastern SSTs that are colder than observed (Penven et al. 2005; Veitch et al. 2010). Since the regional models are not fundamentally different from the GCMs, this suggests that remote influences from the equator might be an important factor in the biases.

Ma et al. (1996) studied the regional impact of subtropical stratocumulus biases. Their study focuses on the southeastern Pacific but should also apply to the southeastern Atlantic, due to the similarity of the two regions. They found that correcting the southeastern tropical Pacific stratocumulus biases could potentially also benefit the equatorial Pacific. When they prescribed 100% cloud cover over the southeastern Pacific in a sensitivity test with the UCLA coupled GCM, they found not only local SST cooling but also a strengthening of the southeast trades that extended all the way to the equator and led to a more pronounced cold tongue. This kind of impact, however, may be due to the idealized set-up of the experiment and also might not be robust across models. A more recent study by Tompkins and Feudale (2010) compared two versions of the ECMWF seasonal forecast system with different physics. The more recent version reduces the stratocumulus bias in the southeast Atlantic but at the same time suffers from a more severe SST bias in the Gulf of Guinea relative to the previ-

ous version. Thus it is not clear whether improving southeast Atlantic stratocumulus biases will necessarily improve equatorial biases in all models.

3.2 Biases originating in the oceanic component

In most GCMs, the largest tropical Atlantic SST bias of up to 8º-10º C is not located on the equator but along the Namibian and Angolan coast near the ABFZ. Another intriguing feature is that the amplitude of the warm bias is significantly larger south of the ABFZ than north of the ABFZ. As mentioned in subsection 3.1, the ABFZ is a unique feature of the southeast Atlantic and maintained by two opposing currents – the southward Angola Current (AC) north of the ABFZ and the northward Benguela Current (BC) south of the ABFZ. Figure 8 gives a schematic depiction of the ABFZ and the associated ocean circulation in the Southeast Tropical Atlantic. The warm AC is fed by the Equatorial Undercurrent (EUC) and South Equatorial Undercurrent (SEUC) and carries warm and saline water from the equatorial region to the ABFZ along the Angola coast against the local southerly wind (Wacongne and Piton 1992; Yamagata and Iizuka 1995). The cold BC is driven by the pressure gradient associated with the strong upwelling maintained by the prevailing southerly winds along the Namibian coast (Peterson and Stramma 1991) and is supplied by the southern limb of the subtropical gyre in the South Atlantic and water from the Indian Ocean through the Agulhas Current (Veitch et al. 2010). The two coastal currents converge near 16°S, forming the ABFZ (Lass et al. 2000), where a sharp temperature gradient is formed. In contrast, no prominent doming structure is present in the Pacific circulation system. The main current in the coastal upwelling system of the southeast Pacific, the Humboldt current, also known as the Peru Current, starts from approximately 43°S, penetrates all the way to the equatorial zone and feeds the South Equatorial Current (SEC) with no major convergence zones or fronts (Penven et al., 2005).

The fact that the location of the largest Atlantic SST bias coincides with the location of the ABFZ raises the possibility that the bias is attributable, at least partially, to the ocean models' failure in correctly simulating the location and strength of the ABFZ. Given the strong SST gradient in the region, it is conceivable that any misrepresentation of the ABFZ can potentially lead to large SST biases. In fact, in a recent study, Xu et al. (2013b) analyzed 38 CMIP5 models and found a statistically significant correlation between the SST biases and ABFZ location errors with a R^2=0.38 among the CMIP5 models. Almost all CMIP5 models simulate a southward-displaced ABFZ with some showing a southward shift as far as 10°.

Another factor that represents a major challenge for ocean models is the sharp contrast in the upper ocean thermal structures north and south of the ABFZ. Figure 9 shows a vertical section of subsurface temperature off the coasts of Angola and Namibia from the equator to 30°S, based on NCEP/CFRS reanalysis data (Saha et al., 2010). The temperature is averaged over a 1° distance from the coast. It is evident that north of the ABFZ the water is considerably warmer and much more stratified with a sharp and shallow thermocline located at 30-40 m below the surface. Conversely, south of the ABFZ, there is no sharp thermocline and the isotherms bulge upward, indicative of strong upwelling that brings cold deep ocean water to the surface. The sharp and shallow thermocline off the Angolan coast shown in the NCEP/CFRS reanalysis is validated by hydrographic measurements (e.g. Lass et al. 2010). Simulating such a steep thermal gradient poses a challenge for global ocean models that typically have rather coarse vertical resolution. Systematic errors in representing the thermocline can result in large subsurface temperature biases that can be advected downstream by the AC to the Benguela coast, affecting the upwelled water and causing a warm bias to form in the Benguela upwelling zone.

Xu et al. (2013a) examined these oceanic mechanisms of generating SST warm biases along the Namibian and Angolan coasts by 1) analyzing ocean data assimilation (ODA) products and 2) conducting eddy-resolving regional ocean model simulations forced by best estimates of observed atmospheric forcing fields. The finding of their study can be summarized as follows: 1) Even with the constraint of existing ocean observations, many ODA products, such as SODA (Carton and Giese 2008) and HYCOM (Chassignet et al., 2007), show warm SST biases that share many common features to those in CGCMs, albeit with a weaker amplitude of ~ 2°C. Many ODA products also exhibit significant subsurface warm biases (~3-4°C) in the sharp and shallow thermocline off the Angolan coast. 2) The warm bias near the ABFZ is related to overshooting of the AC in the ocean models. The overshooting problem could be caused by either underestimation of upwelling in the Benguela region and hence too weak a BC, or by overestimation of the AC. The former may be related to unrealistically weak alongshore winds off the Namibian coast as suggested by Large and Danabasoglu (2006), while the latter may be caused by an unrealistically strong negative wind stress curl north of the ABFZ that has a controlling effect on the strength of the southward AC as shown by Colberg and Reason (2006). 3) The thermocline bias off the Angolan coast makes a significant remote contribution to the warm SST bias south of the ABFZ in the Benguela upwelling zone. The subsurface warm bias makes its way to the Benguela upwelling zone through advection by the AC and subsequently through the Benguela Undercurrent, causing upwelled water to be considerably warmer than observed. Xu et al. (2013a) further shows, using regional model simulations that are confined to the Southeast Atlantic region, that the Angola thermocline bias is linked to the bias in the equatorial thermocline, suggesting that the warm SST bias along the African coast may stem from systematic ocean model

errors in representing the sharp equatorial thermocline, particularly in the eastern Atlantic basin.

3.3 To what extent do model biases affect predictability in the tropical Atlantic?

The tropical Atlantic Ocean hosts several modes of variability that have significant impacts on the climate of the surrounding continents (see Xie and Carton 2004 and Chang et al. 2006 for an overview). The zonal mode of variability (Fig. 10b), also known as Atlantic Niño (Merle et al. 1980; Servain et al. 1982; Hirst and Hastenrath 1983; Philander 1986; Chang et al. 2006) is an equatorial phenomenon with dynamics akin to ENSO in the Pacific (Zebiak 1993) that strongly influences precipitation over the Gulf of Guinea and surrounding coastal areas (Carton and Huang 1994; Giannini et al. 2003) as well as the West African monsoon (Okumura and Xie 2004; Chang et al. 2008). It has an amplitude of about 1 K and typically occurs in JJA at roughly 30 month intervals. (There might be a secondary Atlantic Niño that peaks in November-December, as suggested by Okumura and Xie (2006) though this mode will not be further discussed here).

Another phenomenon called the "meridional mode" (Servain et al. 1999; Fig 10a) relies on a positive feedback involving surface wind, evaporation, and SST (Chang et al. 1997). The meridional mode influences the position of the Atlantic ITCZ and has been associated with droughts and floods on the adjacent continents (Moura and Shukla 1981; Folland et al. 1986; Nobre and Shukla 1996), as well as Atlantic Hurricane variability (Kossin and Vimont 2007). The amplitude is about 1 K and the preferred season is MAM. The frequency spectrum has significant power between 3-10 years but no sharp peak. A third mode, the Benguela Niño (Shannon et al. 1986; Fig 10c), is associated with upwelling and SST anomalies along the southwest African

coast (Florenchie et al. 2003) and can have severe impacts on local fisheries as well as precipitation over southern Africa (Rouault et al. 2007). This mode varies on interannual time scales and can have amplitudes as large as 3-4 K though such strong events only occur about once every 10-15 years. Skillful prediction of these modes of variability could have large benefits to society and it is hoped that prediction systems based on GCMs will be the tools to enable such predictions (Chang et al. 2003). In particular the Atlantic and Benguela Niños are thought to rely on wave dynamics similar to ENSO though there remains some debate on the extent to which these influences are dominant (Richter et al. 2010, Richter et al. 2013). If wave dynamics are indeed dominant this should provide predictability of at least one season in advance.

GCM biases in the tropical Atlantic have been identified as a serious problem well over a decade ago yet progress has been only moderate, and it is likely that it will take many more years to overcome the problem. An important question then is, whether seasonal prediction and global warming projections are significantly affected by such model errors. Previous studies have suggested that the skill of GCM predictions in the tropical Atlantic is usually matched, or even outperformed, by persistence forecasts and statistical models (Repelli and Nobre 2004; Stockdale et al. 2006). A more recent study by Tompkins and Feudale (2010) found a moderate increase in the prediction skill of the West African monsoon in the ECMWF forecasting system. They attributed this increased skill, however, mostly to the improved ocean observation network and noted that the model suffered from a warm SST bias in the Gulf of Guinea. This warm bias, they suggest, contributes to precipitation that is too concentrated along the Guinea coast and thus degrades the prediction of the West African monsoon. The study therefore indicates that equatorial SST biases have to be overcome in order to substantially improve seasonal climate prediction for the region. On

the other hand, the results also illustrate that model-external factors, such as an extensive observational network, are a vital component for skillful prediction systems.

How tropical Atlantic SST biases affect global warming projections has not received much attention so far. One study by Ashfaq et al. (2011) focuses on the projections made with CCSM3. They find that a projection with built-in SST correction scheme produces significantly different precipitation changes in the tropics. The differences are typically larger than the intermodel spread of the CMIP3 ensemble and thus add substantial uncertainty to future projections.

Projected changes in interannual variability and hurricane frequency are even more uncertain. Many models, for example, fail to adequately represent the zonal mode of variability in the tropical Atlantic under present-day conditions (Richter et al. 2012b) and therefore cannot answer the question how that mode will change under global warming. Wan et al. (2011) showed that the simulated tropical Atlantic response to North Atlantic freshwater pulses (thought to have occurred several times in the last 100k years) depends strongly on a GCM's cold tongue bias. Furthermore, the typical cold SST biases in the northern tropical Atlantic, often paired with deficient precipitation, are likely to impair their ability to project changes in hurricane frequency and intensity. Consistent with these biases, studies estimating cyclone activity in GCMs show much lower than observed activity in the North Atlantic (Camargo et al. 2007, Tory et al. 2013), while other basins compare well with observations. We note, however, that other reasons, such as vertical wind-shear, likely contribute to the erroneously low hurricane activity in the North Atlantic.

Downscaling studies using statistical models and high resolution AGCMs have shown that the response of hurricanes to global warming is very sensitive to the details of the projected SST patterns (Chauvin et al. 2006; Emanuel et al. 2008; Zhao et

al. 2009; Bender et al. 2010), which puts even more burden on the accuracy of CGCM projections. More work remains to be done to achieve a qualitative understanding of the impact of tropical Atlantic biases on global warming projections.

4 GCM biases in the tropical Indian Ocean

4.1 Mean state biases

The background state of the Indian Ocean is heavily influenced by the monsoon circulation. In boreal summer, intense precipitation occurs over India and South Asia (Webster et al. 1999), which gives rise to southerlies over the basin and strong upwelling off Sumatra and Somalia with attendant SST cooling. In boreal winter, the center of precipitation migrates to the maritime continent and northern Australia, and northerlies dominate in the tropical Indian Ocean (Webster et al. 1998).

The equatorial Indian Ocean, unlike its Pacific and Atlantic counterparts, is characterized by westerly surface winds in the annual mean (Xie et al. 2002), except for the far western part of the basin. As a consequence equatorial upwelling is largely precluded and SSTs are uniformly warm across the basin (Fig. 2a) except off the African coast. Furthermore, since the surface winds are generally weak, the equatorial thermocline is flat and deep, which reduces its influence on interannual SST variability (Xie et al. 2002).

In most CGCMs the equatorial surface winds are reversed relative to observations, with an easterly bias of about 1-2 m/s (Cai and Cowan 2013, Nagura et al. 2013). As a consequence of the erroneous equatorial easterlies the thermocline is tilted upward toward the east, which gives rise to a Bjerknes feedback (see subsection 2.1) that is more pronounced than in observations (Fig. 11; Cai and Cowan 2013; see subsection 4.2 on variability in the tropical Indian Ocean). The equatorial easterly wind bias also

affects thermocline structure in the off-equatorial region, giving rise to an erroneous eastward displacement of the thermocline dome in the southern tropical Indian Ocean (Fig. 11; Yokoi et al. 2009; Nagura et al. 2013). Nagura et al. report that both the equatorial wind bias and the displaced thermocline dome are insensitive to the choice of model horizontal resolution, atmospheric deep convection scheme, or ocean mixed layer scheme.

As the Indian Ocean mean state is dominated by the monsoon, successful simulation of the monsoon is necessary to adequately represent air-sea interaction in the Indian Ocean. Sperber et al. (2012) performed a comprehensive analysis of the monsoon in CGCMs and found that CMIP3 and CMIP5 models overestimate precipitation in the western Indian Ocean, which is consistent with the easterly wind biases found by Cai and Cowan (2013) and Nagura et al. (2013). Precipitation over the Indian subcontinent is underestimated both in CMIP3 and CMIP5 models, indicating that the Indian monsoon is too weak in current CGCMs (Sperber et al. 2012). The transition from Indian to Australian monsoon is better simulated in CMIP5 models than in CMIP3 models (Li et al. 2012).

4.2 Representation of tropical Indian Ocean variability

A notable climate phenomenon in the tropical Indian Ocean is the Indian Ocean Dipole mode (IOD; Saji et al. 1999; Webster et al. 1999). This interannual mode of variability is akin to ENSO in the tropical Pacific Ocean and thought to involve similar ocean wave dynamics. As in ENSO, equatorial Kelvin and long Rossby waves affect SST variability and determine the time scale of the IOD (Rao et al. 2002; Feng and Meyers 2003; McPhaden and Nagura 2014). The slow ocean dynamics provide the memory of the mode and offer a potential for predictability of Indian Ocean climate.

A positive IOD event is defined by warm SST anomalies in the tropical western Indian Ocean and cool SST anomalies in the equatorial eastern Indian Ocean (Fig. 12); the negative phase is defined by anomalies of the opposite sign. An essential component of the IOD mechanism is the upwelling off Sumatra (the eastern pole of the IOD), which brings wave-induced temperature anomalies to the surface and thus affects SST variability in this region (Murtugudde et al. 2000; Iizuka et al. 2000; Li et al. 2002). SST anomalies in the tropical western Indian Ocean (the western pole of the IOD) are excited by a combination of surface heat flux, and horizontal and vertical oceanic heat advection (Murtugudde et al. 2000; Iizuka et al. 2002; Li et al. 2002). The region northeast of Madagascar is subject to particularly strong SST variability due to strong upwelling (Xie et al. 2002; Foltz et al. 2010; Yokoi et al. 2012). The resulting SST anomalies along the equator are further amplified by the Bjerknes feedback (Saji et al. 1999; Webster et al. 1999; Murtugudde et al. 2000).

The IOD displays a clear seasonality, with the initial phase in boreal summer, mature phase in boreal fall, and termination phase in boreal winter (Fig. 12). This is due to the upwelling off Sumatra being most vigorous in boreal summer, which is forced by southeasterly winds during the Indian monsoon. These conditions allow for rapid growth of SST anomalies in this season (Li et al. 2003). Due to high correlation between indices of ENSO and IOD, it has been suspected that ENSO is a major initiator of the IOD (Hendon 2003; Lau and Nath 2004; Shinoda et al. 2004). In addition, the initiation of the IOD has been ascribed variously to oceanic waves (Rao et al. 2002; Feng and Meyers 2003; Behera et al. 2006) or the Antarctic Oscillation (Lau and Nath 2004). Termination, on the other hand, has been associated with the transition from Indian monsoon to Australian monsoon (Tokinaga and Tanimoto 2004), reflection of oceanic waves at the eastern coast of the African continent (Rao et al.

2002; Feng and Meyers 2003), or atmospheric intraseasonal variability (Rao and Yamagata 2004; Rao et al. 2007).

CGCMs are generally able to reproduce the zonal dipole pattern of SST anomalies and its seasonality (Cai et al. 2005; Spencer et al. 2005; Zhong et al. 2005; Saji et al. 2006; Song et al. 2007; Liu et al. 2011). This success is partly due to the ability of the CGCMs to capture the Indian monsoon and Sumatra upwelling maximum in boreal summer. The simulated wind and SST anomalies along the equator are significantly correlated, indicative of the Bjerknes feedback (Cai et al. 2005; Saji et al. 2006). The models also capture the western deepening and eastern shoaling of the thermocline during positive IOD events, which indicates successful reproduction of upwelling Kelvin and downwelling Rossby waves (Cai et al. 2005; Spencer et al. 2005; Zhong et al. 2005; Saji et al. 2006).

Less successfully simulated are the triggering and terminating mechanisms of the IOD. Cai et al. (2005) found in their CSIRO Mark 3 model that the simulated dipole often develops in the year following El Niño, while in observations the two phenomena typically evolve simultaneously. Their analysis revealed that simulated thermocline depth anomalies erroneously propagate from the tropical western Pacific through the Indonesian passages into the equatorial Indian Ocean, while in observations they propagate poleward along the western coast of Australia (Wijffels and Meyers 2004). This unrealistic propagation of model thermocline depth anomalies initiates model IOD events one year after model El Niño events. Cai et al. attribute this error to the coarse horizontal resolution in the model and the resulting poor representation of the Indonesian passages.

Spencer et al. (2005) found erroneous behavior regarding the IOD termination in the Hadley Centre HadCM3 model. They conducted experiments with two different

vertical resolutions in the oceanic component of the model (20 levels and 40 levels) and found that IOD events in the lower resolution version did not terminate completely in boreal winter but persisted until the following year, which is rare in observations. This error is eliminated in the higher resolution version of the model, leading Spencer et al. to suggest that better representation of thermocline structure and coastal upwelling is necessary to correctly reproduce IOD termination.

Another issue regards the magnitude of simulated IOD variability. Several groups have carried out systematic intermodel comparisons for this climate mode using CGCM output from CMIP3 and CMIP5 models. Liu et al. (2011) and Cai and Cowan (2013) find that models with larger IOD magnitude feature higher sensitivity regarding the response of 1) equatorial winds to eastern pole SST anomalies; 2) eastern pole thermocline depth to equatorial wind anomalies; and 3) eastern pole SST to local thermocline anomalies (Fig. 13). As a result the Bjerknes feedback, which is composed of these three elements (e.g. Keenlyside and Latif 2007), is unrealistically strong. The oversensitivity of the three elements is related to mean state errors, such as too shallow a thermocline in the equatorial eastern Indian Ocean, too strong upwelling, and an excessive vertical temperature gradient off Sumatra (Saji et al. 2006; Liu et al. 2011; Cai and Cowan 2013).

As discussed in subsection 4.1, the overactive Bjerknes feedback is associated with stronger than observed easterlies on the equator. The easterly bias also gives rise to an erroneous eastward displacement of the thermocline dome in the southern tropical Indian Ocean (Fig. 11; Yokoi et al. 2009; Nagura et al. 2013), which, in turn, causes unrealistic patterns of SST anomalies off the equator (Cai et al. 2005; Spencer et al. 2005; Saji et al. 2006). This indicates that equatorial wind biases play an important role in tropical Indian biases, similarly to the Atlantic basin (section 3).

Currently CGCMs are able to predict IOD events at lead times of one to two seasons (e.g., Wajsowicz 2005; Luo et al. 2007; Zhao and Hendon 2009). Longer lead times may be achievable, because thermocline depth anomalies in the southern Indian Ocean, a precursor for IOD events, can be observed a year ahead (McPhaden and Nagura 2014). These thermocline depth anomalies propagate as off-equatorial Rossby waves from the central basin to the western boundary, where they are reflected into equatorial Kelvin waves and eventually trigger IOD events. While previous studies have pointed to a link between mean state biases and IOD variability (Cai and Cowan 2013), more work needs to be done to understand the underlying mechanisms and their relation to GCM parameterizations in order to accomplish more skillful predictions.

4.3 Representation of the southern Indian Ocean

The southern Indian Ocean hosts a coupled ocean-atmosphere mode that is characterized by a dipole structure in SST anomalies and is commonly referred to as the Indian Ocean subtropical dipole (IOSD; Behera et al. 2000; Behera and Yamagata 2001). Studies have found that this subtropical mode has a significant impact on the climate of southern Africa (Reason 2001; Suzuki et al. 2004; Morioka et al. 2012) and Australia (England et al. 2006). During a positive IOSD event warm SST anomalies appear in the southwestern South Indian Ocean, whereas cold SST anomalies appear in the northeastern part. This pattern attains maximum strength in austral summer and is associated with an intensification and southward shift of the South Indian Ocean subtropical high (also known as Mascarene High). The first study of the IOSD using a CGCM was conducted by Suzuki et al. (2004). They found that the simulated magnitude of both positive and negative IOSD events was similar to observations. The duration of IOSD events in their CGCM is also realistic, except that negative events tend

to last a few months longer than observed. More recently, Morioka et al. (2012) used a CGCM to show that SST anomalies can be generated by LHF anomalies through their influence on mixed-layer depth (MLD). Decreased latent heat loss shoals the mixed layer and thus raises its sensitivity to shortwave radiation. On the other hand, increased latent heat loss deepens the mixed layer and thus lowers its sensitivity to shortwave radiation. The mixed-layer temperature tendency is expressed as the sum of the net surface heat flux term and oceanic terms, which comprise horizontal advection, entrainment, and horizontal and vertical diffusion:

$$\frac{\partial T_{\mathrm{mix}}}{\partial t} = \frac{Q}{\rho c_p H} + (oceanic\ terms),$$

where T_{mix} represents mixed-layer temperature, Q denotes surface heat flux, ρ is density, c_p is specific heat, and H is mixed-layer thickness. The CMIP3 ensemble mean composite of each term, averaged from October through December, is shown in Figure 14. The contribution from the surface heat flux term shows a dipole pattern similar to the tendency term. In contrast, the amplitude of the contribution from the oceanic effects is smaller and damps the IOSD. In the CGCM used by Morioka et al. (2012), the IOSD emerges as the first EOF of SST in the area 45-10°S, 40-110°E, whereas in the HadISST (Rayner et al. 2003) it emerges as the second EOF. Nevertheless, spatial pattern and explained variance agree well with observations.

Kataoka et al. (2012) examined how CMIP3 models simulate the IOSD and find that most models simulate some form of dipole pattern and also reproduce the seasonal phase-locking of the IOSD. The latter is expected because almost all CMIP3 models capture the observed MLD minimum in austral summer, which is key to IOSD phase locking (Suzuki et al. 2004). The location and orientation of the SST anomaly poles, however, varies considerably across models. These variations are closely linked to the simulated anomalies of the Mascarene High. Thus errors in the pattern and po-

sition of the IOSD are closely mirrored by SLP errors across models. The results of Morioka et al. (2012) indicate that the Mascarene High is the driving force behind the IOSD. Therefore, it seems that improving the representation of the Mascarene High should also lead to a better representation of the IOSD. Errors in the strength and position of the Mascarene High might be due to several factors. Kataoka et al. (2012) suggested that SLP biases in the region are related to the misrepresentation of a wavenumber 3 or 4 pattern of the atmospheric circulation in the Southern Hemisphere (Fauchereau et al. 2003) and ENSO teleconnections. Huang and Shukla (2006), on the other hand, suggested that the zonally elongated SST poles (which strongly influence SLP) in their CGCM are associated with an excessively strong Southern Annular Mode (Walker 1928; Thompson and Wallace 2000). Such an influence, however, was not evident in the CMIP3 models examined by Kataoka et al. (2012). If the annular mode does play a role in the SLP biases improved sea-ice physics might help remedy the problem. A further error source could be the strength and position of the simulated ITCZ, which is linked to the subtropics through the Hadley circulation.

The IOSD is associated with rainfall anomalies over Southern Africa, which is a region whose population is particularly vulnerable to droughts and floods. Successful prediction of this climate mode is therefore of great importance. Recently, Yuan et al. (2014) assessed predictability of the IOSD and a similar climate mode in the South Atlantic, called the South Atlantic subtropical dipole (SASD; Venegas et al. 1997). Although their coupled model captured the IOSD reasonably well, the prediction skills were relatively low. This was mostly due to problems in simulating the southwestern pole of the IOSD, which is strongly influenced by meridional surface wind anomalies. Yuan et al. (2014) suggest that the failure to capture these meridional wind anomalies is one of the reasons for the relatively low skill in their model. Another rea-

son for the low prediction skill in the southwestern pole might be its relatively high latitude, which renders it subject to inherently unpredictable forcing from the midlatitudes.

5 Challenges in land surface modeling

5.1 Land surface models

Coupled ocean-atmosphere modes of variability in the three major ocean basins affect the climate of the surrounding continents (sections 2-4). ENSO (Pacific Ocean), Atlantic Niño (Atlantic Ocean) and IOD (Indian Ocean) are "hot-spots" of strong ocean-atmosphere coupling. Similarly, "hot-spots" of strong land surface-atmosphere coupling have been identified in North America, the Sahel, equatorial Africa, tropical India, South America, and Central Asia (Koster et al. 2000, 2004; Xue et al. 2010). By modifying the exchanges of momentum, radiation, sensible and latent heat fluxes (Seneviratne et al. 2010, Ma et al. 2013), land processes (water cycle, vegetation), influence the climate over the continents (e.g. Koster et al. 2003, 2004; Taylor et al. 2011, 2012), as well as over the oceans (e.g. Zeng et al. 1996; Richter et al. 2012a; Ma et al. 2013).

The water stored on land is a key variable controlling numerous processes and feedback loops within the climate system (Seneviratne et al. 2010). The interaction between soil moisture and the atmosphere is expressed through the coupling of the former with evapotranspiration, temperature, and precipitation. To represent the land surface-atmosphere coupling in a climate model, a land surface model (LSM) is used. Current LSMs simulate the surface energy fluxes (latent and sensible heat flux, short- and longwave radiation, momentum), the hydrology (evapotranspiration, runoff, infiltration), and the carbon cycle (photosynthesis, nutrient uptake, gas emission) to repro-

duce the exchanges between land surface and atmosphere (Pitman 2003; IPCC 2007; Seneviratne et al. 2010). Thus an accurate simulation of soil moisture-climate interactions and feedbacks is needed in order to correctly simulate the climate system. For example, Richter et al. (2012a) pointed out that the influence of land surface conditions in tropical South America and Africa exert a strong influence on local precipitation, as well as on tropical Atlantic climate. In one of their experiments, the increase of soil moisture leads to less convective activity over the Congo basin. This is consistent with the temperature feedback, in which higher soil moisture induces higher evaporation, which in turn initiates cooling of the surface and overlying air (cf. Seneviratne et al. 2010).

Problems with the representation of rainfall are present in both GCMs (Ines and Hansen 2006) and regional climate models (RCMs; Ceglar and Kajfež-Bogataj 2012). There is a tendency to generate too many rainfall events of too low intensity (Carter et al. 1994; Mearns et al. 1995; Goddard et al. 2001). For observed precipitation on local and regional scales there is a positive feedback, in which wetting of the soil by precipitation enhances the subsequent evaporation by the wetted soil. This increases precipitation, closing the feedback loop (Koster 2011; Koster et al. 2003; Seneviratne at al. 2010). Taylor et al. (2011), e.g., showed that in the Sahelian region, the probability of convective initiation is doubled over strong soil moisture gradients. The variation in soil moisture of length scales ~10-40 km exert a strong control on storm initiation. On the other hand, Taylor et al. (2012) have shown that there is a preference for afternoon rain over locally drier soil on scales of 50-100 km.

Observed soil moisture and precipitation anomalies are also strongly coupled in the midlatitudes (Koster et al. 2003). Using the first phase of the Global Land-Atmosphere Coupling Experiment (GLACE, Koster et al. 2004, 2006; Guo et al.

2006), Dirmeyer et al. (2006) explored the ability of twelve GCMs to represent the observed relationships between surface and atmospheric state variable and fluxes in midlatitude summer. They showed that most of the GCMs appear not to simulate correctly the land surface-atmosphere coupling. Systematic deficiencies in three LSMs have also been shown by Abramowitz et al. (2007).

Land-surface processes form a major component of the West African Monsoon system (Redelsperger et al. 2006; Koster et al. 2004; Boone et al. 2009; Xue et al. 2012). Domínguez et al. (2010) show that introducing fractional cloud cover and new radiation parameterizations in the PROMES RCM improves the latitudinal migration of the precipitation band. This is closely linked to more realistic downward solar radiation at the surface, which reduce biases in surface heat fluxes. However, the timing of the main active and break monsoon periods are not improved, as they are more related to larger scale features such as the African Easterly Jet and Tropical Easterly Jet. The lateral boundary conditions in RCMs likely contribute to the misrepresentation of these large-scale features. More generally, Stevens and Bony (2013) suggest that a deeper understanding of the coupling between water and circulation is needed to improve models. They recommend focusing on how clouds, moist convection and heating couple to the general circulation, in order to enhance the representation of the land-ocean-atmosphere coupling in simulations. This agrees with studies arguing that accurate measurements of observed land surface-atmosphere coupling (latent and sensible heat, carbon exchange) will lead to a better understanding of the mechanisms (Dirmeyer et al. 2006; Koster 2011).

5.2 Agro-hydrological modeling as a specific example

Agro-hydrologic impact studies typically use input provided by GCMs, and therefore their predictive skill is highly dependent on that of the underlying large-

scale model. In the particular case of agriculture, numerous studies have tried to translate climate forecasts from GCMs into seasonal crop predictions (e.g. Hansen et al. 2006). Climate impacts are a particularly sensitive issue in semi-arid regions, where the climate variability may have serious consequences for food security. In the following we describe a few of the challenges facing agro-hydrologic modeling, with an emphasis on the West African monsoon region.

It is difficult to translate GCM output into crop yield predictions, mainly because of scale issues in both time and space (Blöschl and Sivapalan 1995; Schulze 2000). These include (1) the coarse horizontal resolution of GCMs relative to the processes governing yields (Baron et al. 2005), (2) the low variability of simulated GCM variables at the crop model scale, (3) the strong dependence of impact studies on the accuracy of climate input data (Berg et al. 2010) and the propagation of errors, and (4) the GCMs' underrepresentation of local forcing, such as topography or water bodies.

For impact studies, there is a need to handle appropriately the reduced variability of climatological variables through the application of downscaling techniques. This can potentially be achieved using various dynamic, empirical, or statistical-dynamic methods (von Storch 1995). Dynamic downscaling is performed by running an RCM over a limited area, in order to increase the resolution in space and the variability in time. An RCM is typically forced at the boundary by reanalysis or GCM data (Giorgi and Mearns 1999). However, similar problems as in GCMs still exist in RCM simulations (see subsection 5.1).

For crop production, the crucial climate variables are solar radiation (influences biomass and grains), rainfall (modulates the effect of solar radiation), temperature (determines length of vegetative cycle) and potential crop evapotranspiration (ET0 hereafter). ET0 is a climate dependent parameter that estimates the potential loss of

water from both soil and vegetation. The reference value for ET0 (Allen et al. 1998) is calculated using relative humidity, air temperature, wind speed and insolation (or solar radiation) at the surface. It can be considered as an integrative metric of the relevant climate parameters (and their biases).

We illustrate the role of the relevant climate parameters for the case of Senegal (Northwest Africa), which is characterized by a north-to-south gradient in rainfall (Fig. 15a) with high the highest values in the southern part of the country. RCMs tend to underestimate precipitation in the south and thus have a weaker than observed rainfall gradient (Oettli et al. 2011). Another conspicuous feature is the large spread of surface solar radiation and mean temperature estimated by RCMs in the region (Oettli et al. 2011). Many RCMs overestimate the solar radiation (Fig. 15b), particularly in the wet south of Senegal. Half of the RCMs overestimate mean temperatures (Fig. 15c), while the other half underestimates them, with uniform biases throughout the country. The biases in rainfall, shortwave radiation and temperature lead to an overestimation of ET0, particularly in the northern part of the country (Fig. 15d). As a consequence of the RCM biases, particularly those in rainfall, the crop yield is severely underestimated in most case. The intermodel spread of precipitation, temperature, and shortwave radiation is mainly due to different physics and parameterizations in the RCMs, which lead to different simulation of the West African monsoon system, the main driver of climate variability in West Africa.

As another illustration of the impact of climate model biases on yield predictions consider the study of Iizumi et al. (2010). Focusing on Japan, they show that CMIP3 models underestimate summer temperatures (July-August) while overestimating warm-season insolation (May-October), which leads to unrealistic rice yields.

5.3 Ways toward land surface model improvement

Impact studies consistently show that biases in land surface components of GCMs are amplified by RCMs and often lead to unrealistic crop (or hydrologic) simulations. They also point out the need to correct GCM or RCM output before using them to drive any impact model. This can be done using different statistical transformations (Déqué 2007; Gudmundsson 2012). Statistical bias correction shows promising results in reducing biases in the mean.

Abramowitz et al. (2007) showed that most of the biases in the LSM component are drastically reduced after the application of an *a-posteriori* correction. According to the authors, the use of a benchmarking technique at a variety of sites might aid the process of LSM refinement. Some other studies (Dirmeyer et al. 2006; Koster 2011) also argued for the need of a comprehensive observation network, documenting various types of soil and vegetation. This might be achieved by current and upcoming satellite missions, providing an unprecedented quantification of soil-moisture patterns on the global scale (Koster 2011). It should be noted, however, that correction schemes generally do not improve the prediction of interannual variability. Results also point out the uncertainties remaining in our knowledge of atmospheric processes, and the complexity of representing these processes in GCMs or RCMs. Further improvement of climate and weather forecast models will be a vital step for advancing agro-hydrological models.

6 Can increased model resolution overcome biases?

Any kind of numerical model of the atmosphere or ocean requires discretization of some sort, be it in physical space (e.g., finite difference or finite volume methods) or wavenumber space (spectral methods). Both atmosphere and ocean are character-

ized by motions that involve scales ranging from thousands of kilometers (e.g. midlatitude jet streams), to tens of meters (e.g. eddies in the planetary boundary layer), to millimeters (e.g. viscous dissipation). The question then arises what resolution is needed in GCMs to adequately represent the large-scale circulation and to what extent unresolved processes contribute to the GCM biases. We examine this in the following, focusing on AGCMs in subsection 6.1 and OGCMs in subsection 6.2. In the last subsection (6.3) we discuss two particular studies that illustrate resolution issues in the tropical Pacific and Atlantic. We note that there is a rich literature on GCM resolution and that in this section we can merely sketch a few of the important issues. We refer the reader to Hamilton and Ohfuchi (2007) and Hecht and Hasumi (2008) for detailed reviews.

6.1 Atmospheric model resolution

Manabe et al. (1970) were perhaps the first to systematically investigate the impact of model resolution on atmospheric model performance, though their study focused on the midlatitudes. There they showed that reducing grid size from 500 km to 250 km led to much more realistic representation of frontal systems. Williamson et al. (1995) examined the performance of an AGCM at various horizontal resolutions ranging from spectral truncation number T21 (equivalent to about 5.6º grid size) to T106 (about 1.1º). Similarly to Manabe et al. (1970) they found significant midlatitude improvements going from low to medium resolution (~ 1.9º), but no significant changes at higher resolution. In terms of tropical climate they found some improvement in the Hadley Circulation, but other problems such as the double ITCZ bias were rather insensitive to resolution. This was also the conclusion of Deser et al. (2006) and Hack et al. (2006). The latter reported that the improved surface winds and shortwave radiation in the high-resolution atmospheric component had little impact on the coupled

simulation. Furthermore, interannual variability in the tropical Pacific did not improve with resolution, which agrees with the findings of Deser et al. (2006).

Many studies point out the need for retuning model parameterizations when resolution is increased (Boer and Lazare 1988; Williamson et al. 1995; Duffy et al. 2003). Nevertheless, even with careful tuning Duffy et al. (2003) could not achieve general improvements in tropical precipitation and surface winds when increasing resolution from T42 (~ 2.9º) to T239 (~ 0.5º). Pope and Stratton (2002) even report a degradation of the simulated precipitation when they increased resolution. They suggest that convective parameterizations need not only retuning but also modification as resolution increases. Furthermore, as resolution approaches the scales of the parameterized cloud systems (which starts at around 20 km), it is obvious that conventional convective parameterization schemes will have to be modified. This highlights the need for scale aware parameterizations that can adapt to a given model resolution.

In the late 1990s a new type of cumulus parameterization, the so-called super parameterization, started being developed (Khairoutdinov and Randall 2001). The approach is to embed a cloud resolving model (CRM) into each GCM grid cell, using the GCM fields (temperature, humidity, etc.) as boundary condition. The advantage is that only microphysical processes have to be parameterized and that the system seamlessly converges into a global CRM (GCRM) as the embedded model is refined. Super-parameterized GCMs have shown promising results in the tropics, where they reduce the wet precipitation bias over the oceans, alleviate the double ITCZ bias, and are also quite successful at simulating the Asian monsoon and intraseasonal phenomena that remain elusive to most GCMs (Khairoutdinov et al. 2005; Stan et al. 2010; DeMott et al. 2011). On the other hand, not all aspects of the tropical circulation im-

prove and the computational burden is substantial (though much lower than that of a GCRM).

As computing power continues to increase there are many efforts at further refining model resolution. A relatively recent simulation using horizontal resolution of 0.25º in the atmosphere and 0.1º in the ocean (McClean et al. 2011) showed some promising results in simulating tropical cyclones but shared many SST and precipitation biases with CMIP5 era GCMs. Experiments with a GCRM (Tomita et al. 2005, Satoh et al. 2008) have also shown promising results but current computing resources do not permit simulation beyond a few months so that is not yet possible to establish a model climatology for comparison with observations. While long-term GCRM simulations are not feasible yet, regional numerical weather prediction (NWP) models are already routinely run at cloud-resolving scales of up to 1 km (Hong and Dudhia 2011). The experience of these modeling centers will provide valuable guidance for GCRM development.

6.2 Oceanic model resolution

Mesoscale eddies contain most of the ocean's kinetic energy (Scharffenberg and Stammer 2010) and are an important feature of the oceanic circulation due to their horizontal and vertical transport of heat, momentum, salinity and other tracers. They are particularly prevalent in regions of strong mean currents such as the Antarctic Circumpolar Current (Hallberg et al. 2006), the Agulhas Current (Biastoch and Krauss 1999), or the Kuroshio Current (Miyazawa et al. 2004). Moreover, they might play a role in setting the vertical temperature structure of the ocean (Marshall et al. 2002). Since these eddies occur at scales of 100 km or less, an OGCM resolution of 10 km or higher is required for their adequate simulation. Models that could marginally resolve mesoscale eddies were developed in the 1990s (Semtner and Chervin 1992, e.g., used

a global OGCM with 0.25° horizontal resolution), with eddy resolving models starting to appear in the 2000s (e.g. Smith et al. 2000; Masumoto et al. 2004; Maltrud and McClean 2005).

Several studies have investigated to what extent the effect of mesoscale eddies can be parameterized in OGCMs (Danabasoglu et al. 2008; Farneti et al. 2011; Bryan et al. 2014). The studies found that current parameterization schemes, such as the one developed by Gent and McWilliams (1990), can present eddy effects to some extent but that further refinements should be implemented. These analyses, however, focused on the mid and high latitudes. The impact of unresolved mesoscale eddies on the tropics has received less attention. Kirtman et al. (2012) compared two experiments with the NCAR CCSM 3.5. The control experiment uses a 0.5º atmospheric component coupled to an oceanic component with zonal resolution of 1.2º and meridional resolution varying from 0.27º at the equator to 0.54º in the mid-latitudes. The second simulation uses the same atmospheric and land-surface models but is coupled to an eddy-resolving 0.1º oceanic component. Their results suggest that increasing the horizontal resolution of the ocean model does not improve significantly the warm SST biases over the eastern tropical Pacific and Atlantic.

6.3 Illustrative example: coupled high-resolution simulations with the GFDL model

Delworth et al. (2012) present results from the high-resolution GFDL CM2.5. The model has an atmospheric resolution of approximately 50 km in the horizontal, with 32 vertical levels. The horizontal resolution in the ocean ranges from 28 km in the tropics to 8 km at high latitudes, with 50 vertical levels. Results are compared to the GFDL CM2.1 climate model, which has somewhat similar physics but coarser

resolution, with 2.5° longitude by 2° latitude and 24 vertical levels in the atmosphere, and 1° (decreasing to 1/3° toward the equator) and 40 vertical levels in the ocean. Figure 16 shows the annual mean SST biases, relative to Reynolds SST (Smith et al. 2008), of the GFDL CM2.1 control run and high-resolution GFDL CM2.5. The eastern Pacific warm SST bias is significantly reduced in CM2.5 relative to CM2.1. This appears to be at least partly due to the steep topography of the Andes, which is much better resolved by the high resolution in CM2.5. The topography plays an important role in simulating southerly winds and coastal upwelling over the eastern Pacific and thus reduces the warm SST bias there. The bias in the eastern Atlantic, however, shows little improvement. This suggests that the mechanism for the eastern Pacific SST bias is different from that of the eastern Atlantic.

Doi et al. (2012) used the CM 2.1 and CM 2.5 models described above to investigate the characteristics and sources of SST and precipitation biases associated with the Atlantic ITCZ. CM 2.5 has an improved simulation of the annual mean and the annual cycle of the rainfall over the Sahel and northern South America, while CM2.1 shows excessive Sahel rainfall and lack of northern South America rainfall in boreal summer (Fig. 17). The marked improvement in CM2.5 is due not only to the high-resolved orography but also a significant reduction of biases in the seasonal meridional migration of the ITCZ. In particular, the seasonal northward migration of the ITCZ in boreal summer is coupled to the seasonal variation of SST and the subsurface doming of the thermocline in the northeastern tropical Atlantic, known as the Guinea Dome. Improved simulation of the ITCZ allows for better representation of the coupled processes that are important for an abrupt seasonally phase-locked decay of interannual SST anomalies in the northern tropical Atlantic related to the meridional mode of variability. Nevertheless, the differences between CM2.5 and CM2.1 are not

sufficient to reduce the warm SST biases in the eastern equatorial region and Angola–Benguela area. The weaker than observed southerly winds along the southwestern African coast associated with the excessive southward migration bias of the ITCZ may be a key to improve the warm SST biases there (see also Richter et al. 2012b).

7 Summary and discussion

7.1 Summary

We first summarize the challenges highlighted in sections 2 through 6. Figure 18 provides a visual summary of some of the features discussed here.

In the tropical Pacific GCMs tend to simulate too vigorous a Walker circulation with excessive convection over the western warm pool and stronger than observed easterly wind stress on the equator. In boreal spring, the simulated ITCZ is often located well south of the equator whereas in observations it tends to be close to the equator. The south-equatorial ITCZ is associated with pronounced cross-equatorial surface winds, which, in combination with the stronger than observed equatorial easterlies, cause excessive upwelling and cooling in the equatorial ocean. The resulting cool bias on the equator further discourages deep convection there and thus reinforces the precipitation and wind biases.

The simulated southeastern Pacific SST tends to be 3-4K warmer than observed. This is at least partly related to the models' failure to simulate sufficient low-level cloud cover over the region. Deficiencies in the representation of low-level cloud, however, are not enough to account for the lack of eastern Pacific meridional asymmetry that plagues most coupled simulations.

Many models simulate a realistic amplitude of the interannual variability associated with ENSO, though this may partly be due to cancellation of errors. Common

shortcomings regarding the simulation of ENSO are insufficient seasonal phase locking and failure to reproduce the observed asymmetry between warm and cold events. Despite these GCM biases, some current prediction systems are able to provide skillful forecasts at lead times of one year and beyond. To what extent further model improvement can push the envelope remains to be seen.

Mean state biases in the equatorial Atlantic are, to some extent, of opposite sign to those in the Pacific. The equatorial surface easterlies are too weak and eastern SSTs too warm. There is a pronounced seasonality in the biases, with wind and SST biases dominant in boreal spring and summer, respectively. The weaker than observed easterlies in MAM are associated with deficient precipitation over tropical South America, and excessive precipitation over tropical Africa and south of the equator over the ocean. These errors are also present, albeit weaker, in standalone AGCM experiments with SST prescribed from observations, which points to an atmospheric error source. Sensitivity tests with various convection schemes support the notion that the partitioning between oceanic and terrestrial convection plays a vital role in setting up equatorial surface winds.

There are also oceanic sources of tropical Atlantic biases. One of them lies in the OGCMs' inability to adequately resolve the sharp temperature gradients in the equatorial thermocline, which leads to the under-representation of upwelling-related cooling. This OGCM deficiency also plays a major role in the severe warm SST biases along the southwest African coast. Moreover, the poleward Angola current further exacerbates these biases by advecting warmer than observed waters from the equator toward the coastal upwelling regions in the South Atlantic.

Due to the severe Atlantic cold tongue biases many models cannot adequately represent the zonal mode that dominates equatorial Atlantic variability. The warm bi-

as in the cold tongue region leads to too much precipitation over the ocean, which hampers skillful prediction of the West African monsoon. As a consequence most seasonal prediction systems still show little skill in the region, though lack of observational data for model initialization may also play a role in this. Climate change projections may also be affected by the cold SST bias in the tropical North Atlantic, where most GCMs underpredict present day cyclone activity.

Over the equatorial Indian Ocean, GCMs typically simulate easterly surface winds, in contrast to the observations where surface winds are westerly. Thus models suffer from an easterly surface wind bias, an error that is also prevalent in the equatorial Pacific. Consistent with the easterly bias, equatorial SSTs in the equatorial Indian Ocean tend to have a cold bias and the thermocline is too shallow in the eastern part of the basin. Precipitation biases also resemble those in the Pacific, with excessive precipitation south of the equator. A feature that is unique to Indian Ocean simulations is the insufficient meridional shear of zonal wind stress in many GCMs. This weakens wind stress-curl-related upwelling south of the equator and leads to a warm bias in the southwestern Indian Ocean. In the absence of southwest Indian Ocean Ekman upwelling, the excessive equatorial easterlies and associated Kelvin and Rossby waves produce a "false" thermocline dome in the southeastern Indian Ocean.

Despite significant biases in the tropical Indian Ocean, many GCMs are able to reproduce some aspects of the dominant interannual mode of variability in the region, the Indian Ocean dipole. Common GCM shortcomings regarding the dipole mode are spurious transmission of Rossby waves through the poorly resolved Indonesian passages and insufficient vertical temperature stratification, which affect event onset and termination, respectively. Another important mode of interannual variability, the subtropical Indian Ocean dipole mode, is captured by many GCMs but often shifted rela-

tive to its observed position. This appears to be a consequence, rather than the cause, of a similarly shift in the South Indian Ocean subtropical high.

Many studies ask the question how slowly evolving ocean anomalies influence conditions over land. However, convection over land surfaces also has an important influence on the tropical oceans, particularly for the comparatively small Indian and Atlantic Ocean basins. Thus biases in the land surface components of GCMs have the potential to induce biases over the oceans as well, and this is apparent for the case of the tropical Atlantic Ocean and, to some extent, that of the Indian Ocean. To what extent terrestrial precipitation biases are due to deficiencies in land surface models needs further analysis. While for the midlatitudes there is a clear indication that models misrepresent the coupling between soil moisture and precipitation, the tropical land surfaces are typically covered by rain forests, which are difficult to observe from satellite. Since ground-based observations for these regions are also sparse, there is little data to compare models against.

An important application for GCM simulations is to provide input for agro-hydrological models, such as crop models. As the example of the West African monsoon region shows, both GCM rainfall and insolation biases associated with sub-grid scale parameterizations as well as shortcomings in large-scale circulation features conspire to create unrealistic input values for crop models. The scale difference between GCMs and crop models necessitates the use of downscaling techniques, which further amplifies initial errors. These factors partly explain why reliable crop yield predictions remain a challenge.

Increasing model resolution improves many aspects of the simulated climate in both the atmosphere and ocean, though these improvements mainly concern the mid and high latitudes. Increased resolution also has the potential to alleviate some of the

tropical issues, such as resolving steep orography, the sharp oceanic thermocline, and the Indonesian passages. This can also contribute to reducing the scale difference between GCM and agro-hydrological models. On the other hand, several examples in this chapter illustrate that increasing model resolution is not a panacea. Furthermore, the central issue of (at least partially) resolving cumulus convection remains out of reach for current climate simulations and may continue to be so for years to come. Thus improving subgrid-scale parameterizations must remain a focus of GCM development.

7.2 Discussion

A problem common to most GCMs is the cold SST bias that prevails over the tropical oceans. Only the eastern subtropical Pacific and Atlantic Oceans are marked by warm biases in all GCMs. These biases are particularly pronounced in the Southern Hemisphere.

Despite the dominance of cold SST biases over the tropical oceans, GCMs tend to overpredict precipitation there. The only notable exception is the equatorial Pacific, where models underpredict precipitation over colder than observed SST. It is therefore also the only region where there is a good match between the patterns of SST and precipitation errors. Thus it seems that, generally speaking, SST errors cannot explain the wet precipitation biases over large portions of the tropical oceans. This view is also supported by AGCM experiments forced with observed SST, which typically suffer from much the same precipitation biases as their coupled counterparts, albeit in weaker form. Thus factors other than the underlying SST must contribute to localizing deep convection in GCMs. Such factors might be convection over the adjacent continents, remote forcing from the Pacific warm pool, and lower tropospheric moisture

convergence, which does not necessarily occur over SST maxima (see e.g. Biasutti et al. 2006).

A possible explanation for the pervasive cold SST biases in GCMs might be the excessive precipitation and associated cloud cover. Results by Lin (2007), however, seem to contradict this notion. Another explanation might be the models' tendency to produce too much mixing in the upper ocean, which brings too much cold water to the ocean surface while eroding the sharp temperature gradient of the thermocline.

The simulated equatorial trades are stronger than observed in the Pacific and Indian Oceans but weaker than observed in the Atlantic. The easterly bias is consistent with an ITCZ and associated equatorial doldrums that, in the annual average, are farther from the equator than observed. This explanation works for the equatorial Pacific and Indian Oceans, but not for the equatorial Atlantic where westerly biases prevail despite an ITCZ that is south of the equator in boreal winter and spring. Possibly this is related to the continental influences on the equatorial trades in the relatively small Atlantic basin (Richter and Xie 2008; Richter et al. 2012a).

Two issues appear to be central to GCM biases in the tropics. The first is the realistic representation of deep convection and its relation to surface winds. The second concerns the oceanic equatorial thermocline, which is closely related to the parameterization of oceanic vertical mixing. Certainly, the importance of both these issues has been recognized by the community since the early days of general circulation modeling. Accordingly many scientists have worked hard to improve parameterizations and, as a result, models have improved substantially over the last few decades. Notwithstanding this progress, many problems persist in state-of-the-art GCMs, such as the Pacific double ITCZ and the Atlantic warm SST bias. How should the community address these issues? Recent diagnostic studies have narrowed down on the error

sources but this is not sufficient to improve models. More effort needs to be spent on bridging the gap between diagnostic studies and model development. Many of the deficiencies we identify in model output, such as the double ITCZ, are emergent properties of numerical model simulations. That is to say, they are not related in any simply way, to a GCM's parameterizations but rather arise out of the complex interactions between individual model components. In order to provide actionable advice to model developers we need to have a better understanding of how these interactions combine to produce certain model features. Such efforts should benefit from the increasing body of ground and satellite based observations.

While there is reason to be optimistic about overcoming some of the problems in current GCMs, it is likely that many issues will remain unsolved for a long time. Since seasonal predictions and climate projections are central applications for GCMs, it will be important to better understand how and to what extent these are affected by model biases. While it is generally thought that there is a close correspondence between general model performance and prediction skills, this might not hold true in all circumstances and awaits deeper analysis. Such efforts should provide valuable guidance for model development and may inform schemes for correcting model output.

Acknowledgments

The authors thank the two anonymous reviewers for their helpful comments. Tomoki Tozuka is supported by the Japan Society for Promotion of Science through Grant-in-Aid for Exploratory Research 24654150.

References

Abramowitz, G., A. Pitman, H. Gupta, E. Kowalczyk, and Y. Wang, 2007: Systematic bias in land surface models. *J. Hydrometeor*, **8**, 989–1001.

AchutaRao, K., and K. R. Sperber, 2006: ENSO simulation in coupled ocean-atmosphere models: are the current models better? *Clim. Dyn.*, **27,** 1-15.

Adler, R. F., G. J. Huffman, D. T. Bolvin, S. Curtis, and E. J. Nelkin, 2000: Tropical rainfall distributions determined using TRMM combined with other satellite and rain gauge information. *J. Appl. Meteor.*, **39**, 2007–2023.

Adler, R. F., G. J. Huffman, A. Chang, R. Ferraro, P. Xie, J. Janowiak, B. Rudolf, U. Schneider, S. Curtis, D. Bolvin, A. Gruber, J. Susskind, and P. Arkin, 2003: The Version 2 Global Precipitation Climatology Project (GPCP) Monthly Precipitation Analysis (1979-Present). *J. Hydrometeor*, **4**, 1147-1167.

Allen, R. G., L. S. Pereira, D. Raes, and M. Smith, 1998: Crop evapotranspiration - guidelines for computing crop water requirements. *Irrigation and Drainage Paper 56*, FAO, Rome. 328 p.

An, S.-I., Y.-G. Ham, J.-S. Kug, F.-F. Jin, and I.-S. Kang, 2005: El Niño-La Niña Asymmetry in the Coupled Model Intercomparison Project Simulations. *J. Climate*, **18,** 2617-2627.

Arakawa, A., and W. H. Schubert, 1974: Interaction of a cumulus cloud ensemble with the large-scale environment. Part I. *J. Atmos. Sci*, **31,** 674–701.

Arakawa, A., 2004: The cumulus parameterization problem: Past, present, and future. *J. Climate*, **17**, 2493–2525.

Ashfaq, M., C. B. Skinner, N. S. Diffenbaugh: Influence of SST biases on future climate change projections. *Clim. Dyn.,* **36,** 1303-1319.

Barnston, A. G., M. K. Tippett, M. L. L'Heureux, S. Li, and D. G. DeWitt, 2012: Skill of Real-Time Seasonal ENSO Model Predictions During 2002: Is Our Capability Increasing? *Bull. Amer. Meteorol. Soc.*, **93,** ES48-ES50.

Baron, C., B. Sultan, M. Balme, B. Sarr, S. Traore, T. Lebel, S. Janicot, and M. Dingkuhn, 2005: From GCM grid cell to agricultural plot: scale issues affecting modelling of climate impact. *Phil. Trans. R. Soc. B*, **360**, 2095–2108.

Behera, S. K., P. S. Salvekar, and T. Yamagata, 2000: Simulation of interannual SST variability in the tropical Indian Ocean. *J. Climate*, **13**, 3487-3499.

Behera, S.K., and T. Yamagata, 2001: Subtropical SST dipole events in the southern Indian Ocean. *Geophys. Res. Lett.*, **28**, 327-330.

Behera, S.K., J.-J. Luo, S. Masson, S.A. Rao, H. Sakuma, and T. Yamagata, 2006: A CGCM study on the interaction between IOD and ENSO. *J. Climate*, **19**, 1688-1705.

Bellenger, H., E. Guilyardi, J. Leloup, M. Lengaigne, and J. Vialard, 2013: ENSO representation in climate models: from CMIP3 to CMIP5. *Clim. Dyn.***,**, 10.1007/s00382-013-1783-z.

Bender, M. A., T. R. Knutson, R. E. Tuleya, J. J. Sirutis, G. A. Vecchi, S. T. Garner, and I. M. Held, 2010: Modeled impact of anthropogenic warming on the frequency of intense Atlantic hurricances. *Science,* **327,** 454-458.

Berg, A., B. Sultan, and N. de Noblet-Ducoudré, 2010: What are the dominant features of rainfall leading to realistic large-scale crop yield simulations in West Africa?. *Geophys. Res. Lett.*, **37**, L05405.

Biastoch, A., and W. Krauss, 1999: The role of mesoscale eddies in the source regions of the Agulhas Current. *J. Phys. Oceanogr.*, **29**, 2303–2317.

Biasutti, M., A. H. Sobel, and Y. Kushnir, 2006: AGCM precipitation biases in the tropical Atlantic. *J. Climate*, **19,** 935–958.

Bjerknes, V., 1904: Das Problem der Wettervorhersage, betrachtet vom Standpunkte der Mechanik und der Physik (The problem of weather prediction, considered from the viewpoints of mechanics and physics). Meteorol. Zeitschrift, **21**, 1–7.

Bjerknes, V., 1900: The Dynamic principles of the circulatory movements in the atmosphere. *Mon. Wea. Rev.*, **28**, 434–443.

Bjerknes, J., 1969: Atmospheric teleconnections from the equatorial Pacific. *Mon. Wea. Rev.*, **97,** 163-172.

Blösch, G., and M. Sivapalan, 1995: Scale issues in hydrological modelling: A review. *Hydrol. Process.*, **9**, 251–290.

Boer, G. J., and M. Lazare, 1988: Some results concerning the effect of horizontal resolution and gravity–wave drag on simulated climate. *J. Climate*, **1**, 789–806.

Bony, S., and J.-L. Dufresne, 2005: Marine boundary layer clouds at the heart of tropical cloud feedback uncertainties in climate models. *Geophys. Res. Lett.,* **32,** L20806, doi:10.1029/2005GL023851.

Boone, A., P. de Rosnay, G. Basalmo, A. Beljaars, F. Chopin, B. Decharme, C. Delire, A. Ducharne, S. Gascoin, M. Grippa, F. Guichard, Y. Gusev, P. Harris, L. Jarlan, L. Kergoat, E. Mougin, O. Nasonova, A. Norgaard, T. Orgeval, C. Ottlé, I. Poccard-Leclercq, J. Polcher, I. Sandholt, S. Saux-Picart, C. Taylor, and Y. Xue, 2009: The AMMA Land Surface Model Intercomparison Project. *Bull. Amer. Meteor. Soc.,* **90**, 1865-1880.

Braconnot, P., F. Hourdin, S. Bony, J. L. Dufresne, J. Y. Grandpeix, and O. Marti, 2007: Impact of different convective cloud schemes on the simulation of the tropical seasonal cycle in a coupled ocean-atmosphere model. *Clim. Dyn.*, **29,** 501-520.

Bryan, K., 1963: A numerical investigation of a nonlinear model of a wind-driven ocean, *J. Atmos. Sci.*, **20,** 594-606

Bryan K., and M. Cox, 1967: A numerical investigation of the oceanic general circulation. *Tellus*, **19**, 54-80.

Bryan K., and M. Cox, 1968: A nonlinear model of an ocean driven by wind and differential heating. I. Description of the three-dimensional velocity and density fields. II. An analysis of the heat, vorticity, and energy balance. *J. Atmos. Sci.*, **25**, 945-78.

Bryan, K., S. Manabe, and R. C. Pacanowski, 1975: A global ocean-atmosphere climate model. Part II: the ocean circulation. *J. Phys. Oceanogr.* **5**, 30-46.

Bryan, F.O., P.R. Gent, and R. Tomas, 2014: Can Southern Ocean eddy effects be parameterized in climate models? *J. Climate,* **27,** 411-425.

Cai, W., H.H. Hendon, and G. Meyers, 2005: Indian Ocean Dipolelike variability in the CSIRO Mark 3 coupled climate model. *J. Climate*, **18**, 1449-1468.

Cai, W., and T. Cowan, 2013: Why is the amplitude of the Indian Ocean Dipole overly large in CMIP3 and CMIP5 climate models? *Geophys. Res. Lett.*, doi:10.1002/grl.50208.

Camargo, S. J., Sobel, A. H., Barnston, A. G., and K. A. Emanuel, 2007: Tropical cyclone genesis potential index in climate models. *Tellus A*, **59**, 428–443.

Carter, T. R., M. L. Parry, H. Harasawa, and S. Nishioka, 1994: IPCC technical guidelines for assessing climate change impacts and adaptations. *Special report to Working Group II, Intergovernment Panel on Climate Change*, 59 pp.

Carton, J. A., and B. Huang, 1994: Warm events in the tropical Atlantic. *J. Phys. Oceanogr.*, **24,** 888–903.

Carton, J. A., and B. S. Giese, 2008: A reanalysis of ocean climate using Simple Ocean Data Assimilation (SODA), *Mon. Wea. Rev.,* **136,** 2999-3017.

Ceglar, A., and L. Kajfež-Bogataj, 2012: Simulation of maize yield in current and changed climatic conditions: addressing modelling uncertainties and the importance of bias correction in climate model simulations. *Europ. J. Agronomy*, **37**, 83–95.

Chang, P., L. Ji, and H. Li, 1997: A decadal climate variation in the tropical Atlantic Ocean from thermodynamic air-sea interactions. *Nature*, **385,** 516–518.

Chang, P., and Coauthors, 2006: Climate fluctuations of tropical coupled systems – the role of ocean dynamics, *J. Climate*, **19**, 5122-5174.

Chang, P., Y. Fang, R. Saravanan, L. Ji, and H. Seidel, 2006: The cause of the fragile relationship between Pacific El Niño and the Atlantic Niño, *Nature*, **443**, 324-328.

Chang, P., R. Zhang, W. Hazeleger, C. Wen, X. Wan, L. Ji,, R. J. Haarsma, W.-P. Breugem, and H. Seidel, 2008: An oceanic teleconnection between abrupt changes in high-latitude North Atlantic climate and the African Monsoon, *Nature Geoscience*, **1**, 444-448.

Chang, P., R. Saravanan, and L. Ji, 2003: Tropical Atlantic seasonal predictability: the roles of El Nino remote influence and thermodynamic air-sea feedback, *Geophys. Res. Lett.*, **30**, 1501-1504.

Chang, C.-Y., J. A. Carton, S. A. Grodsky, and S. Nigam, 2007: Seasonal climate of the tropical Atlantic sector in the NCAR Community Climate System Model 3: Error structure and probable causes of errors. *J. Climate*, **20**, 1053–1070.

Chang, C.-Y., S. Nigam, and J. A. Carton, 2008: Origin of the springtime westerly bias in equatorial Atlantic surface winds in the Community Atmosphere Model version 3 (CAM3) simulation. *J. Climate*, **21**, 4766–4778.

Charney, J. G., R. Fjörtoft, and J. von Neumann, 1950: Numerical integration of the barotropic vorticity equation. *Tellus*, **2**, 237-254.

Chassignet, E. P., H. E. Hurlburt, O. M. Smedstad, G. R. Halliwell, P. J. Hogan, A. J. Wallcraft, R. Baraille, and R. Bleck, 2007: The HYCOM (HYbrid Coordinate Ocean Model) data assimilative system. *J. Mar. Syst.*, **65**, 60–83.

Chauvin, F., J.-F. Royer, and M. Déqué, 2006: Response of hurricane-type vortices to global warming as simulated by ARPEGE-Climat at high resolution. *Clim. Dyn.*, **27**, 377–399.

Colberg, F., and C. J. C. Reason, 2006: A model study of the Angola Benguela frontal zone sensitivity to atmospheric forcing. *Geophys. Res. Lett.* **33**, L19608, doi:10.1029/2006GL027463.

Dai, A., 2006: Precipitation characteristics in eighteen coupled climate models. *J. Climate*, **19,** 4605-4630.

Danabasoglu, G., R. Ferrari, and J. C. McWilliams, 2008: Sensitivity of an ocean general circulation model to a parameterization of near-surface eddy fluxes. *J. Clim.*, **21**, 1192–1208.

Davey, M. K., and Coauthors, 2002: STOIC: A study of coupled model climatology and variability in tropical ocean regions. *Clim. Dyn.*, **18**, 403–420.

Dee, D. P., and Coauthors, 2011: The ERA-Interim reanalysis: configuration and performance of the data assimilation system. *Quart. J. R. Meteorol. Soc.*, **137**, 553-597.

Delworth, and coauthors, 2012: Simulated climate and climate change in the GFDL-CM2.5 high-resolution coupled climate model. *J. Climate,* **25,** 2755–2781.

Déqué, M., 2007: Frequency of precipitation and temperature extremes over France in an anthropogenic scenario: Model results and statistical correction according to observed values. *Glob. Planet. Change,* **57**, 16-26.

DeWitt, D. G., 2005: Diagnosis of the tropical Atlantic near-equatorial SST bias in a directly coupled atmosphere–ocean general circulation model. *Geophys. Res. Lett.*, **32,** L01703, doi:10.1029/2004GL021707.

Dewitte B., S. Illig, L. Renault, K. Goubanova, K. Takahashi, D. Gushchina, K. Mosquera, and S. Purca, 2011: Modes of covariability between sea surface temperature and wind stress intraseasonal anomalies along the coast of Peru from satellite observations (2000-2008). *J. Geophys. Res.*, **116**, doi:10.1029/2010JC006495.

de Szoeke, S. P., Y. Wang, S.-P. Xie, and T. Miyama, 2006: Effect of shallow cumulus convection on the eastern Pacific climate in a coupled model. *Geophys. Res. Lett.*, **33,** L17713, 10.1029/2006GL026715.

de Szoeke, S. P., and S.-P. Xie, 2008: The tropical eastern Pacific seasonal cycle: Assessment of errors and mechanisms in IPCC AR4 coupled ocean-atmosphere general circulation models. *J. Climate*, **21,** 2573-2590.

de Szoeke, S. P., S. E. Yuter, D. B. Mechem, C. W. Fairall, C. Burleyson, and P. Zuidema, 2012: Observations of stratocumulus clouds and their effect on the eastern Pacific surface heat budget along 20°S. *J. Climate***, 25,** 8542-8567.

DeMott, C.A., C. Stan, D.A. Randall, J.L. Kinter, and M. Khairoutdinov, 2011: The Asian Monsoon in the Superparameterized CCSM and Its Relationship to Tropical Wave Activity. *J. Climate,* **24,** 5134–5156.

Deser, C., A. Capotondi, R. Saravanan, and A.S. Phillips, 2006: Tropical Pacific and Atlantic Climate Variability in CCSM3. *J. Climate*, **19,** 2451-2481.

Dirmeyer, P. A., R. D. Koster, Z. Guo, 2006: Do global models properly represent the feedback between land and atmosphere? *J. Hydrometeor*, **7**, 1177–1198.

Doi, T., G. A. Vecchi, A. J. Rosati, and T. L. Delworth, 2012: Biases in the Atlantic ITCZ in seasonal-interannual variations for a coarse and a high resolution coupled climate model. *J. Climate,* **25,** 5494-5511.

Duffy, P.B., and coauthors 2003: High-resolution simulations of global climate, part 1: present climate. *Clim. Dyn,,* **21,** 371-390.

Edwards, P. N., 2000: A brief history of atmospheric general circulation modeling. *General Circulation Model Development: Past, Present, and Future*, D. A. Randall, Ed., Academic Press, 67–90.

Emanuel, K., 1991: A scheme for representing cumulus convection in large-scale models. *J. Atmos. Sci.*, **48,** 2313-2335.

Emanuel, K., R. Sundararajan, and J. Williams, 2008: Hurricanes and global warming: Results from downscaling IPCC AR4 simulations. *Bull. Amer. Meteor. Soc.,* **89,** 347–367.

England, M. H., C. C. Ummenhofer, and A. Santoso, 2006: Interannual rainfall extremes over southwest western Australia linked to Indian Ocean climate variability. *J. Climate*, **19**, 1948-1969.

Farneti, R., and P. R. Gent, 2011: The effects of the eddy--induced advection coefficient in a coarse--resolution coupled climate model. *Ocean Modelling,* **39,** 135-145.

Fauchereau, N., S. Trzaska, Y. Richard, P. Roucou, and P. Camberlin, 2003: Sea-surface temperature co-variability in the southern Atlantic and Indian Oceans and its connections with the atmospheric circulation in the southern hemisphere. *J. Climate*, **23**, 663-677.

Feng, M., and G. Meyers, 2003: Interannual variability in the tropical Indian Ocean: a two-year time-scale of Indian Ocean Dipole. *Deep-Sea Res.*, **50**, 2263-2284.

Florenchie, P., J. R. E. Lutjeharms, C. J. C. Reason, S. Masson, and M. Rouault, 2003: The source of Benguela Niños in the South Atlantic Ocean. *Geophys. Res. Lett.*, **30**, 1505, doi:10.1029/2003GL017172.

Folland, C. K., T. N. Palmer, and D. E. Parker, 1986: Sahel rainfall and world-wide sea temperatures. *Nature*, **320,** 602-607.

Foltz, G.R., J. Vialard, B.P. Kumar, and M.J. McPhaden, 2010: Seasonal mixed layer heat balance of the southwestern tropical Indian Ocean. *J. Climate*, **23**, 947-965.

Gates, W. L., Y. J. Han, and M. E. Schlesinger, 1985: The global climate simulated by a coupled atmosphere-ocean general circulation model: preliminary results. *Coupled Ocean-Atmosphere Modeling.* J. C. J. Nihoul, ed., Elsevier, 313 pp.

Gent, P. R., and J. C. McWilliams, 1990: Isopycnal mixing in ocean circulation models. *J. Phys. Oceanogr.*, **20,** 150–155.

Giannini, A., R. Saravanan, and P. Chang, 2003: Oceanic forcing of Sahel rainfall on interannual to interdecadal timescales. *Science*, **302**, 1027-1030.

Giorgi, F., and L. O. Mearns, 1999: Introduction to special section: Regional Climate Model revisiting. *J. Geophys. Res.*, **104**, 6335–6352.

Goddard, L., S. J. Mason, S. E. Zebiak, C. F. Ropelewski, R. Basher, and M. A. Cane, 2001: Current approaches to seasonal to interannual climate predictions. *Int. J. Climatol.*, **21**, 1111–1152.

Gordon, C. T., A. Rosati, and R. Gudgel, 2000: Tropical sensitivity of a coupled model to specified ISCCP low clouds. *J. Climate*, **13,** 2239-2260.

Grodsky, S. A., J. A. Carton, and S. Nigam, 2003: Near surface westerly wind jet in the Atlantic ITCZ. *Geophys. Res. Lett.*, **30**. doi:10.1029/2003GL017867

Grodsky, S. A., J. A. Carton, S. Nigam, and Y. M Okumura, 2012: Tropical Atlantic Biases in CCSM4, *J. Clim.*, **25**, 3684-3701.

Gudmundsson, L., J. B. Bremnes, J. E. Haugen, and T. Engen-Skaugen, 2012: Technical note: downscaling RCM precipitation to the station scale using statistical transformations – a comparison of methods. *Hydrol. Earth Syst. Sci.*, **16**, 3383-3390.

Guilyardi, E., 2006: El Niño–mean state–seasonal cycle interactions in a multi-model ensemble. *Clim. Dyn.*, **26,** 329-348, 10.1007/s00382-005-0084-6.

Guo, Z., P. A. Dirmeyer, R. D. Koster, Y. C. Sud, G. Bonan, K. W. Oleson, E. Chan, D. Verseghy, P. Cox, C. T. Gordon, J. L. McGregor, S. Kanae, E. Kowalczyk, D. Lawrence, P. Liu, D. Mocko, C.-H. Lu, K. Mitchell, S. Malyshev, B. McAvaney, T. Oki, T. Yamada, A. Pitman, C. M. Taylor, R. Vasic and Y. Xue, 2006. GLACE: The Global Land–Atmosphere Coupling Experiment. Part II: Analysis. *J. Hydrometeor.*, **7**, 611–625.

Hack, J.J., and coauthors, 2006: CCSM-CAM3 Climate Simulation Sensitivity to Changes in Horizontal Resolution. *J. Climate,* **19,** 2267-2287.

Hallberg, R., and A. Gnanadesikan, 2006: The role of eddies in determining the structure and response of the wind-driven Southern Hemisphere overturning: Results from the Modeling Eddies in the Southern Ocean (MESO) project. *J. Phys. Oceanogr.*, **36**, 2232–2252.

Halley, E., 1686: An Historical Account of the Trade Winds, and Monsoons, Observable in the Seas between and Near the Tropicks, with an Attempt to Assign the Phisical Cause of the Said Winds, By E. Halley. *Philosophical Transactions (1683-1775)*, **16,** 153-168.

Hamilton, K., and W. Ohfuchi, Eds., 2007: *High Resolution Numerical Modelling of the Atmosphere and Ocean*. Springer, 310 pp.

Hansen, J. W., A. J. Challinor, A. Ines, T. R. Wheeler, and V. Moron, 2006: Translating climate forecasts into agricultural terms: advances and challenges. *Clim. Res.*, **33**, 27–41.

Hartmann, D. L., M. E. Ockert-Bell, and M. L. Michelsen, 1992: The effect of cloud type on Earth's energy balance: Global analysis. *J. Climate*, **5,** 1281-1304.

Hecht, M. W., and H. Hasumi, Eds., 2008: Ocean Modeling in an Eddying Regime, Geophys. Monogr. Ser., vol. 177, 409 pp., AGU, Washington, D. C., doi:10.1029/GM177.

Hendon, H.H., 2003: Indonesian rainfall variability: Impacts of ENSO and local air-sea interaction. *J. Climate*, **16**, 1775-1790.

Hirst, A. C., and S. Hastenrath, 1983: Atmosphere–ocean mechanisms of climate anomalies in the Angola–tropical Atlantic sector. *J. Phys. Oceanogr.*, **13,** 1146–1157.

Hong, S.-Y., and J. Dudhia, 2012: Next--Generation Numerical Weather Prediction: Bridging Parameterization, Explicit Clouds, and Large Eddies. *Bull. Amer. Meteor. Soc.,* **93,** 6–9.

Hoskins, B. J., and D. J. Karoly, 1981: The Steady Linear Response of a Spherical Atmosphere to Thermal and Orographic Forcing. *J. Atmos. Sci.*, **38,** 1179-1196.

Hu, Z.-Z., B. Huang, Y.-T. Hou, W. Wang, F. Yang, C. Stan, and E. K. Schneider, 2011: Sensitivity of tropical climate to low-level clouds in the NCEP climate forecast system. *Clim. Dyn.,* **36,** 1795-1811.

Huang, B., and J. Shukla, 2006: Interannual SST variability in the southern subtropical and extra-tropical ocean. *COLA Technical Report*, **223**, 20pp.

Huang B., Z.-Z. Hu, and B. Jha, 2007: Evolution of model systematic errors in the tropical Atlantic basin from coupled climate hindcasts. *Clim. Dyn.*, **28**, 661-682.

Iizuka, S., T. Matsuura, and T. Yamagata, 2000: The Indian Ocean SST dipole simulated in a coupled general circulation model. *Geophys. Res. Lett.*, **27**, 3369-3372.

Iizumi, T., M. Nishimori, and M. Yokozawa, 2010: Diagnostics of climate model biases in summer temperature and warm-season insolation for the simulation of regional paddy rice yield in Japan. *J. Appl. Meteorol. Clim.*, **49**, 574–591.

Ines, A. M. V., and J. W. Hansen, 2006: Bias correction of daily GCM rainfall for crop simulations studies. *Agr. Forest Meteorol.*, **138**, 44–53.

IPCC, 2007. Climate Change 2007: The physical science basis. In: Solomon, S., Qin, D., Manning, M., Chen, Z., Marquis, M., Averyt, K.B., Tignor, M., Miller, H.L. (Eds.), Contribution of Working Group I to the Fourth Assessment Report of the Intergovernmental Panel on Climate Change. Cambridge University Press, Cambridge, United Kingdom. 996 pp.

Jin, F. F., 1997: An equatorial ocean recharge paradigm for ENSO: 1. Conceptual model. *J. Atmos. Sci.*, **54,** 811-829.

Kalnay, E., and Coauthors, 1996: The NCEP/NCAR 40-year reanalysis project. *Bull. Am. Meteorol. Soc.* **77**, 437–471.

Kataoka, T., T. Tozuka, Y. Masumoto, and T. Yamagata, 2012: The Indian Ocean subtropical dipole mode simulated in the CMIP3 models. *Clim. Dyn.*, **39**, 1385–1399.

Khairoutdinov, M., and D. A. Randall, 2001: A cloud resolving model as a cloud parameterization in the NCAR Community Climate System Model: Preliminary results. *Geophys. Res. Lett.*, **28**, 3617–3620.

Khairoutdinov, M., D. A. Randall, and C. A. DeMott, 2005: Simulation of the atmospheric general circulation using a cloud-resolving model as super-parameterization of physical processes. *J. Atmos. Sci.*, **62**, 2136 – 2154.

Keenlyside, N. S., and M. Latif, 2007: Understanding equatorial Atlantic interannual variability. *J. Climate*, **20,** 131-142.

Kim, D., and Coauthors, 2009: Application of MJO simulation diagnostics to climate models. *J. Climate,* **22,** 6413–6436.

Kirtman, B., and coauthors, 2012: Impact of ocean model resolution on CCSM climate simulation. *Clim. Dyn.,* **39,** 1303–1328.

Klein, S. A., and D. L. Hartmann, 1993: The seasonal cycle of low stratiform clouds. *J. Climate*, **6,** 1588-1606.

Kossin, J. P., and D. J. Vimont, 2007: A more general framework for understanding Atlantic hurricane variability and trends. *Bull. Amer. Meteor. Soc.*, **88**, 1767-1781.

Koster, R. D., P. Dirmeyer, Z. Guo, G. Bonan, P. Cox, C. Gordon, S. Kanae, E. Kowalczyk, D. Lawrence, P. Liu, C. Lu, S. Malyshev, B. McAvaney, K. Mitchell, D. Mocko, T. Oki, K. Oleson, A. Pitman, Y. Sud, C. Taylor, D. Verseghy, R. Vasic, Y. Xue, and T. Yamada, 2004: Regions of strong coupling between soil moisture and precipitation. *Science*, **305**, 1138–1140.

Koster, R. D., 2011: Climate science: Storm instigation from below. *Nat. Geosci*., **4**, 427–428.

Koster, R. D., M. J. Suarez and M. Heiser, 2000: Variance and predictability of precipitation at seasonal-to-interannual timescales. *J. Hydrometeor.*, **1**, 26–46.

Koster, R. D., M. J. Suarez, R. W. Higgins and H. M. Van den Dool, 2003: Observational evidence that soil moisture variations affect precipitation. *Geophys. Res. Lett.*, **30**, 1241, doi:10.1029/2002GL016571.

Koster, R. D., Y. C. Sud, Z. Guo. P. A. Dirmeyer, G. Bonan, K. W. Oleson, E. Chan, D. Verseghy, P. Cox, H. Davies, E. Kowalczyk, C. T. Gordon, S. Kanae, D. Lawrence, P. Liu, D. Mocko, C.-H. Lu, K. Mitchell, S. Malyshev, B. McAvaney, T. Oki, T. Yamada, A. Pitman, C. M. Taylor, R. Vasic and Y. Xue, 2006: GLACE: The Global Land–Atmosphere Coupling Experiment. Part I: Overview. *J. Hydrometeor.*, 7, 590–610.

Koster, R. D., S. P. P. Mahanama, T. J. Yamada, G. Balsamo, A. A. Berg, M. Boisserie, P. A. Dirmeyer, F. J. Doblas-Reyes, G. Drewitt, C. T. Gordon, Z. Guo, J.-H. Jeong, W.-S. Lee, Z. Li, L. Luo, S. Malyshev, W. J. Merryfield, S. I. Seneviratne, T. Stanelle, B. J. J. M. van den Hurk, F. Vitart, and E. F. Wood, 2011: The second phase of the Global Land–Atmosphere Coupling Experiment: Soil moisture contributions to subseasonal forecast skill. *J. Hydrometeor*, 12, 805–822.

Kuo, H. L., 1974: Further studies of the parameterization of the influence of cumulus convection on large-scale flow. *J. Atmos. Sci.*, **31,** 1232-1240.

Large, W. G., and G. Danabasoglu, 2006: Attribution and impacts of upper-ocean biases in CCSM3. *J. Climate*, **19**, 2325–2346.

Lass, H. U., M. Schmidt, V. Mohrhol, and G. Nausch, 2000: Hydrographic and current measurements in the area of the Angola–Benguela front. *J. Phys. Oceanogr.* **30**, 2589–609.

Latif, M., J. Biercamp, and H. von Storch, 1988: The response of a coupled ocean-atmosphere general circulation model to wind bursts. *J. Atmos. Sci.*, **45**, 964-979.

Lau, N.-C., and M.J. Nath, 2004: Coupled GCM simulation of atmosphere-ocean variability associated with zonally asymmetric SST changes in the tropical Indian Ocean. *J. Climate*, **1**, 245-265.

Lauer, A., K. Hamilton, Y. Wang, V. T. J. Phillips, and R. Bennartz, 2010: The impact of global warming on marine boundary layer clouds over the eastern Pacific - a regional model study. *J. Climate*, **23,** 5844-5863.

Li, T., Y. Zhang, E. Lu, and D. Wang, 2002: Relative role of dynamic and thermodynamic processes in the development of the Indian Ocean dipole: An OGCM diagnosis. *Geophys. Res. Lett.*, **29**, 2110, doi:10.1029/2002GL015789.

Li, T., B. Wang, C-P. Chang, and Y. Zhang, 2003: A theory for the Indian Ocean dipole– zonal mode. *J. Atmos. Sci.*, **60**, 2119–2135.

Li, Y., N.C. Jourdain, A.S. Taschetto, C.C. Ummenhofer, K. Ashok, and A.S. Gupta, 2012: Evaluation of monsoon seasonality and the tropospheric biennial oscillation transitions in the CMIP models. *Geophys. Res. Lett.*, **39**, doi:10.1029/2012GL053322.

Lin, J.-L., 2007: The double-ITCZ problem in IPCC AR4 coupled GCMs: Ocean atmosphere feedback analysis. *J. Climate*, **20,** 4497-4525.

Liu, L., W. Yu, and T. Li, 2011: Dynamic and thermodynamic air-sea coupling associated with the Indian Ocean Dipole diagnosed from 23 WCRP CMIP3 models. *J. Climate*, **24**, 4941-4958.

Lloyd, J., E. Guilyardi, and H. Weller, 2012: The Role of Atmosphere Feedbacks during ENSO in the CMIP3 Models. Part III: The Shortwave Flux Feedback. *J. Climate*, **25,** 4275-4293.

Locarnini RA, Mishonov AV, Antonov JI, Boyer TP, Garcia HE (2006) World Ocean Atlas 2005, Volume 1: Temperature. S. Levitus, Ed. NOAA Atlas NESDIS 61, U.S. Government Printing Office, Washington, D.C., 182 pp

Lübbecke, J. F., C. W. Böning, N. S. Keenlyside, and S.-P. Xie, 2010: On the connection between Benguela and equatorial Atlantic Niños and the role of the South Atlantic anticyclone. *J. Geophys. Res.*, **115**, C09015, doi:10.1029/2009JC005964.

Luo, J.-J., S. Masson, E. Roeckner, G. Madec, and T. Yamagata, 2005: Reducing climatology bias in an ocean–atmosphere CGCM with improved coupling physics. *J. Climate*, **18**, 2344–2360.

Luo, J.-J., S. Masson, S. Behera, and T. Yamagata, 2007: Experimental forecasts of the Indian Ocean Dipole using a coupled OAGCM. *J. Climate*, **20**, 2178-2190.

Luo, J.-J., S. Masson, S. K. Behera, and T. Yamagata, 2008: Extended ENSO predictions using a fully coupled ocean–atmosphere model. *J. Climate*, **21**, 84–93.

Ma, C.-C., C. R. Mechoso, A. W. Robertson, and A. Arakawa, 1996: Peruvian stratus clouds and the tropical Pacific circulation: a coupled ocean-atmosphere GCM study. *J. Climate*, **9,** 1635-1645.

Ma, H.-Y., H. Xiao, C. R. Mechoso and Y. Xue, 2013: Sensitivity of global tropical climate to land surface processes: mean state and interannual variability. *J. Climate*, **26**, 1818–1837.

Maltrud, M.E., and J.L. McClean, 2005: An eddy resolving global 1/10° ocean simulation. *Ocean Modelling,* **8,** 31-54.

Manabe, S., and K. Bryan, 1969: Climate calculations with a combined ocean-atmosphere model. *J. Atmos. Sci.*, **26**, 786-789.

Manabe, S., J. Smagorinsky, J.L. Holloway, and H.M. Stone, 1970: Simulated climatology of a general circulation model with a hydrologic cycle: III. Effects of increased horizontal computational resolution. *Mon. Wea. Rev.,* **98,** 175-212.

Manabe, S., K. Bryan, and M. J. Spelman, 1975: A global ocean-atmosphere climate model: Part I. The atmosphere circulation. *J. Phys. Oceanogr.*, **5**, 3-29.

Manabe, S., K. Bryan, and M. J. Spelman, 1990: Transient response of a global oceanatmosphere model to a doubling of atmospheric carbon dioxide. *J. Phys. Oceanogr*. **20**, 722-749.

Marshall, J., H. Jones, R. Karsten, and R. Wardle, 2002: Can eddies set ocean stratification? *J. Phys. Oceanogr*, **32,** 26–38.

Masumoto, Y., and coauthors, 2004: A fifty-year eddy-resolving simulation of the world ocean—Preliminary outcomes of OFES (OGCM for the Earth Simulator). *J. Earth Simulator,* **1,** 35–56.

(available at http://www.jamstec.go.jp/esc/publication/journal/)

McClean, J. L., and coauthors, 2011: A prototype two-decade fully-coupled fine-resolution CCSM simulation. *Ocean Modelling,* **39,** 10–30.

McPhaden, M.J., and M. Nagura, 2014: Indian Ocean dipole interpreted in terms of recharge oscillator theory. *Clim. Dyn.*, **42,** 1569-1586.

McWilliams, J. C., 1996: Modeling the oceanic general circulation. *Ann. Rev. Fluid. Mech.*, **28**, 215-248.

Mearns, L. O., F. Giorgi, L. McDaniel, and C. Shields, 1995: Analysis of climate of daily variability of precipitation in a nested regional climate model: Comparison with observations and doubled CO_2 results. *Global. Planet. Change*, **10**, 55–70.

Mechoso, C. R., and Coauthors, 1995: The seasonal cycle over the tropical Pacific in coupled ocean–atmosphere general circulation models. *Mon. Wea. Rev.*, **123**, 2825–2838.

Meehl, G. A., and Coauthors, 2007: The WCRP CMIP3 multi-model dataset: A new era in climate change research. *Bull. Amer. Meteorol. Soc.*, **88,** 1383-1394.

Merle, J., 1980: Annual and interannual variability of temperature in the eastern equatorial Atlantic Ocean – hypothesis of an Atlantic El Niño, *Oceanol. Acta*, *3*, 209-220.

Mitchell, T. P., and J. M. Wallace, 1992: The annual cycle in equatorial convection and sea surface temperature. *J. Climate*, **5,** 1140-1156.

Miyazawa, Y., X. Guo, and T. Yamagata, 2004: Roles of mesoscale eddies in the Kuroshio paths. *J. Phys. Oceanogr.*, **34**, 2203–2222.

Moeng, C.-H., and B. Stevens, 2000: Representing the stratocumulus-topped boundary layer in GCMs. *General Circulation Model Development: Past, Present, and Future*, D. A. Randall, Ed., Academic Press, 577–604.

Morioka, Y., T. Tozuka, S. Masson, P. Terray, J.-J. Luo, and T. Yamagata, 2012: Subtropical dipole modes simulated in a coupled general circulation model. *J. Climate*, **25**, 4029-4047.

Moura, A., and J. Shukla, 1981: On the dynamics of droughts in northeast Brazil: Observations, theory and numerical experiments with a general circulation model. *J. Atmos. Sci.,* **38,** 2653-2675.

Murtugudde, R., J.P. McCreary Jr., and A.J. Busalacchi, 2000: Oceanic processes associated with anomalous events in the Indian Ocean with relevance to 1997-1998. *J. Geophys. Res.*, **105**, 3295-3306.

Nagura, M., W. Sasaki, T. Tozuka, J.-J. Luo, S.K. Behera, and T. Yamagata, 2013: Longitudinal biases in the Seychelles Dome simulated by 35 ocean-atmosphere

coupled general circulation models. *J. Geophys. Res. Oceans*, **118**, doi:10.1029/2012JC008352.

Neelin, J. D., and Co-authors, 1992: Tropical air-sea interaction in general circulation models. *Clim. Dyn.* **7,** 73-104.

Neelin, J. D., and H. A. Dijkstra, 1995: Ocean–atmosphere interaction and the tropical climatology. Part I: The dangers of flux correction. *J. Climate*, **8**, 1325–1342.

Nobre, P., and J. Shukla, 1996: Variations of sea surface temperature, wind stress, and rainfall over the tropical Atlantic and South America. *J. Climate*, **9,** 2464-2479.

Oettli, P., B. Sultan, C. Baron, and M. Vrac, 2011: Are regional climate models relevant for crop yield prediction in West Africa? *Environ. Res. Lett.*, **6**, 014008.

Okumura, Y., and S.-P. Xie, 2004: Interaction of the Atlantic equatorial cold tongue and African monsoon. *J. Climate*, **17,** 3589–3602.

Okumura, Y., and S.-P. Xie, 2006: Some overlooked features of tropical Atlantic climate leading to a new Niño-like phenomenon. *J. Climate,* **19,** 5859-5874.

Patricola, C. M., M. Li, Z. Xu, P. Chang, R. Saravanan, and J.-S. Hsieh, 2012: An investigation of tropical Atlantic bias in a high-resolution coupled regional climate model, *Clim. Dyn.*, **39,** 2243-2463.

Penven, P., J. Pasapera, J. Tam, and V. Echevin, 2005: Mean circulation, seasonal cycle and mesoscale dynamics of the Peruvian upwelling system : a modelling approach. *J. Geophys. Res.*, **110**, C10021. doi: 10.1029/2005JC002945.

Peterson, R. and G., L. Stramma, 1991: Upper-level circulation in the South Atlantic Ocean. *Prog. Oceanogr.*, **26**, 1–73.

Philander, S. G. H., 1986: Unusual conditions in the tropical Atlantic Ocean in 1984. *Nature*, **322,** 236–238.

Philander, S. G. H., D. Gu, D. Halpern, G. Lambert, N. C. Lau, T. Li, and R. C. Pacanowski, 1996: Why the ITCZ is mostly north of the equator. *J. Climate*, **9,** 2958-2972.

Phillips, N. A., 1956: The general circulation of the atmosphere: a numerical experiment. *Quart. J. Roy. Meteor. Soc.*, **82**, 123-165.

Pitman, A.J., 2003. The evolution of, and revolution in, land surface schemes designed for climate models. *Int. J. Climatol.,* **23**, 479–510.

Polo, I., A. Lazar, B. Rodríguez-Fonseca, and S. Arnault, 2008: Oceanic Kelvin Waves and Tropical Atlantic Intraseasonal Variability. Part I: Kelvin Wave Characterization. *J. Geophys. Res.,* **113,** C07009. doi:10.1029/2007JC004495

Pope, V.D., and R.A. Stratton, 2002: The processes governing horizontal resolution sensitivity in a climate model. *Clim. Dyn.,* **19,** 211-236.

Ramanathan, V., and W. Collins, 1991: Thermodynamic regulation of ocean warming by cirrus clouds deduced from observations of the 1987 El Nino. *Nature*, **351,** 27-32.

Randall, D. A., 1980: Conditional instability of the first kind upside-down. *J. Atmos. Sci.*, **37**, 125 - 130.

Rao, S.A., S.K. Behera, Y. Masumoto and T. Yamagata, 2002: Interannual subsurface variability in the tropical Indian Ocean with a special emphasis on the Indian Ocean Dipole. *Deep-Sea Res.*, **49**, 1549-1572.

Rao, S.A., and T. Yamagata, 2004: Abrupt termination of Indian Ocean dipole events in response to intraseasonal disturbances. *Geophys. Res. Lett.*, **31**, L19306, doi:10.1029/2004GL020842.

Rao, S.A., S. Masson, J.-J. Luo, S.K. Behera, and T. Yamagata, 2007: Termination of Indian Ocean Dipole events in a coupled general circulation model. *J. Climate*, **20**, 3018-3035.

Rayner, N. A., E. B. Horton, D. E. Parker, C. K. Folland, and R. B. Hackett, 1996: Version 2.2 of the Global Sea-Ice and Sea Surface Temperature Data Set, 1903–1994 (Clim. Res. Tech. Note 74, UK Meteorological Office, Bracknell).

Rayner, N. A., D. E. Parker, E. B. Horton, C. K. Folland, L. V. Alexander, D. P. Rowell, E. C. Kent, and A. Kaplan, 2003: Global analyses of sea surface temperature, sea ice, and night marine air temperature since the late nineteenth century. *J. Geophys. Res.*, **108**, 4407, doi:10.1029/2002JD002670.

Reason, C.J.C., 2001: Subtropical Indian Ocean SST dipole events and southern African rainfall. *Geophys. Res. Lett.*, **28**, 2225-2227.

Redelsperger, J.-L., C. D. Thorncroft, A. Diedhiou, T. Lebel, D. J. Parker, and J. Polcher, 2006: African monsoon multidisciplinary analysis: an international research project and field campaign. *Bull. Amer. Meteor. Soc.*, **87**, 1739–1746.

Repelli, C. A., and P. Nobre, 2004: Statistical prediction of sea surface temperature over the tropical Atlantic. *Int. J. Climatol.*, **24**, 45–55.

Reynolds, R.W., N. A. Rayner, T. M. Smith, D. C. Stokes, and W. Wang, 2002: An improved in situ and satellite SST analysis for climate. *J. Climate,* **15,** 1609-1625.

Richardson, L. F., 1922: Weather Prediction by Numerical Processes. Cambridge University Press, Cambridge.

Richter, I., and S.-P. Xie, 2008: On the origin of equatorial Atlantic biases in coupled general circulation models. *Clim. Dyn.*, **31**, 587–598.

Richter, I., S. K. Behera, Y. Masumoto, B. Taguchi, N. Komori, T. Yamagata, 2010: On the triggering of Benguela Niños – remote equatorial vs. local influences. *Geophys. Res. Lett.*, **37**, doi:10.1029/2010GL044461.

Richter, I., S. P. Xie, A. T. Wittenberg, and Y. Masumoto, 2012a: Tropical Atlantic biases and their relation to surface wind stress and terrestrial precipitation. *Clim. Dyn.*, **38**, 985–1001.

Richter, I., S.-P. Xie, S. K. Behera, T. Doi, and Y. Masumoto, 2012b: Equatorial Atlantic variability and its relation to mean state biases in CMIP5. *Clim. Dyn.,* doi: 10.1007/s00382-012-1624-5

Richter, I., S. K. Behera, Y. Masumoto, B. Taguchi, H. Sasaki, and T. Yamagata, 2013: Multiple causes of interannual sea surface temperature variability in the equatorial Atlantic Ocean. *Nature Geosci.,* **6,** 43-47.

Roach, W. T., R. Brown, S. J. Caughey, B. A. Crease, and A. Slingo, 1982: A field-study of nocturnal stratocumulus: 1. Mean structure and budgets. *Quart. J. Roy. Meteor. Soc.*, **108**, 103–123.

Rouault, M., S. Illig, C. Bartholomae, C. J. C. Reason, and A. Bentamy, 2007: Propagation and origin of warm anomalies in the Angola Benguela upwelling system in 2001. *J. Mar. Syst.*, **68**, 473–488.

Saha, S., and Coauthors, 2010: The NCEP Climate Forecast System Reanalysis. *Bull. Amer. Meteor. Soc.*, **91**, 1015–1057.

Saji, N. H., B. N. Goswami, P. N. Vinayachandran, and T. Yamagata, 1999: A dipole mode in the tropical Indian Ocean. *Nature*, **401**, 360-363.

Saji, N.H., S.-P. Xie, and T. Yamagata, 2006: Tropical Indian Ocean variability in the IPCC twentieth-century climate simulations. *J. Climate*, **19**, 4397-4417.

Sarkisyan A. S., 1962: On the dynamics of the origin of wind currents in the baroclinic ocean. *Okeanologia*, **11**, 393-409.

Satoh, M., T. Matsuno, H. Tomita, H. Miura, T. Nasuno, and S. Iga, 2008: Nonhydrostatic Icosahedral Atmospheric Model (NICAM) for global cloud-resolving simulations. *J. Comput. Phys.*, **227**, 3486–3514.

Scharffenberg, M., and D. Stammer, 2010: Seasonal variations of the large-scale geostrophic flow field and eddy kinetic energy inferred from the TOPEX/Poseidon

and *Jason-1* tandem mission data. *J. Geophys. Res.*, **115**, C02008, doi:10.1029/2008JC005242.

Schneider, E. K., 2002: Understanding differences between the equatorial Pacific as simulated by two Coupled GCMs. *J. Climate*, **15,** 449-469.

Schulze, R., 2000: Transcending scales of space and time in impact studies of climate and climate change on agrohydrological responses. *Agric. Ecosyst. Environ.*, **82**, 185–212.

Semtner, A.J., and R.M. Chervin, 1992: Ocean general circulation from a global eddy-resolving model. *J. Geophys. Res.,* **97,** 5493–5550.

Servain, J., J. Picaut, and J. Merle, 1982: Evidence of remote forcing in the equatorial Atlantic Ocean. *J. Phys. Oceanogr.*, **12,** 457–463.

Seneviratne, S. I., T. Corti, E. L. Davin, M. Hirschi, E. B. Jaeger, I. Lehner, B. Orlowsky and A. J. Teuling, 2010: Investigating soil moisture–climate interactions in a changing climate: A review. *Earth Sci. Rev*., **99**, 125–161.

Servain, J., I. Wainer, J. P. McCreary, and A. Dessier, 1999: Relationship between the Equatorial and meridional modes of climatic variability in the tropical Atlantic. *Geophys. Res. Lett.,* **26,** 485–488.

Shannon, L.V., A.J. Boyd, G.B. Brundrit, and J. Taunton-Clark, 1986: On the existence of an El Nino-type phenomenon in the Benguela system. *J. Mar. Res.*, **44**, 495-520.

Shinoda, T., M. Alexander, and H.H. Hendon, 2004: Remote response of the Indian Ocean to interannual SST variations in the tropical Pacific. *J. Climate*, **17**, 362-372.

Smagorinsky, J., 1958: On the numerical integration of the primitive equations of motion for baroclinic flow in a closed region. *Mon. Wea. Rev.*, **86**, 457-466.

Smith, R. D., M. E. Maltrud, F. Bryan, and M. W. Hecht, 2000: Numerical simulation of the North Atlantic Ocean at 1/10°. *J. Phys. Oceanogr.*, **30**, 1532–1561.

Smith, T. M., R. W. Reynolds, T. C. Peterson, and J. Lawrimore, 2008: Improvements to NOAA's historical merged land–ocean surface temperature analysis (1880–2006). *J. Climate*, **21**, 2283–2296.

Song, Q., G.A. Vecchi, and A.J. Rosati, 2007: Indian Ocean variability in the GFDL coupled climate model. *J. Climate*, **20**, 2895-2916.

Spencer, H., R.T. Sutton, J.M. Slingo, M. Roberts, and E. Black, 2005: Indian ocean climate and dipole variability in Hadley Centre coupled GCMs. *J. Climate*, **18**, 2286-2307.

Sperber, K.R., H. Annamalai, I.-S. Kang, A. Kitoh, A. Moise, A. Turner, B. Wang, and T. Zhou, 2012: The Asian summer monsoon: an Intercomparison of CMIP5 vs. CMIP3 simulations of the late 20th century. *Clim. Dyn.*, **41,** 2711-2744.

Stan, C., M. Khairoutdinov, C. A. DeMott, V. Krishnamurthy, D. M. Straus, D. A. Randall, J. L. Kinter, III, and J. Shukla, 2010: An ocean-atmosphere climate simulation with an embedded cloud resolving model. *Geophys. Res. Lett*., **37**, L01702, doi:10.1029/2009GL040822.

Stensrud, D. J., 2007: Parameterization schemes: Keys to understanding numerical weather prediction models. Cambridge University Press, New York, 459 pp

Stephens, G. L., and T. J. Greenwald, 1991: Observations of the Earth's radiation budget in relation to atmospheric hydrology. Part II: Cloud effects and cloud feedback. *J. Geophys. Res.*, **96**, 15 325–15 340.

Stevens, B., and S. Bony, 2013: What are climate models missing?. *Nature*, **340**, 1053–1054.

Stockdale, T. N., M. A. Balmaseda, and A. Vidard, 2006: Tropical Atlantic SST prediction with coupled ocean–atmosphere GCMs. *J. Climate*, **19**, 6047–6061.

von Storch, H., 1995: Inconsistencies at the interface of climate impacts studies and global climate research. *Z. Meteorol.*, **4**, 72–80.

Suarez, M. J., A. Arakawa, and D. A. Randall, 1983: The parameterization of the planetary boundary layer in the UCLA general circulation model: Formulation and results. *Mon. Wea. Rev.*, **111**, 2224–2243.

Suzuki, R., S.K. Behera, S. Iizuka, and T. Yamagata, 2004: Indian Ocean subrtopical dipole simulated using a coupled general circulation model. *J. Geophys. Res.*, **109**, C09001, doi:10.1029/2003JC001974.

Taylor, C. M., A. Gounou, F. Guichard, P. P. Harris, R. J. Ellis, F. Couvreux and M. De Kauwe, 2011: Frequency of Sahelian storm initiation enhanced over mesoscale soil-moisture patterns. *Nat. Geosci*., **4**, 430–433.

Taylor, C. M., R. A. M. de Jeu, F. Guichard, P. P. Harris and W. A. Dorigo, 2012: Afternoon rain more likely over drier soils. *Nature*, **489**, 423–426.

Taylor, K. E., R. J. Stouffer, and G. A. Meehl, 2012: An Overview of CMIP5 and the Experiment Design. Bull. Amer. *Meteorol. Soc.,* **93,** 485-498.

Thompson, D. W. J., and J. M. Wallace, 2000: Annular modes in the extratropical circulation. Part I: Month-to-month variability. *J. Climate*, **13**, 1000-1016.

Tiedtke, M., 1989: A comprehensive mass flux scheme for cumulus parameterization in large-scale models. *Mon. Wea. Rev.*, **117,** 1779-1800.

Tokinaga, H., and Y. Tanimoto, 2004: Seasonal transition of SST anomalies in the tropical Indian Ocean during El Niño and Indian Ocean Dipole years. *J. Meteor. Soc. Japan*, **82**, 1007-1018.

Tomita, H., H. Miura, S. Iga, T. Nasuno, and M. Satoh, 2005: A global cloud-resolving simulation: Preliminary results from an aqua planet experiment. *Geophys. Res. Lett.*, **32**, L08805, doi:10.1029/2005GL022459.

Tompkins, A. M., and L. Feudale, 2010: Seasonal ensemble predictions of West African Monsoon precipitation in the ECMWF system 3 with a focus on the AMMA special observing period in 2006. *Wea. Forecasting*, **25**, 768–788.

Tory, K. J., S. S. Chand, R. A. Dare, and J. L. McBride, 2013: An assessment of a model-, grid-, and basin-independent tropical cyclone detection scheme in selected CMIP3 global climate models. *J. Climate*, **26**, 5508-5522.

Tozuka, T., T. Doi, T. Miyasaka, N. Keenlyside, and T. Yamagata, 2011: Key factors in simulating the equatorial Atlantic zonal sea surface temperature gradient in a coupled general circulation model. *J. Geophys. Res.*, **116**, C06010, doi:10.1029/2010JC006717.

Uppala, S. M., and Coauthors, 2005: The ERA-40 re-analysis. *Quart. J. R. Meteorol. Soc.*, **131**, 2961-3012.

Veitch, J., P. Penven, and F. Shillington, 2010: Modeling equilibrium dynamics of the Benguela Current system. J. Phys. Oceanogr., 40, 1942–1964.

Venegas, S. A., L. A. Mysak, and D. N. Straub, 1997: Atmosphere-ocean coupled variability in the South Atlantic. *J. Climate*, **10**, 2904-2920.

Wacongne, S., and B. Piton, 1992: The near-surface circulation in the northeastern corner of the South Atlantic Ocean. *Deep-Sea Res.*, **39,** 1273–1298.

Wahl, S., M. Latif, W. Park, and N. Keenlyside, 2011: On the tropical Atlantic SST warm bias in the Kiel Climate Model. *Clim. Dyn.*, **36**, 891–906.

Wajsowicz, R.C., 2005: Potential predictability of tropical Indian Ocean SST anomalies. *Geophys. Res. Lett.*, **32**, L24702, doi:10.1029/2005GL024169.

Wallace, J. M., and D. S. Gutzler, 1981: Teleconnections in the geopotential height field during the Northern Hemisphere winter. *Mon. Wea. Rev.*, **109,** 784-812.

Walker, G.T., 1923: Correlation in seasonal variations of weather, VIII: a preliminary study of world weather. *Memoirs of the Indian Meteorological Department,* **24**, 75-131.

Walker, G. T., 1924: Correlation in seasonal variations of weather, IX: a further study of world weather. *Memoirs of the India Meteorological Department,* **24**, 275-332.

Walker, G. T. 1928: World weather. *Quart. J. Roy. Meteor. Soc.*, **54**, 79-87.

Wan, X., Chang, P., Jackson, C.S., Ji, L. and Li, M. 2011: Plausible effect of climate model bias on abrupt climate change simulations in Atlantic sector. *Deep-Sea Res. II,* **58**, 1904-1913.

Washington, W. M., A. J. Semtner, G. A. Meehl, D. J. Knight, and T. A. Mayer, 1980: A general circulation experiment with a coupled atmosphere, ocean and sea ice model. *J. Phys. Oceanogr.,* **10**, 1887-908.

Washington, W. M., and G. A. Meehl, 1989: Climate sensitivity due to increased CO2: experiments with a coupled atmosphere and ocean general circulation model. *Clim. Dyn.*, **4**,1-38.

Webster, P.J., A.M. Moore, J.P. Loschnigg, and R.R. Leben, 1999: Coupled ocean-atmosphere dynamics in the Indian Ocean during 1997-98. *Nature*, **401**, 356-360.

Wijffels, S., and G. Meyers, 2004: An intersection of oceanic waveguides: Variability in the Indonesian throughflow region. *J. Phys. Oceanogr.*, **34**, 1232-1253.

Williamson, D. L., J. T. Kiehl, and J. J. Hack, 1995: Climate sensitivity of the NCAR Community Climate Model (CCM2) to horizontal resolution. *Clim. Dyn*, **11,** 377–397.

Woodruff, S.D., and Coauthors, 2011: ICOADS Release 2.5: Extensions and enhancements to the surface marine meteorological archive. *Int. J. Climatol.*, **31**, 951-967.

Xie, P. and P. A. Arkin, 1996: Analysis of global monthly precipitation using gauge observations, satellite estimates, and numerical model predictions, *J. Climate*, **9**, 840-858.

Xie, S.-P., and S. G. H. Philander, 1994: A coupled ocean-atmosphere model of relevance to the ITCZ in the eastern Pacific. *Tellus A*, **46,** 340-350.

Xie, S.-P., 1996: Westward propagation of latitudinal asymmetry in a coupled ocean-atmosphere model. *J. Atmos. Sci.*, **53**, 3236-3250.

Xie, S.-P., H. Annamalai, F.A. Schott, and J.P. McCreary Jr., 2002: Structure and mechanisms of south Indian Ocean climate variability. *J. Climate*, **15**, 864-878.

Xie, S.-P., and J. A. Carton, 2004: Tropical Atlantic variability: Patterns, mechanisms, and impacts. *Earth's Climate: The Ocean-Atmosphere Interaction, Geophys. Monogr.,* Vol. 147, Amer. Geophys. Union, 121–142.

Xu, Z., M. Li, C. M. Patricola, and P. Chang, 2013a: Oceanic origin of southeast tropical Atlantic bias. *Clim. Dyn.,* doi:10.1007/s00382-013-1901-y.

Xu, Z., P. Chang, and W. Kim, 2013b: Diagnosing Southeast Tropical Atlantic SST and Ocean Circulation Biases in the CMIP5 Ensemble. *Clim. Dyn.*, submitted.

Xue, Y., F. De Sales, R. Vasic, C. R. Mechoso, A. Arakawa, S. Prince, 2010: Global and seasonal assessment of interactions between climate and vegetation biophysical processes: A GCM study with different land–vegetation representations. *J. Climate*, **23**, 1411–1433.

Xue, Y., A. Boone, and C. M. Taylor, 2012: Review of recent developments and the future prospective in west African atmosphere/land interaction studies. *Int. J. Geophys.*, doi:10.1155/2012/748921.

Yamagata, T., and S. Iizuka, 1995: Simulation of the tropical thermal domes in the Atlantic: a seasonal cycle. *J. Phys. Oceanogr.*, **25**, 2129-2140.

Yokoi, T., T. Tozuka, and T. Yamagata, 2009: Seasonal variations of the Seychelles Dome simulated in the CMIP3 models. *J. Phys. Oceanogr.*, **39**, 449-457.

Yokoi, T., T. Tozuka, and T. Yamagata, 2012: Seasonal and interannual variations of the SST above the Seychelles Dome. *J. Climate*, **25**, 800-814.

Yu, J.-Y., and C. R. Mechoso, 1999: Links between annual variations of Peruvian stratocumulus clouds and of SST in the eastern equatorial Pacific. *J. Climate*, **12**, 3305–3318.

Yuan, C., T. Tozuka, J. J. Luo, and T. Yamagata, 2014: Predictability of the subtropical dipole modes in a coupled ocean-atmosphere model. *Climate Dyn.*, **42,** 1291-1308.

Zebiak, S. E., 1993: Air–sea interaction in the equatorial Atlantic region. *J. Climate*, **6,** 1567–1586.

Zermeno, D., and C. Zhang, 2013: Possible root causes of the surface westerly biases over the equatorial Atlantic in global climate models. *J. Climate*, **26,** 8154–8168.

Zhao, M., and H. H. Hendon, 2009: Representation and prediction of the Indian Ocean Dipole in the POAMA seasonal forecast model. *Q. J. R. Meteorol. Soc.*, **135**, 337-352.

Zeng, N., R. E. Dickinson, and X. Zeng, 1996: Climatic impact of Amazon deforestation—A mechanistic model study. *J. Climate*, **9**, 859–883.

Zhao, M., M. I. Held, S.-J. Lin, and G. A. Vecchi, 2009: Simulations of global hurricane climatology, internannual variability, and response to global warming using a 50-km resolution GCM. *J. Climate*, **22**, 6653–6678.

Zhong, A., H.H. Hendon, and O. Alves, 2005: Indian Ocean variability and its association with ENSO in a global coupled model. *J. Climate*, **18**, 3634-3649.

Captions

Table 1. List of the 25 coupled GCMs that are part of the CMIP5 ensemble mean shown in Figs. 1b, 2b, and 3, and list of the 22 coupled GCMs that are part of the CMIP3 ensemble mean shown in Fig. 14.

Figure 1. Schematic equatorial cross sections of tropical Pacific for (a) neutral conditions, and (b) El Niño conditions. The Walker cell (yellow arrows) dominates the atmospheric circulation with surface winds flowing from the eastern Pacific cold tongue (blue ellipse in panel a) toward the western Pacific warm pool (red ellipse in a), where high SST drive deep convection. In the upper troposphere this is accompanied by divergent flow, with winds blowing toward the eastern Pacific, where they sink over the relatively cool SST. The surface winds drive the westward equatorial ocean current at the surface and, indirectly, the eastward undercurrent. Upwelling of cold waters (dark blue shading) from below the sharp vertical temperature gradient (thermocline) helps to keep the eastern Pacific cool. During El Niño events (panel b), the surface winds weaken, warm waters and convection move to the center of the basin, and upwelling weakens. This is accompanied by deepening of the thermocline in the east and shoaling in the west.

Figure 2. Climatological annual mean precipitation (mm/day) in (a) the GPCP observations (a blend of satellite and rain gauge data; Adler et al. 2003), and (b) the ensemble mean of CMIP5 pre-industrial control simulations (see Table 1). Features of interest are labeled in panel a. These are: the North Pacific and North Atlantic storm

tracks, the Intertropical Convergence Zone (ITCZ), the South Pacific Convergence Zone (SPCZ), and the South Atlantic Convergence Zone (SACZ).

Figure 3. (a) Climatological annual mean SST (ºC) in the OISST observations (a blend of in-situ and satellite data; Reynolds et al. 2002). (b) SST errors (K) relative to OISST for an ensemble mean of CMIP5 pre-industrial control simulations.

Figure 4. Annual mean wind stress (vectors; N m^{-2}; reference vector in upper right corner) over the tropical oceans (TropFlux, http://www.locean-ipsl.upmc.fr/tropflux/). The shading indicates the vector magnitude.

Figure 5. Seasonal cycle of zonal mean SST (colors) and precipitation (gray shaded) in the eastern tropical Pacific Ocean (140-90°W). Vectors represent the wind on the equator. Panel (0) shows OISST and TRMM satellite data (Adler et al. 2000). Panels (1-f) are CMIP3-generation GCMs. (from de Szoeke and Xie 2008)

Figure 6. Biases of the CMIP5 ensemble mean (see Table 1) relative to observed precipitation from GPCP, near-surface winds from ICOADS ship-based observations (Woodruff et al. 2011), and SST from OISST. (a) Boreal spring (MAM) biases of precipitation (shading; mm d^{-1}) and near-surface winds (reference vector 1 m s^{-1}). (b) Boreal summer (JJA) biases of SST (K).

Figure 7. Boreal spring (MAM) precipitation (shading; mm/day) and SST (contours; interval 1ºC) in (a) Climate Prediction Center (CPC) Merged Analysis of precipitation (CMAP; Xie and Arkin, 1996), (b) UTCM with Kuo convection scheme, (c)

UTCM with Emanuel convection scheme, and (d) UTCM with Tiedtke convection scheme.

Figure 8. Schematics of the Angola Benguela Frontal Zone (ABFZ) and the regional ocean circulation system. Vectors indicate the annual-mean winds, color and contour show the annual mean SST, and solid (dashed) arrows show major surface (subsurface) currents. The features shown include the equatorward Benguela Current (BC), the poleward Guinea and Angola currents (GC and AC, respectively), and the eastward South Equatorial Counter Current (SECC). Subsurface currents include the eastward Equatorial Under Current (EUC) and South Equatorial Under Current (SEUC). At about 10ºS there is a clockwise circulation associated with the shallow mixed layer of the Angola Dome (AD).

Figure 9. The alongshore temperature in °C averaged within a 1° wide band adjacent to the coast of Angola and Namibia from the equator to 30°S in NCEP/CFSR reanalysis product (Saha et al. 2010).

Figure 10. Composites of anomalous SST (shading; units K), precipitation (contours; interval 1 mm/d), and surface winds (vectors; reference 1 m/s), based on ERA 40 data from 1958-2001 (Uppala et al. 2005). The panels show (a) the meridional mode, composited on 2 standard deviations of the SST difference between NTA (40-10ºW, 10-20ºN) and STA (20ºW-20ºE, 25-5ºS), (b) the zonal mode (Atlantic Niño), based on 2 standard deviations of SST in the ATL3 region (20ºW-0, 3ºS-3ºN), and (c) the Benguela Niño, based on 2 standard deviations of SST in the ABA region (8ºE-

coast, 20-10ºS). The averaging areas for the three indices are marked by grey rectangles in the individual panels.

Figure 11. (a) Annual mean 20°C isotherm depth based on the World Ocean Atlas 2009 observations (Locarnini et al. 2006). (b) Same as (a), but for the ensemble average of three CGCMs that erroneously displace the upwelling dome (shallow thermocline) eastward (IPSL-CM5B-LR, BCC-CSM1.1, and FGOALS-g2). The CGCM results are from experiment "historical" of the CMIP5 intercomparison, in which models are forced with historical concentrations of greenhouse gases. The dome is located in the southwestern Indian Ocean in observations, whereas it is near Indonesia in the models.

Figure 12: A composite dipole mode event derived from GISST 2.3b SST (Rayner et al. 1996), NCEP reanalysis winds (Kalnay et al. 1996), and CMAP precipitation. Evolution of composite SST and surface wind anomalies are shown from (a) May-June to (d) November-December. The statistical significances of the analyzed anomalies were estimated by the two-tailed *t*-test. Anomalies of SSTs and winds exceeding 90% significance are indicated by shading and bold arrows, respectively. (from Saji et al. 1999)

Figure 13. Intermodel relationship between the amplitude of the IOD (measured by the Dipole Mode Index, DMI), and components of the Bjerknes feedback, including the sensitivity (per one standard deviation of the predictor) of (a) 850-mb winds to the DMI, (b) SST to thermocline depth, and (c) thermocline depth to 850-mb winds. The sensitivity is obtained by multiplying regression coefficient with a one-standard

deviation value of the predictor. Wind is averaged over the central-eastern equato-rial tropical Indian Ocean (EEIO, Eq.-10°S, 80°E-100°E). SST and thermocline are averaged over the eastern pole of the IOD (Eq.-10°S, 90°E-110°E). Observations used are listed in the legend. The p-values for all three correlation coefficients are less than 0.0001. (from Cai and Cowan 2013)

Figure 14. CMIP3 ensemble mean (see Table 1) composites of (a) mixed-layer temperature tendency, (b) surface heat flux, and (c) oceanic term, which is sum of the horizontal advection, entrainment, and horizontal and vertical diffusion. Units are 10^{-8} K s^{-1}.

Figure 15. Seasonal mean biases of rainfall (a), solar radiation (b), mean temperature (c) and potential evapotranspiration (d) for ERA-Interim reanalysis (Dee et al. 2011) and nine regional configurations for 12 synoptic stations across Senegal. Mean biases are computed over the 1990-2000 period from 1 May-30 November (from Oettli et al. 2011, Environ. Res. Lett. 6 (2011), doi:10.1088/1748-9326/6/1/014008).

Figure 16. Maps of errors in simulation of annual mean sea-surface temperature (SST) from the Reynolds SST data (provided by the NOAA-CIRES Climate Diagnostics Center, Boulder, Colorado, USA, from their Web site at http:// http://www.esrl.noaa.gov/psd/). Units are K. (a) CM2.1. (b) CM2.5. (from Delworth et al. 2012)

Figure 17. (a) Seasonal cycle of rainfall (mm/day) averaged in the Sahel region (10º–20ºN, 20ºW–10ºE) for CMAP (black line with circles), GPCP (grey line with

crosses), CM 2.1 (red line with squares), and CM 2.5 (blue line with triangles). (b) As in (a) but for the northern South American region: 10ºS–10ºN, 75º–55ºW. (from Doi et al. 2012)

Figure 18. Schematic summarizing common GCM biases in the tropics. The individual features highlighted are: surface wind biases (hollow arrows), cold and warm SST biases (blue and red ellipses, respectively), and wet and dry precipitation biases (grey ellipses and yellow dots, respectively). The shading over the continents represents orographic heights.

A. Tables

modeling center	CMIP5 ensemble	CMIP3 ensemble
Commonwealth Scientific and Industrial Research Organization (CSIRO) and Bureau of Meteorology (BOM) Australia	ACCESS1-0	
	ACCESS1-3	
Beijing Climate Center, China Meteorological Administration	bcc-csm1-1	
College of Global Change and Earth System Science, Beijing Normal University	BNU-ESM	
Canadian Centre for Climate Modelling and Analysis	CanESM2	cccma_cgcm3_1 cccma_cgcm3_1_t63
National Center for Atmospheric Research	CCSM4	ncar_ccsm3_0
		ncar_pcm1
Centre National de Recherches Météorologiques		cnrm_cm3
Commonwealth Scientific and Industrial Research Organization	CSIRO-Mk3-6-0	csiro_mk3_0
EC-EARTH consortium	EC-EARTH	
Istituto Nazionale di Geofisica e Vulcanoglogia		ingv_echam4
LASG, Institute of Atmospheric Physics, Chinese Academy of Sciences	FGOALS-g2	iap_fgoals1_0_g
	FGOALS-s2	
The First Institute of Oceanography, SOA, China	FIO-ESM	
NOAA Geophysical Fluid Dynamics Laboratory	GFDL-CM3	gfdl_cm2_0
	GFDL-ESM2G	gfdl_cm2_1
	GFDL-ESM2M	
NASA Goddard Institute for Space Studies	GISS-E2-H	giss_aom
	GISS-E2-R	giss_model_e_h giss_model_e_r
Met Office Hadley Centre	HadGEM2-ES	ukmo_hadcm3
		ukmo_hadgem1
Institute for Numerical Mathematics	inmcm4	inmcm3_0
Institut Pierre-Simon Laplace		ipsl_cm4
Meteorological Institute, University of Bonn		miub_echo_g
Atmosphere and Ocean Research Institute (The University of Tokyo), National Institute for Environmental Studies, and Japan Agency for Marine-Earth Science and Technology	MIROC4h	miroc3_2_medres
	MIROC5	miroc3_2_hires
	MIROC-ESM	
Max-Planck-Institut für Meteorologie (Max Planck Institute for Meteorology)	MPI-ESM-LR	mpi_echam5
	MPI-ESM-MR	
Meteorological Research Institute	MRI-CGCM3	mri_cgcm2_3_2a
Norwegian Climate Centre	NorESM1-M	

Table 1. List of the 25 coupled GCMs that are part of the CMIP5 ensemble mean shown in Figs. 1b, 2b, and 3, and list of the 22 coupled GCMs that are part of the CMIP3 ensemble mean shown in Fig. 14.

B. Figures

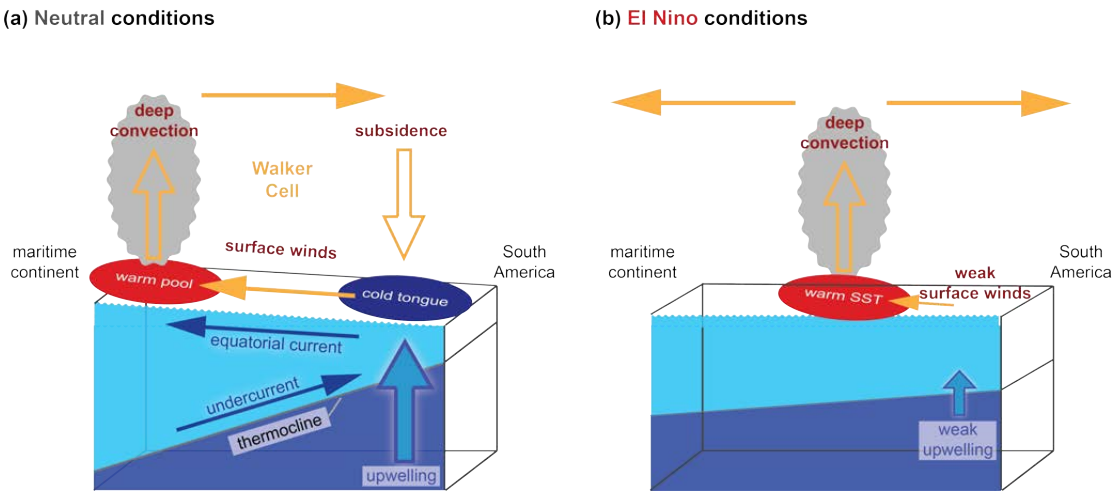

Figure 1. Schematic equatorial cross sections of tropical Pacific for (a) neutral conditions, and (b) El Niño conditions. The Walker cell (yellow arrows) dominates the atmospheric circulation with surface winds flowing from the eastern Pacific cold tongue (blue ellipse in panel a) toward the western Pacific warm pool (red ellipse in a), where high SST drive deep convection. In the upper troposphere this is accompanied by divergent flow, with winds blowing toward the eastern Pacific, where they sink over the relatively cool SST. The surface winds drive the westward equatorial ocean current at the surface and, indirectly, the eastward undercurrent. Upwelling of cold waters (dark blue shading) from below the sharp vertical temperature gradient (thermocline) helps to keep the eastern Pacific cool. During El Niño events (panel b), the surface winds weaken, warm waters and convection move to the center of the basin, and upwelling weakens. This is accompanied by deepening of the thermocline in the east and shoaling in the west.

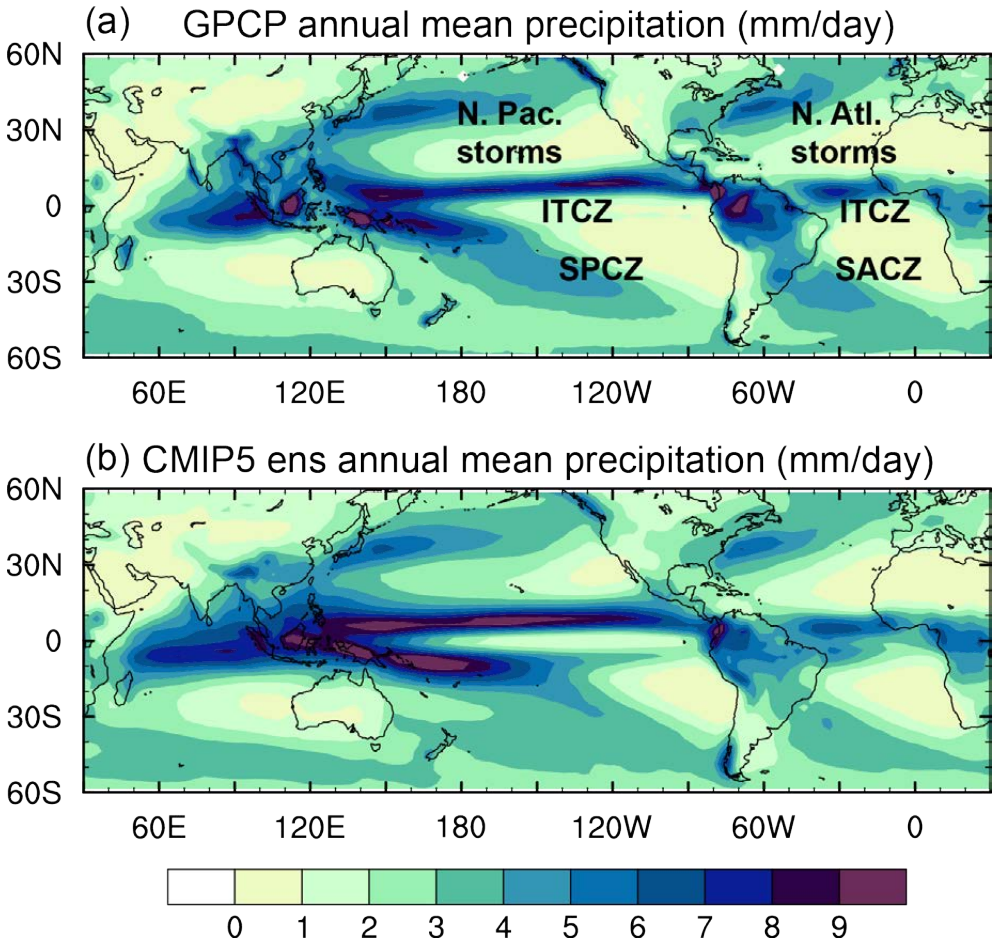

Figure 2. Climatological annual mean precipitation (mm/day) in (a) the GPCP observations (a blend of satellite and rain gauge data; Adler et al. 2003), and (b) the ensemble mean of CMIP5 pre-industrial control simulations (see Table 1). Features of interest are labeled in panel a. These are: the North Pacific and North Atlantic storm tracks, the Intertropical Convergence Zone (ITCZ), the South Pacific Convergence Zone (SPCZ), and the South Atlantic Convergence Zone (SACZ).

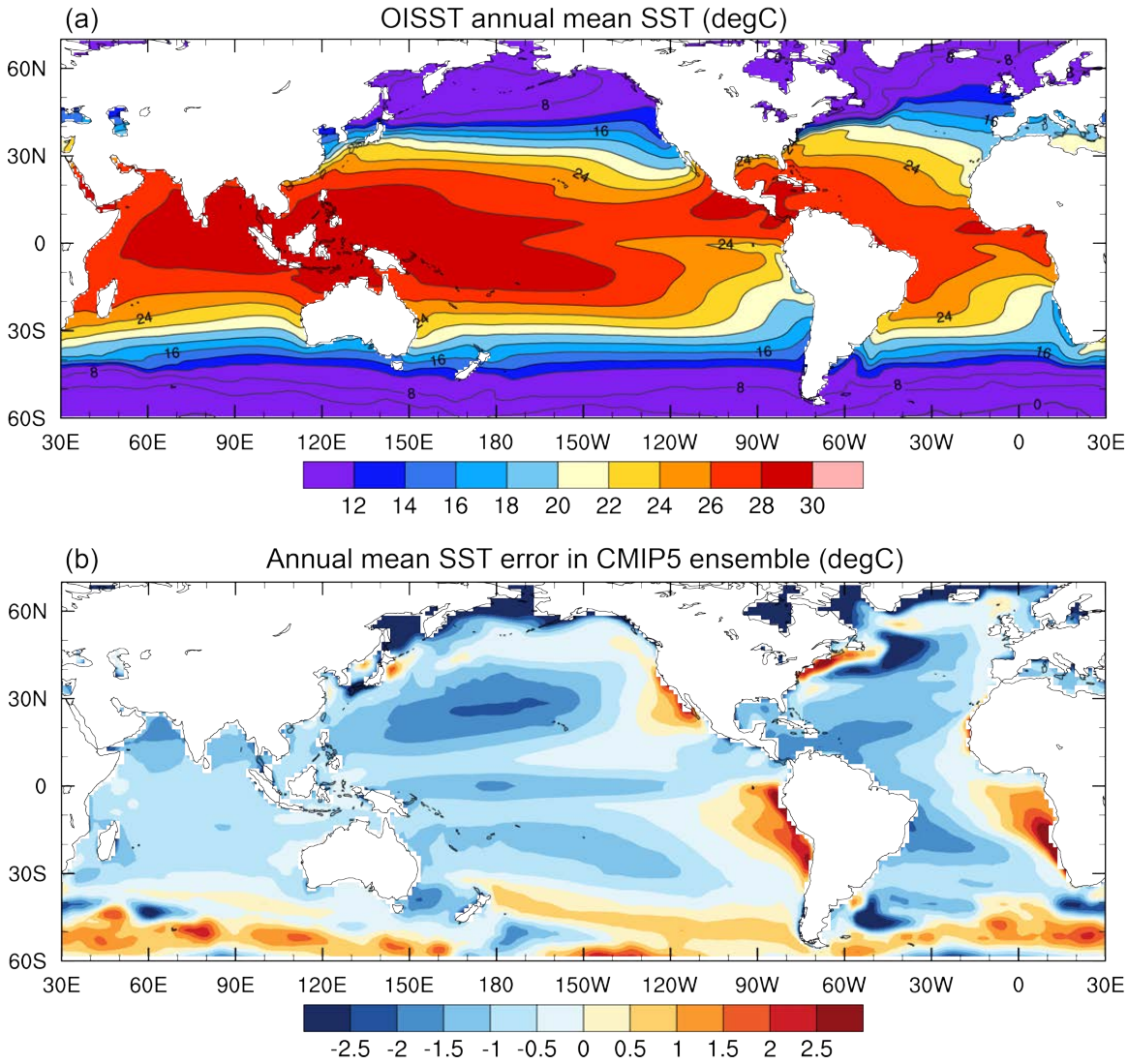

Figure 3. (a) Climatological annual mean SST (ºC) in the OISST observations (a blend of in-situ and satellite data; Reynolds et al. 2002). (b) SST errors (K) relative to OISST for an ensemble mean of CMIP5 pre-industrial control simulations.

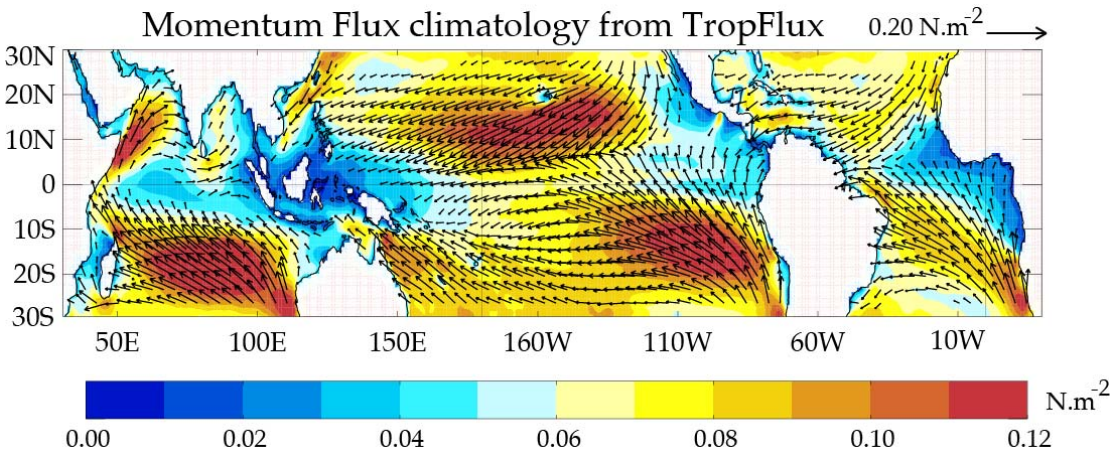

Figure 4. Annual mean wind stress (vectors; N m^{-2}; reference vector in upper right corner) over the tropical oceans (TropFlux, http://www.locean-ipsl.upmc.fr/tropflux/). The shading indicates the vector magnitude.

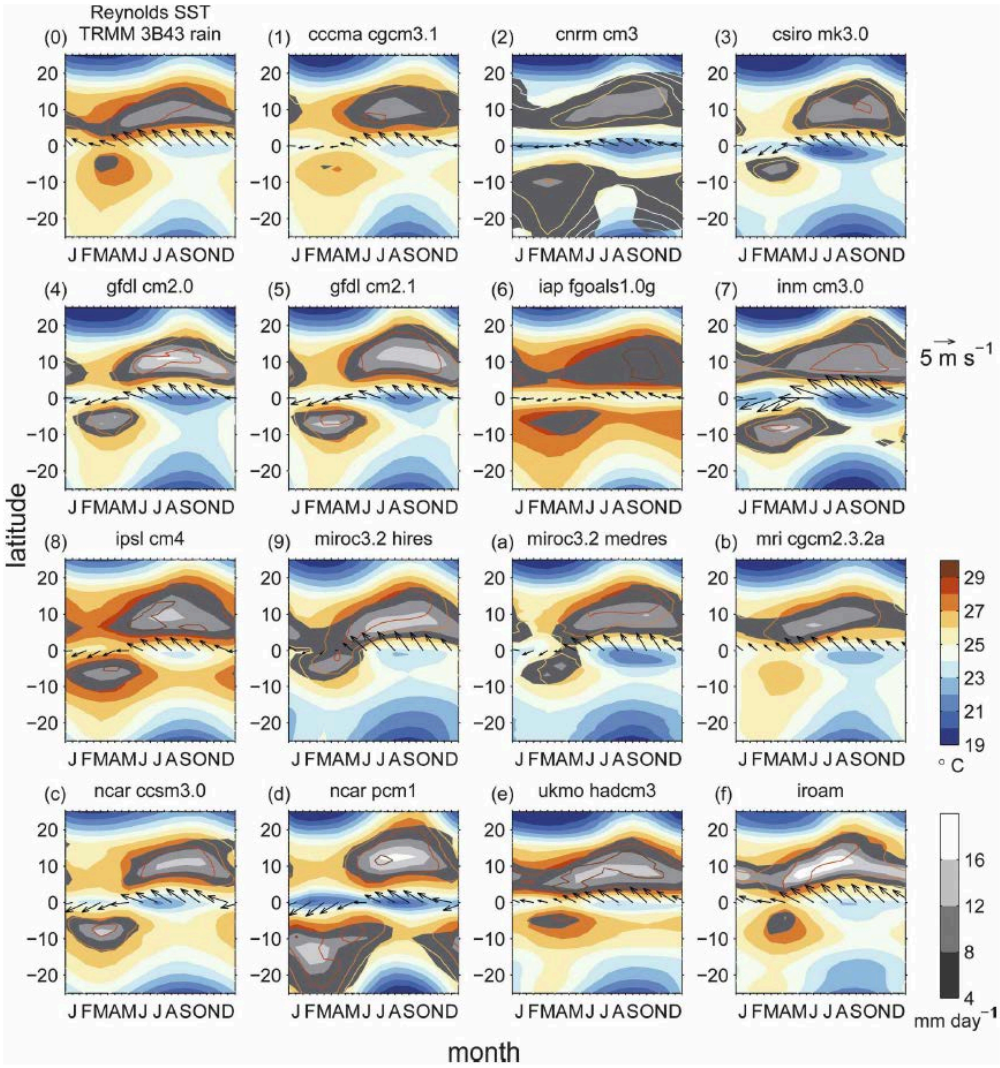

Figure 5. Seasonal cycle of zonal mean SST (colors) and precipitation (gray shaded) in the eastern tropical Pacific Ocean (140-90°W). Vectors represent the wind on the equator. Panel (0) shows OISST and TRMM satellite data (Adler et al. 2000). Panels (1-f) are CMIP3-generation GCMs. (from de Szoeke and Xie 2008)

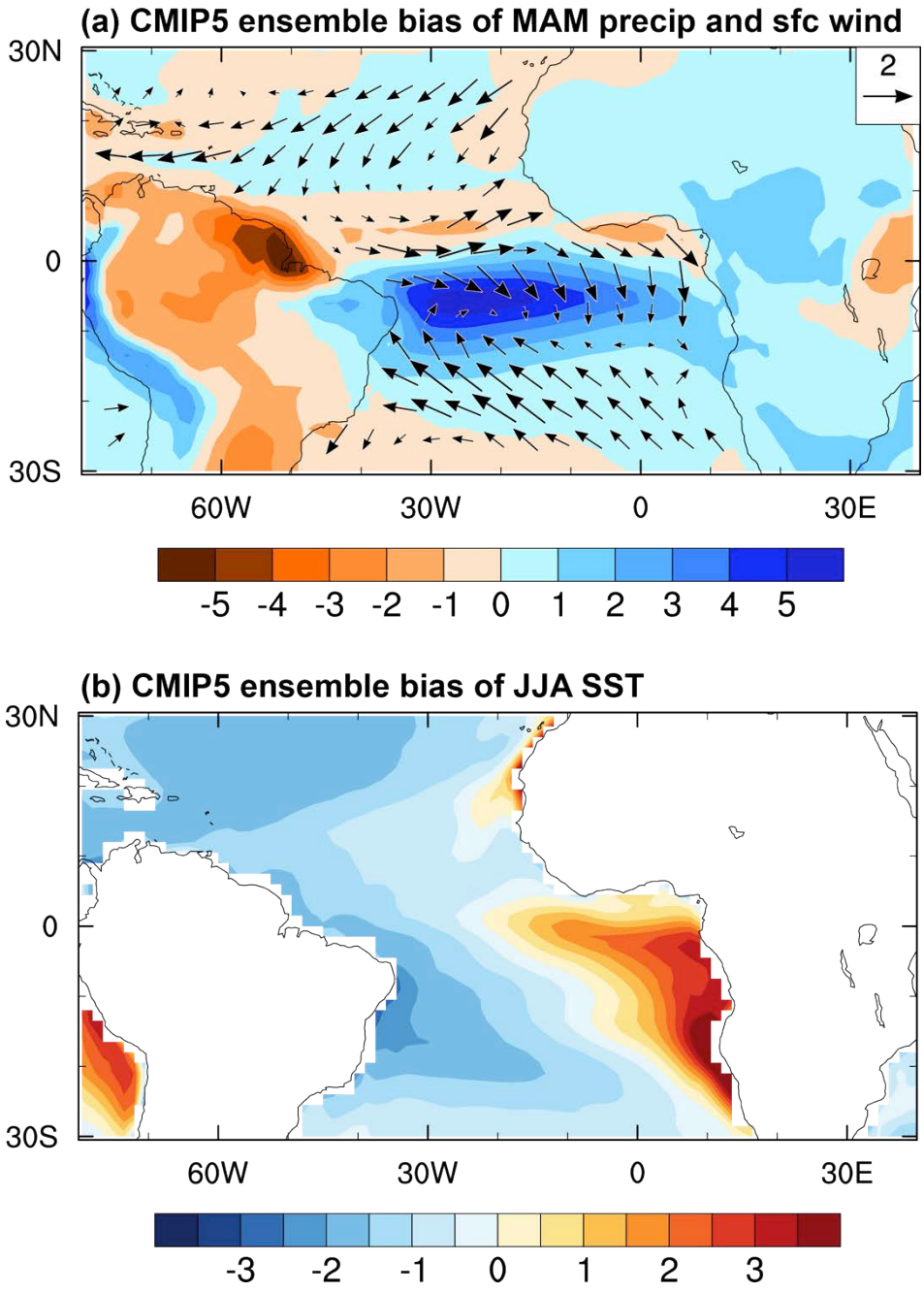

Figure 6. Biases of the CMIP5 ensemble mean (see Table 1) relative to observed precipitation from GPCP, near-surface winds from ICOADS ship-based observations (Woodruff et al. 2011), and SST from OISST. (a) Boreal spring (MAM) biases of precipitation (shading; mm d^{-1}) and near-surface winds (reference vector 1 m s^{-1}). (b) Boreal summer (JJA) biases of SST (K).

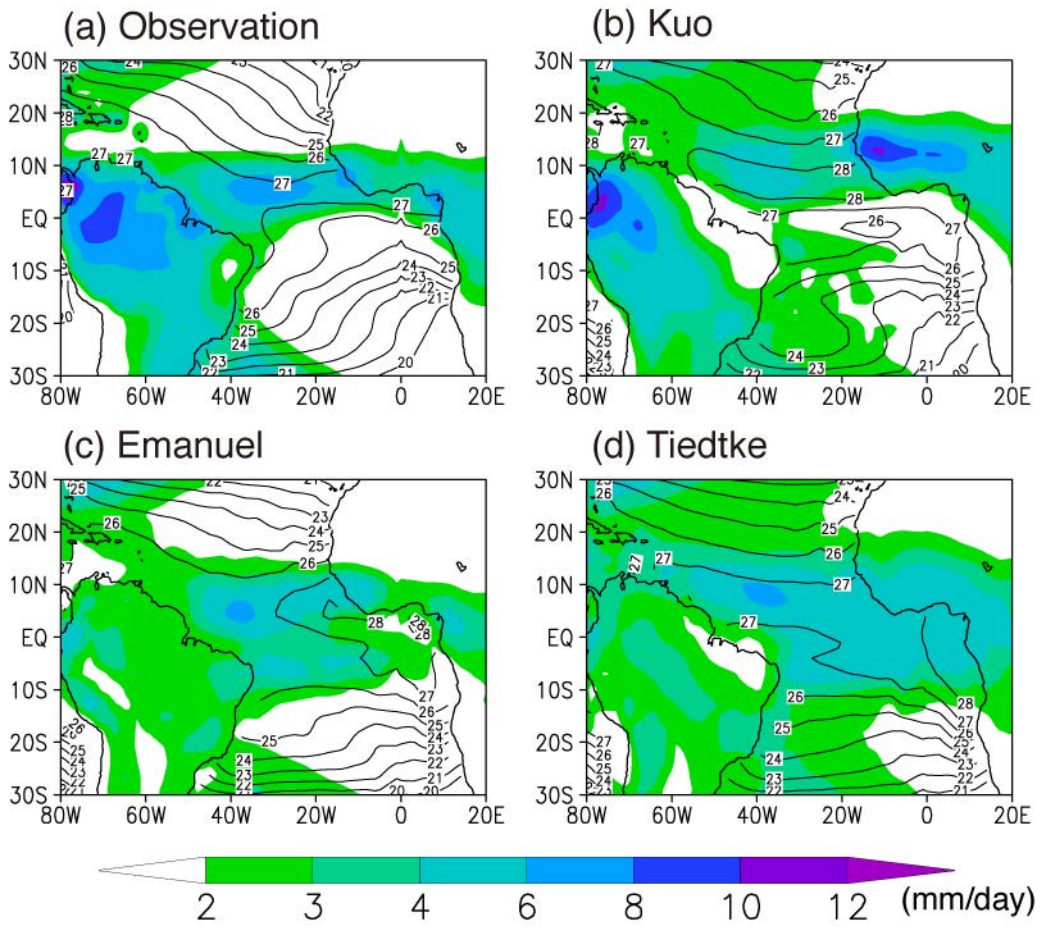

Figure 7. Boreal spring (MAM) precipitation (shading; mm/day) and SST (contours; interval 1ºC) in (a) Climate Prediction Center (CPC) Merged Analysis of precipitation (CMAP; Xie and Arkin, 1996), (b) UTCM with Kuo convection scheme, (c) UTCM with Emanuel convection scheme, and (d) UTCM with Tiedtke convection scheme.

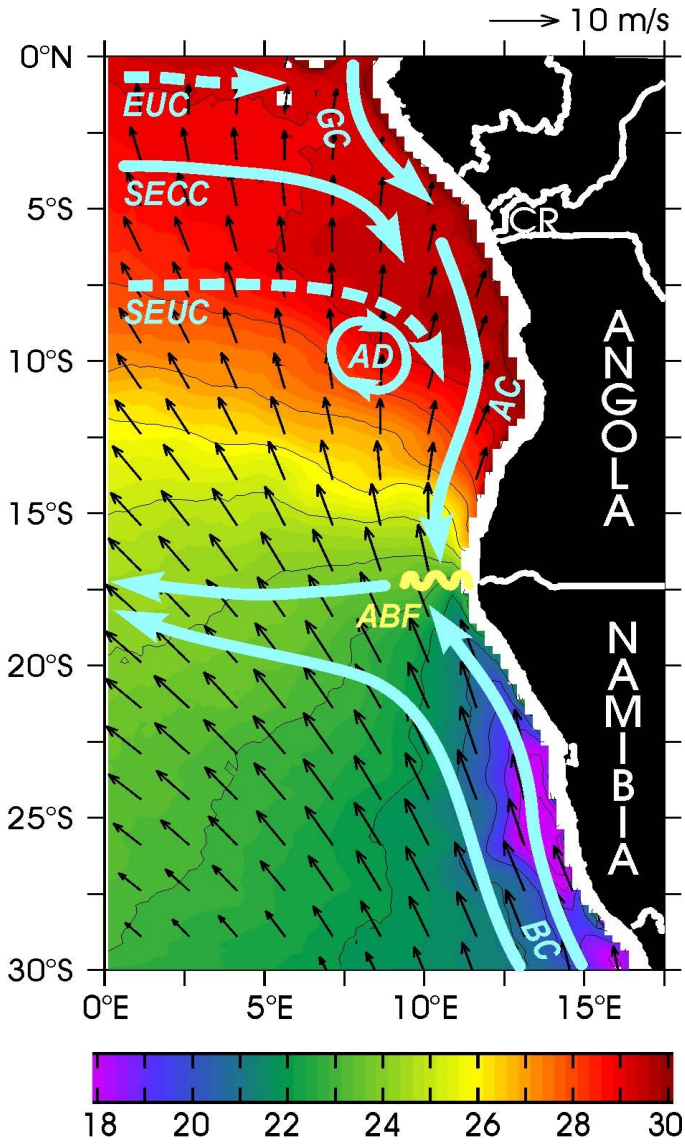

Figure 8. Schematics of the Angola Benguela Frontal (ABF) zone and the regional ocean circulation system. Vectors indicate the annual-mean winds, color and contour show the annual mean SST, and solid (dashed) arrows show major surface (subsurface) currents. The features shown include the equatorward Benguela Current (BC), the poleward Guinea and Angola currents (GC and AC), and the eastward South Equatorial Counter Current (SECC). Subsurface currents include the eastward Equatorial Under Current (EUC) and South Equatorial Under Current (SEUC). At about 10ºS there is a clockwise circulation associated with the shallow mixed layer of the Angola Dome (AD).

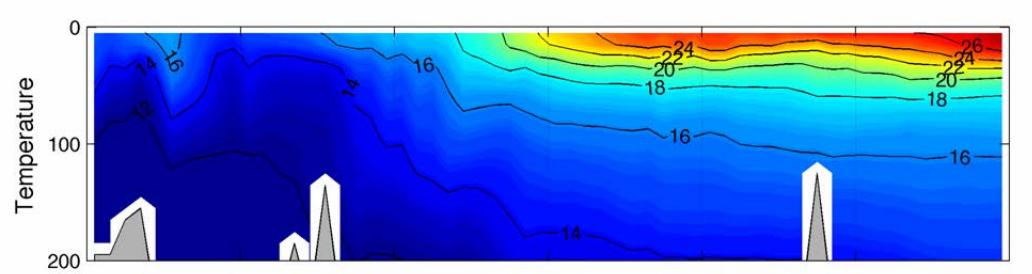

Figure 9. The alongshore temperature in °C averaged within a 1° wide band adjacent to the coast of Angola and Namibia from the equator to 30°S in NCEP/CFSR reanalysis product (Saha et al. 2010).

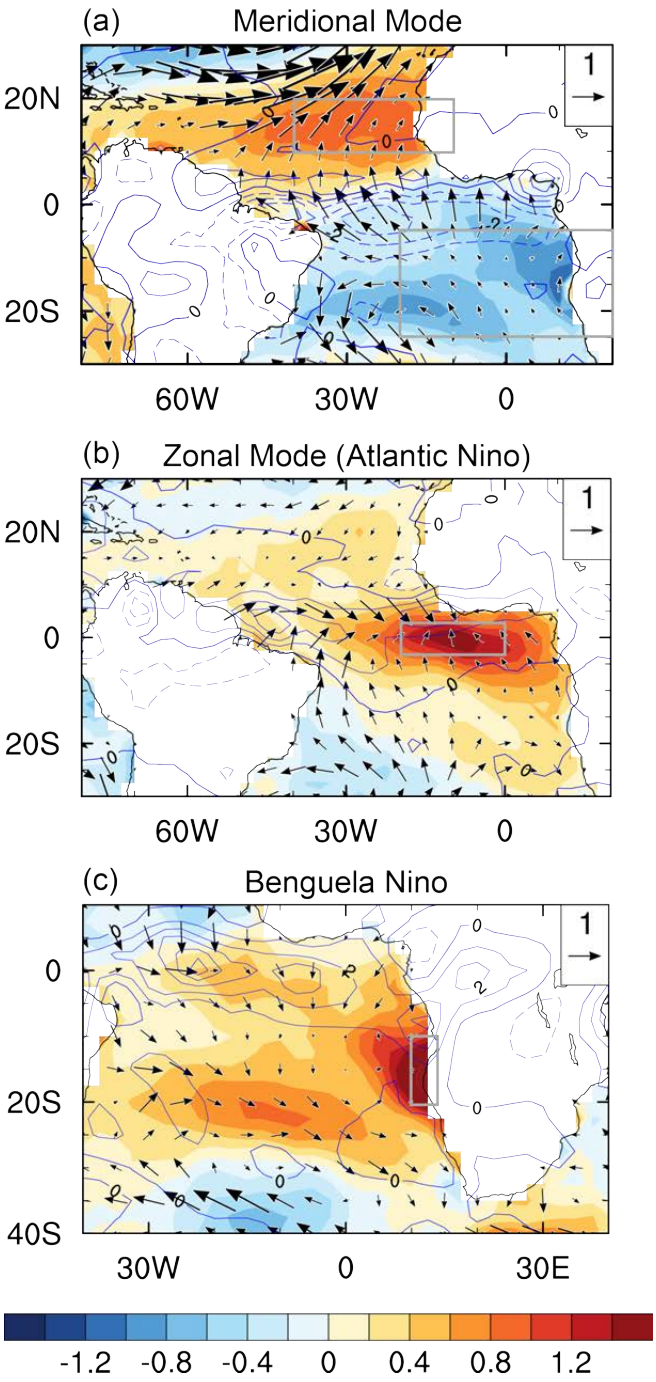

Figure 10. Composites of anomalous SST (shading; units K), precipitation (contours; interval 1 mm/d), and surface winds (vectors; reference 1 m/s), based on ERA 40 data from 1958-2001 (Uppala et al. 2005). The panels show (a) the meridional mode, composited on 2 standard deviations of the SST difference between NTA (40-10ºW, 10-20ºN) and STA (20ºW-20ºE, 25-5ºS), (b) the zonal mode (Atlantic Niño), based on 2 standard deviations of SST in the ATL3 region (20ºW-0, 3ºS-3ºN), and (c) the Benguela Niño, based on 2 standard deviations of SST in the ABA region (8ºE-coast, 20-10ºS). The averaging areas for the three indices are marked by grey rectangles in the individual panels.

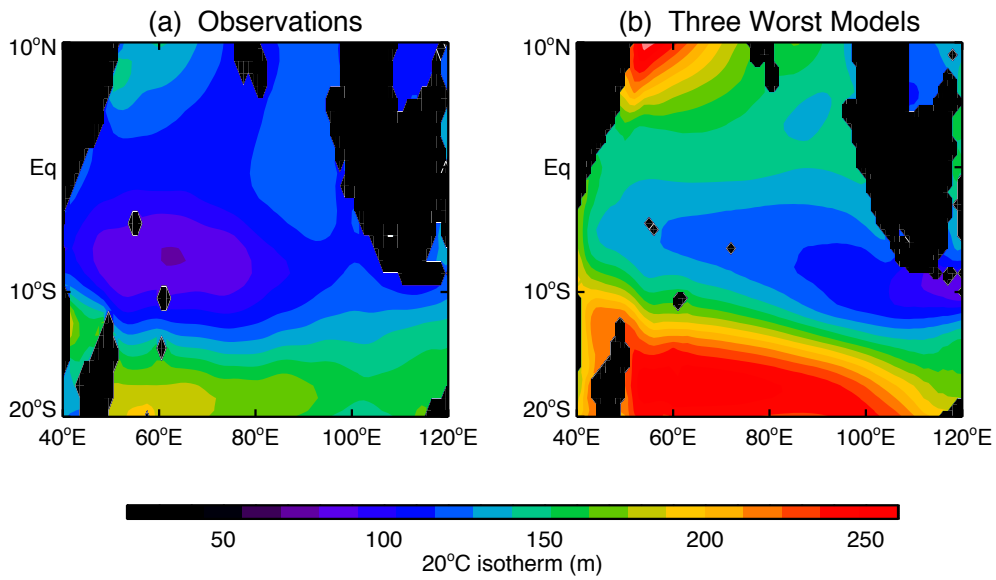

Figure 11. (a) Annual mean 20°C isotherm depth based on the World Ocean Atlas 2009 observations (Locarnini et al. 2006). (b) Same as (a), but for the ensemble average of three CGCMs that erroneously displace the upwelling dome (shallow thermocline) eastward (IPSL-CM5B-LR, BCC-CSM1.1, and FGOALS-g2). The CGCM results are from experiment "historical" of the CMIP5 intercomparison, in which models are forced with historical concentrations of greenhouse gases. The dome is located in the southwestern Indian Ocean in observations, whereas it is near Indonesia in the models.

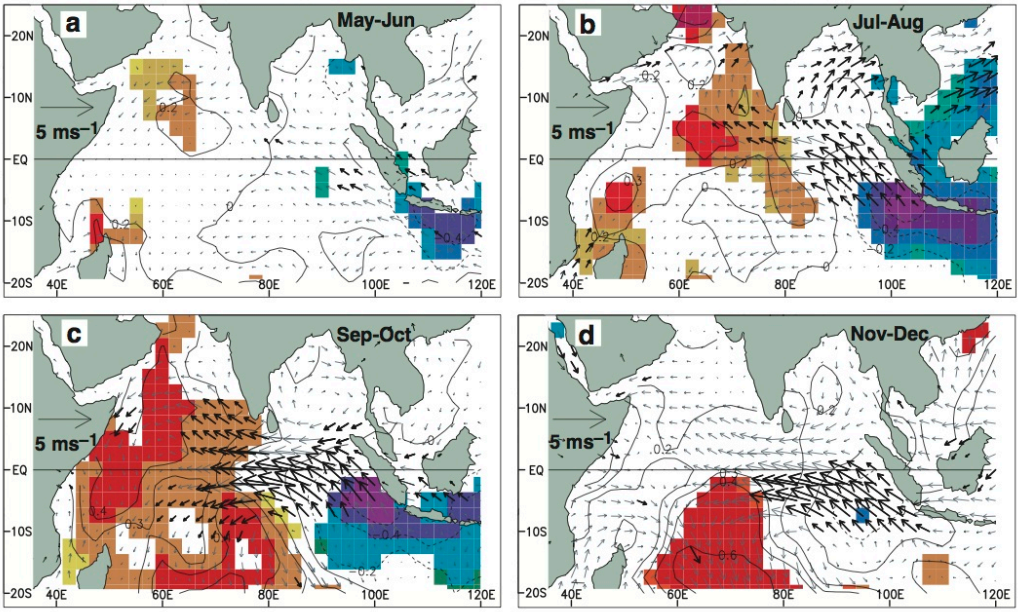

Figure 12: A composite dipole mode event derived from GISST 2.3b SST (Rayner et al. 1996), NCEP reanalysis winds (Kalnay et al. 1996), and CMAP precipitation. Evolution of composite SST and surface wind anomalies are shown from (a) May-June to (d) November-December. The statistical significances of the analyzed anomalies were estimated by the two-tailed *t*-test. Anomalies of SSTs and winds exceeding 90% significance are indicated by shading and bold arrows, respectively. (from Saji et al. 1999)

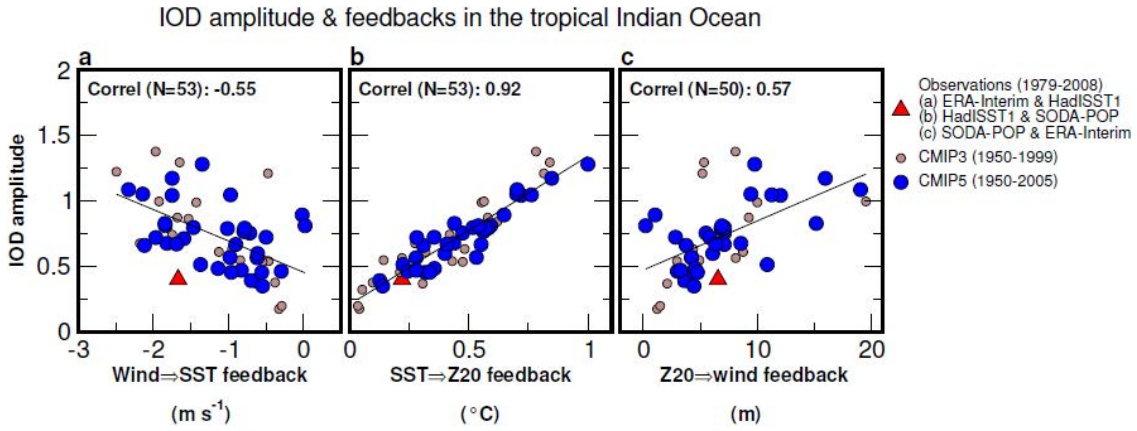

Figure 13. Intermodel relationship between the amplitude of the IOD (measured by the Dipole Mode Index, DMI), and components of the Bjerknes feedback, including the sensitivity (per one standard deviation of the predictor) of (a) 850-mb winds to the DMI, (b) SST to thermocline depth, and (c) thermocline depth to 850-mb winds. The sensitivity is obtained by multiplying regression coefficient with a one-standard deviation value of the predictor. Wind is averaged over the central-eastern equatorial tropical Indian Ocean (EEIO, Eq.-10°S, 80°E-100°E). SST and thermocline are averaged over the eastern pole of the IOD (Eq.-10°S, 90°E-110°E). Observations used are listed in the legend. The p-values for all three correlation coefficients are less than 0.0001. (from Cai and Cowan 2013)

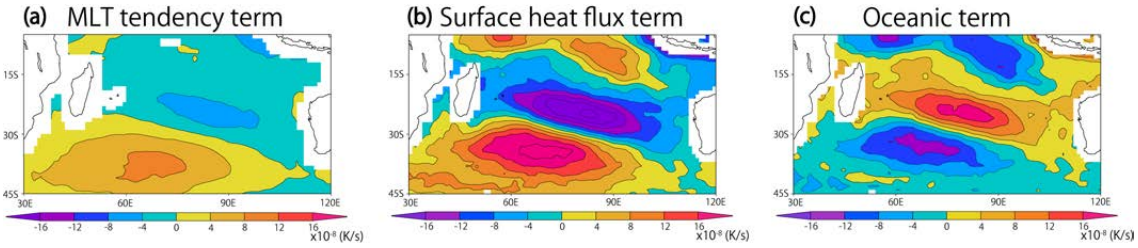

Figure 14. CMIP3 ensemble mean (see Table 1) composites of (a) mixed-layer temperature tendency, (b) surface heat flux, and (c) oceanic term, which is sum of the horizontal advection, entrainment, and horizontal and vertical diffusion. Units are 10^{-8} K s^{-1}.

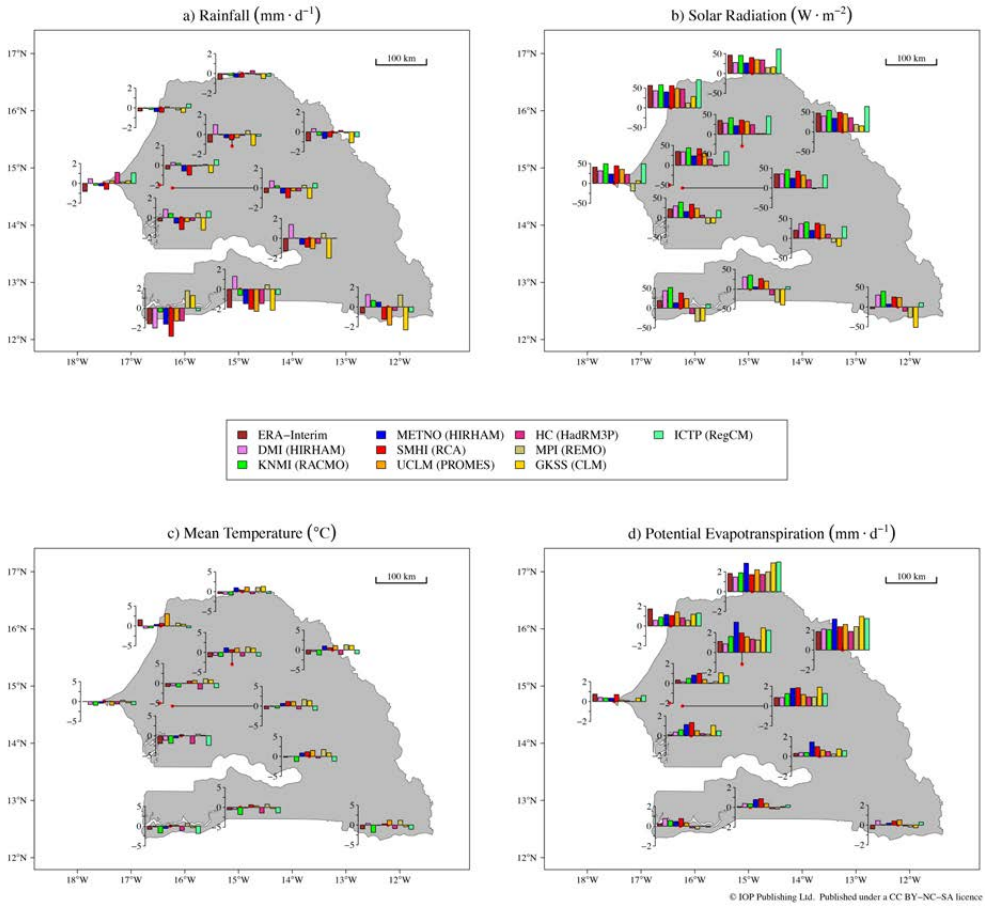

Figure 15. Seasonal mean biases of rainfall (a), solar radiation (b), mean temperature (c) and potential evapotranspiration (d) for ERA-Interim reanalysis (Dee et al. 2011) and nine regional configurations for 12 synoptic stations across Senegal. Mean biases are computed over the 1990-2000 period from 1 May-30 November (from Oettli et al. 2011, Environ. Res. Lett. 6 (2011), doi:10.1088/1748-9326/6/1/014008).

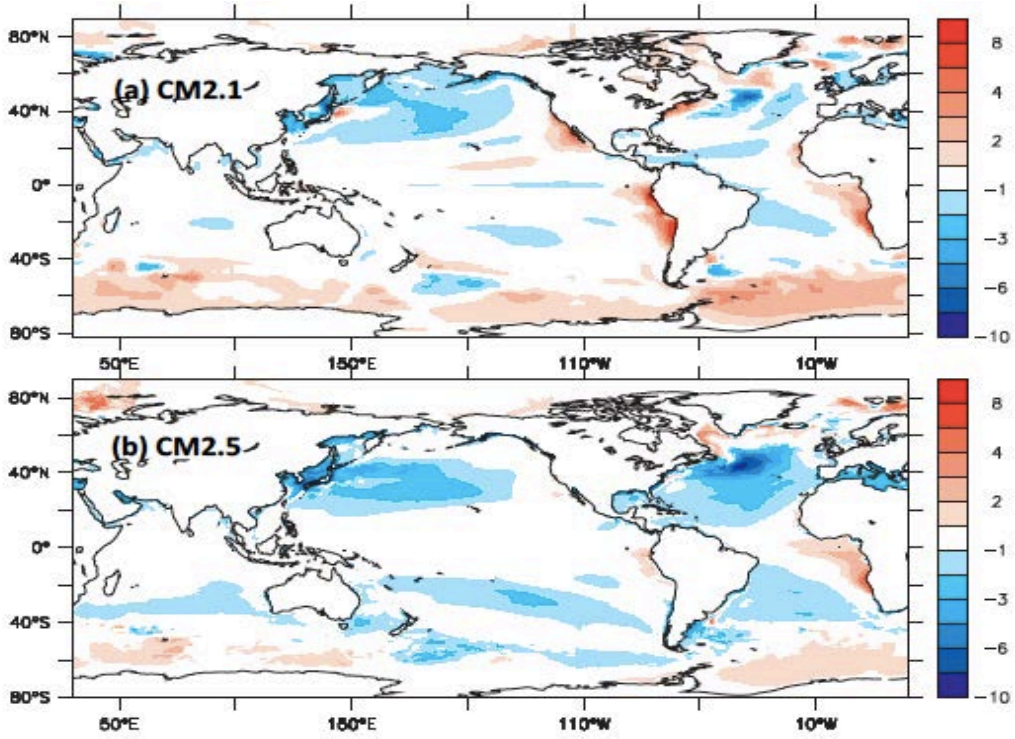

Figure 16. Maps of errors in simulation of annual mean sea-surface temperature (SST) from the Reynolds SST data (provided by the NOAA-CIRES Climate Diagnostics Center, Boulder, Colorado, USA, from their Web site at http:// http://www.esrl.noaa.gov/psd/). Units are K. (a) CM2.1. (b) CM2.5. (from Delworth et al. 2012)

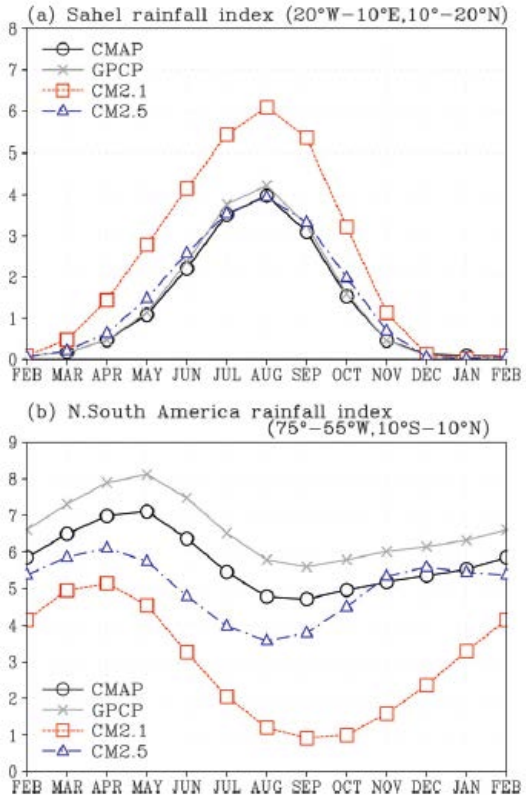

Figure 17. (a) Seasonal cycle of rainfall (mm/day) averaged in the Sahel region (10º–20ºN, 20ºW–10ºE) for CMAP (black line with circles), GPCP (grey line with crosses), CM 2.1 (red line with squares), and CM 2.5 (blue line with triangles). (b) As in (a) but for the northern South American region: 10ºS–10ºN, 75º–55ºW. (from Doi et al. 2012)

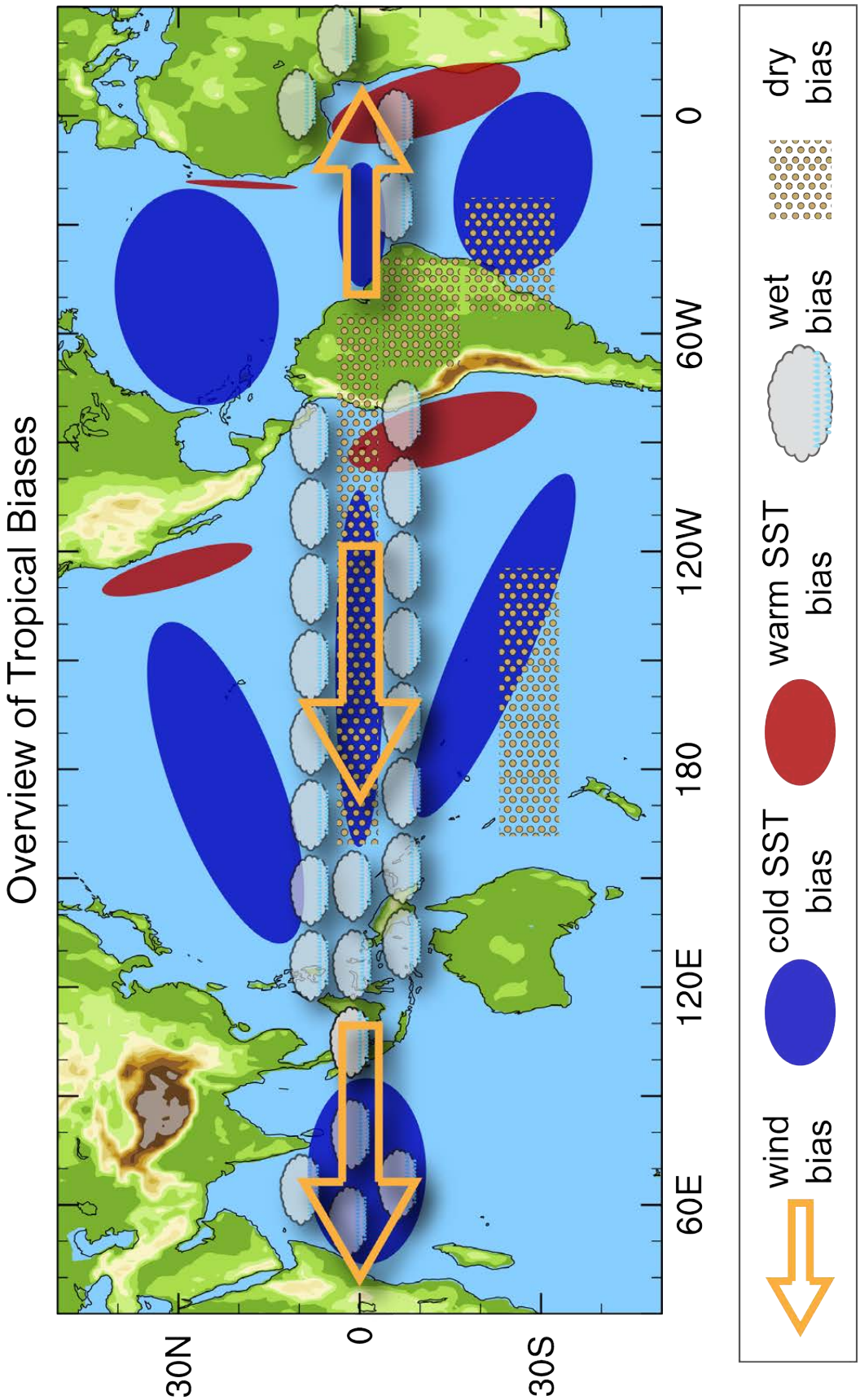

Figure 18. Schematic summarizing common GCM biases in the tropics. The individual features highlighted are: surface wind biases (hollow arrows), cold and warm SST biases (blue and red ellipses, re-

spectively), and wet and dry precipitation biases (grey ellipses and yellow dots, respectively). The shading over the continents represents orographic heights.